Electrical transport phenomena in MnTe, an antiferromagnetic semiconductor

ELECTRICAL TRANSPORT PHENOMENA IN MnTe, AN ANTIFERROMAGNETIC SEMICONDUCTOR

J. D. WASSCHER

ELECTRICAL TRANSPORT PHENOMENA IN $MnTe_x$ AN ANTIFERROMAGNETIC SEMICONDUCTOR

PROEFSCHRIFT

TER VERKRIJGING VAN DE GRAAD VAN DOCTOR IN DE TECHNISCHE WETENSCHAPPEN AAN DE TECHNISCHE HOGESCHOOL TE EINDHOVEN OP GEZAG VAN DE RECTOR MAGNIFICUS PROF. DR. IR. A. A. TH. M. VAN TRIER, HOOGLERAAR IN DE AFDELING DER ELEKTROTECHNIEK, VOOR EEN COMMISSIE UIT DE SENAAT TE VERDEDIGEN OP DINSDAG 30 SEPTEMBER 1969 DES NAMIDDAGS TE 4 UUR

DOOR

JAN DOUWE WASSCHER

GEBOREN TE GRONINGEN

DIT PROEFSCHRIFT IS GOEDGEKEURD DOOR DE PROMOTOR
PROF. DR. F. VAN DER MAESEN

Aan de nagedachtenis van
mijn ouders

CONTENTS

INTRODUCTION

The relation between electrical and magnetic properties of magnetic metals [1]) and magnetic semiconductors [2]) is a problem with many aspects. With regard to antiferromagnetic semiconductors, investigations have been mainly restricted to transition-metal oxides (see, e.g., ref. 3). The question of the proper description of their electrical conduction has a long history and has not yet been solved.

This thesis*) is devoted to a study of the electrical properties of MnTe, which is a non-oxidic antiferromagnetic semiconductor [4–9]). By suitable doping it can be made relatively low-ohmic and, in the temperature range from 77 to 500 °K, the resistivity and Seebeck coefficient (thermoelectric power) of such material increases with rising temperature. The increase is particularly marked just below 307 °K and weak above 307 °K. This behaviour is clearly connected with the magnetic properties of the compound since 307 °K is the Néel temperature, T_N, of MnTe (at which a second-order phase transition occurs from the low-temperature antiferromagnetically ordered phase to the high-temperature paramagnetic phase).

Similar effects near T_N appear to be absent in oxidic antiferromagnetic semiconductors. Some of these have, however, one interesting phenomenon in common with MnTe, viz. a very anomalous behaviour of the Hall coefficient at temperatures near and above T_N. The effects mentioned are not due to a change in energy gap. In MnTe the optical-energy gap is 1·2 eV both below and above T_N.

At the present moment it is difficult to evaluate the relation between the electrical properties of MnTe and those of the oxidic antiferromagnetic semiconductors. It may be significant that the effective mass of the charge carriers is relatively low in MnTe while it is much larger in the oxides. According to Albers and Haas [10–12]) such a difference might stem from the fact that in the oxides the charge carriers occupy states of a narrow energy band derived mainly from nearly non-overlapping $3d$ orbitals of the transition-metal atoms, while in (p-type) MnTe the holes occupy states of a broad energy band predominantly originating from markedly overlapping $5p$ Te orbitals. In addition to the low effective mass ($\approx 0{\cdot}6\ m_0$) another argument for a model based on broad-band conduction in p-type MnTe is the relatively high mobility of the holes (about 5 cm^2/V s at T_N and 100 cm^2/V s at 77 °K). In this work a model of this kind will be used for the theoretical description of the observed properties.

In two brief communications published some time ago [13,14]) we have reported the results of measurements on the resistivity, Hall coefficient and

*) This work will also be published as Philips Res. Repts Suppl. 1969, No. 8.

Seebeck coefficient of MnTe at temperatures between 77 and 350 °K. The change in the temperature dependence of the resistivity at T_N mentioned above was attributed to spin-disorder scattering, which is known to give rise to a similar behaviour of the resistivity in ferromagnetic metals. The temperature dependence of the Seebeck coefficient could be accounted for by magnon drag — a phenomenon similar to phonon drag in non-magnetic semiconductors — the existence of which was theoretically predicted by Bailyn [15]), but which had never previously been observed (Bailyn also had ferromagnetic metals at low temperatures in mind rather than an antiferromagnetic semiconductor at T_N). The anomalous behaviour of the Hall coefficient observed above 240 °K could not be explained at the time.

In the meantime the following developments have taken place. (1) The anomalous behaviour of the Hall coefficient was interpreted by Maranzana [16]) as being due to an "extraordinary" contribution to the Hall coefficient like that found in ferromagnetic metals (as remarked above, a similar effect has now been found in the oxidicanti ferromagnetic semiconductors too [17])). (2) The theoretical mobility in magnetic semiconductors due to spin-disorder scattering was recently calculated by Haas [18]). The temperature dependence of this mobility is quite different from that previously assumed. (3) In connection with optical work on MnTe [19]) it was pointed out by Zanmarchi and Haas [20,21]) that in considering magnon drag in MnTe second-order effects may have to be taken into account.

In this thesis more experimental data on the electrical properties of *p*-type MnTe are given than in the papers cited above [13,14]). With respect to this earlier work the main new features of this thesis are:
(1) a temperature-dependent anisotropy is found in the resistivity, indicating a temperature-dependent anisotropy in either the effective mass or the relaxation time for scattering,
(2) proposals are made for extensions of Haas' theory of spin-disorder scattering, on the basis of discrepancies found in comparing the experimental data with the theory,
(3) considerations involving second-order drag effects suggest that the effective mass and the acceptor-level depth may change with temperature near T_N (in accordance with one of the proposed modifications of the theory).

The presentation of the various subjects is arranged as follows.

In chapter 1 we briefly indicate the physical meaning of the transport properties investigated, as well as their interpretation as given in our previous papers [13,14]). The method used for preparing MnTe is given and also some of the physico-chemical and magnetic properties of MnTe.

Chapter 2 contains a description of the experimental arrangements employed

for the measurements, and of a new and sensitive method for determining anisotropies of the resistivity.

In chapter 3 the experimental results are presented and different possibilities for their interpretation are indicated. The main difficulty here is that the anomalous behaviour of the Hall coefficient does not allow the temperature dependence of the hole concentration near T_N to be established unambiguously.

Chapter 4 reviews Haas' theory of spin-disorder scattering and the model on which it is based. From the discrepancy between the result of this theory and the experimental data some suggestions are made as to points in which the theory could be improved. Among these is a proposal of a model in which the band parameters (such as the effective mass) depend on the magnitude of the sublattice magnetization. In the last section of this chapter the spin-disorder mobility in antiferromagnetic semiconductors is calculated on the basis of magnon scattering.

In chapter 5 a brief account is given of the physical origin of the first-order and second-order drag effects. Equations are presented which have been derived from a simplified model and from detailed calculations published for the case of phonon drag. Assuming that the hole concentration is essentially independent of temperature one finds that first-order magnon-drag effects give a satisfactory description of the anomalous behaviour of the Seebeck coefficient in MnTe. For degenerate samples second-order effects have to be taken into account at temperatures near T_N. In this case no agreement between theory and experiment is found.

In the final chapter the main points of disagremeent between theory and experiment are reviewed and it is concluded that a magnetization dependence of the band parameters contributes significantly to the observed behaviour of the electrical transport properties of MnTe.

1. SOME PROPERTIES OF MnTe

In this chapter an introductory discussion is given of the most prominent features of the electrical properties of MnTe reported earlier. The method used for preparing MnTe and some of its physico-chemical and magnetic properties are briefly discussed.

1.1. Previous work on the electrical properties of MnTe

The anomalous behaviour of the transport properties of (p-type) MnTe near its Néel temperature, $T_N = 307$ °K, has been noted by several authors [4–9]), but no consistent or complete explanation of these phenomena has been given. In two brief earlier communications [13,14]) we reported additional experimental data of which the most important was the discovery of a large anisotropy in the Hall coefficient at temperatures above 240 °K. The explanation of the experimental data given in these papers will now be summarized.

In normal (non-magnetic and extrinsic) semiconductors the *Hall coefficient*, R_H, is a simple (nearly) isotropic quantity which is a direct measure for the concentration and the sign of the charge carriers responsible for the electrical conductivity (see sec. 3.1.2),

$$R_H = \gamma_H/pe \ (p\text{-type}); \ R_H = -\gamma_H/ne \ (n\text{-type}), \tag{1.1}$$

where γ_H is a numerical constant of the order of unity, and where e is the absolute value of the electronic charge, while p and n are the concentrations of holes and electrons, respectively. As just mentioned, it is found that in MnTe the Hall coefficient is anisotropic above 240 °K. Above T_N (307 °K) this anisotropy is so large that R_H has a different sign when measured with the magnetic field parallel or perpendicular to the crystallographic c-axis *). From this unusual anisotropy it was concluded that in MnTe above 240 °K relation (1.1) is not valid, but from secondary evidence it was possible to show that it holds at least approximately at temperatures below 240 °K. At these temperatures R_H is positive so that conduction occurs by holes.

With hole concentrations p derived by use of the Hall coefficient below 240 °K we obtained from the resistivity

$$\varrho = (p\, e\, \mu)^{-1} \tag{1.2}$$

the hole *mobility* μ, i.e. the average drift velocity acquired by the holes due to the combined action of an applied electrical field of unit strength and scattering processes. This mobility is found to decrease with increasing temperature, the decrease being particularly marked just below T_N, but rather weak above T_N. It was remarked that this behaviour is very similar to that observed in ferro-

*) MnTe has a hexagonal NiAs structure below 1312 °K.

magnetic metals and should be ascribed to spin-disorder scattering. This scattering arises from an exchange interaction between the spin of the charge carrier and the magnetic spins of the Mn atoms. It is expected to be strong when the Mn spins are disordered and to vanish with perfect ordering of all Mn spins.

In general the Seebeck coefficient, or thermoelectric power, of non-magnetic semiconductors contains two components. The first, the purely electronic contribution S_e, arises from the thermodiffusion of the charge carriers in a temperature gradient, which is balanced by the diffusion due to the concentration gradient and electrical field created. The value of S_e at a given temperature can be calculated from the concentration and the effective mass of the charge carriers (the energy dependence of the mean free path should also be known, cf. eq. (3.3)). A second contribution to the Seebeck coefficient may arise from drag effects. If the carriers are (predominantly) scattered by phonons, the phonon-drag contribution originates from the fact that in these scattering processes crystal momentum is conserved so that the carriers are dragged along with the thermodiffusion current of the phonons. This enlarges the thermal e.m.f. and thus the Seebeck coefficient.

Describing the scattering of the charge carriers by spin disorder as a scattering by magnons, magnon-drag effects are to be expected in magnetic semiconductors. Although the magnon description of spin disorder is strictly valid at temperatures well below T_N, it was shown that such a drag effect can explain the anomaly in the Seebeck coefficient of MnTe observed near T_N.

Other work carried out on MnTe in the Philips' Research Laboratories relates to its optical properties [19–21]), the thermal hysteresis of its resistivity at high temperatures [22]), the extraordinary behaviour of the Hall effect and magnetoresistance in Cu-doped MnTe [23,24]), the attenuation of ultrasonic waves [25]) and, more recently, the phase diagram of MnTe [26]). A discussion of this work falls outside the scope of this thesis. It will suffice to note that an energy gap of 1·2 eV at room temperature is found from the optical properties, and an effective mass $m_\perp = 0{\cdot}4\, m_0$ for motions perpendicular to the c-axis and $m_{||} = 1{\cdot}6\, m_0$ for motions parallel to the c-axis, both for temperatures below 150 °K (for higher temperatures, see sec. 3.3).

1.2. Physico-chemical properties

The MnTe crystals used in the present investigation were obtained by slowly cooling a melt of MnTe contained in a carbon boat *). The ambient gas was argon at a pressure of 200 mm Hg. This pressure was found to prevent the formation of macroscopic holes in the ingot formed when working in a vacuum.

*) During the first stage of the investigation the preparation was carried out by Dr W. Albers. This work was continued by Mr A. J. M. H. Seuter.

The temperature of the melt before cooling was begun was 1470 °K.

Under the above conditions of preparation, solidification occurs at about 1440 °K and the crystals formed have the NaCl structure initially. Upon further cooling a first-order transition point is reached at 1312 °K where the crystals transform into the NiAs structure. This modification appears to be stable down to the lowest temperature used in the present investigation (cf. ref. 27). The first-order transition is the probable cause of the fact that the crystals finally obtained are far from perfect and show many fractures and dislocations.

Recently Van den Boomgaard [26]) has investigated the phase diagram of the Mn-Te system near the equiatomic composition. He finds that it should be possible to obtain crystals of MnTe which grow directly in the NiAs structure. The conditions which must be satisfied are, however, rather difficult to fulfil and no crystals have been grown in this manner. At ordinary temperatures the crystals made by the method followed by Seuter always contain precipitates of $MnTe_2$.

The homogeneity range of MnTe is found to be very small and to lie probably entirely on the Te-rich side of the stoichiometric composition. It may be assumed that the *p*-type conductivity found in undoped material is connected with the deviation from stoichiometry. Changes in the equilibrium between the single-phase MnTe and the $MnTe_2$ precipitates or the vapour phase also cause a change in hole concentration. This mechanism was proposed by Seuter [22]) as being the probable origin of the effects of thermal hysteresis in the resistivity which are observed in MnTe at temperatures above 400 °K [4,27]).

Doping of the crystals may be achieved by adding the dopants to the starting material. Incorporation of Na increases the *p*-type conductivity [6]), indicating that Na acts as an acceptor. High-resistivity material may be obtained by adding

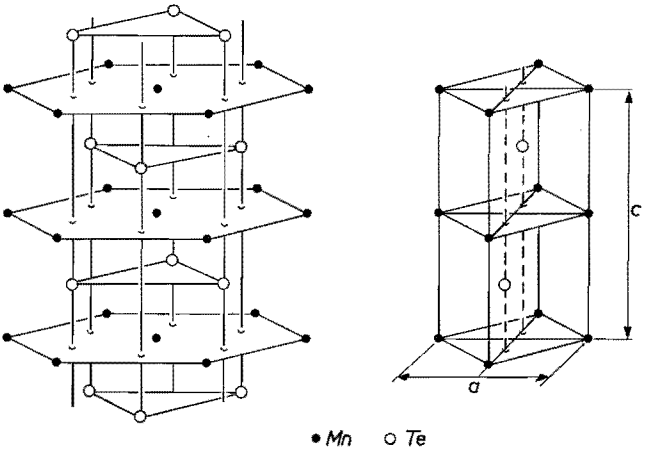

Fig. 1.1. The crystal structure of MnTe; the right-hand figure is the unit cell.

Cr (cf. ref. 7), but the MnTe thus prepared remains *p*-type. Apparently Cr acts as a donor but its solubility does not exceed the concentration of native defects acting as acceptors. Another possibility is that the concentration of Cr atoms exceeds the concentration of native defects but that their donor level is closer to the valence band than to the conduction band.

The NiAs structure is shown in fig. 1.1. It may be thought of as an h.c.p. lattice of the anions in whose octahedral sites the cations are located. The latter form a simple hexagonal lattice. For MnTe the c/a ratio is 1·62 [28]), which is close to the ideal value of $(8/3)^{1/2} = 1{\cdot}63$, corresponding to a perfect octahedral coordination of the cations. The crystallographic unit cell contains two anions and two cations, all belonging to different *c*-planes (planes perpendicular to the *c*-axis).

1.3. Magnetic properties

The magnetic susceptibility of MnTe has a maximum near 328 °K [4]), but the magnetic-ordering temperature, or Néel temperature T_N, is somewhat lower, 307 °K. This value has been established in several ways, e.g. from an abrupt decrease in the specific heat [29]) and, very accurately, from a sharp peak in the attenuation of ultrasonic waves [25]), both effects presumably taking place at T_N. The change of slope at T_N of the resistivity vs temperature curve has been used to investigate the pressure dependence of T_N [30]).

Above 600 °K the susceptibility follows the Curie-Weiss law $\chi = C/(T + \theta)$ with an asymptotic Curie temperature θ of 600 to 700 °K [4,31]). The Curie constant C corresponds to a magnetic moment of five Bohr magnetons per Mn atom, in agreement with an expected ^6S configuration for five unpaired $3d$ electrons on each Mn atom [27]).

The magnetic structure in the antiferromagnetic phase below T_N has been determined from the anisotropy of the magnetic susceptibility [31]) and from neutron diffraction [27,32]). It is found that the average spin directions of the Mn atoms in each *c*-plane are parallel to each other and antiparallel to those of the Mn atoms in the next *c*-plane. The magnetic unit cell is thus identical with the crystallographic unit cell.

There are relatively strong anisotropy forces causing the spin direction to be oriented perpendicularly to the *c*-axis, but the forces coupling the orientation to any particular direction within the *c*-plane are much weaker [31]). This direction has not been determined experimentally. It can be shown, however, that if the preferred direction of sublattice magnetization is not along the Mn-Mn direction, weak ferromagnetism is possible [23,24]). Since weak ferromagnetism is not usually observed in MnTe, it seems likely that the direction of preferred sublattice magnetization is normally along the Mn-Mn direction.

2. EXPERIMENTAL METHODS

This chapter contains a description of the experimental set-up used for measuring the resistivity, Hall coefficient and Seebeck coefficient. Calculations and applications of a new and sensitive method for determining anisotropies of the resistivity are given.

2.1. Experimental arrangements

2.1.1. *Resistivity and Hall effect*

Most measurements on MnTe reported here were performed using the method of Van der Pauw [33,34]) (see also sec. 2.2). The dimensions of the samples were about $5 \times 5 \times 0{\cdot}5$ mm^3 and silver paste was used for making electrical contacts.

The various components of the electrical equipment used for the measurements are shown in the block diagram of fig. 2.1. The measuring current is

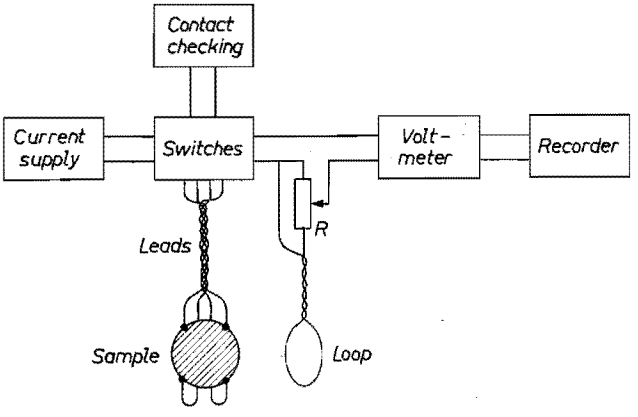

Fig. 2.1. Block diagram of apparatus used for resistivity and Hall-effect measurements.

drawn from ten 1·5-V air-depolarized cells. Currents ranging from 0·5 to 100 mA are obtained by stepwise variation of the series resistance of the circuit. The voltmeter is a Keithley model 150A d.c. Microvolt-Ammeter. The zero suppression up to 100 times full scale of this instrument can be used conveniently for compensating the voltage drop across the Hall probes. Its output is connected to a Philips PR 4069 M/06 recorder. For the Hall measurements the use of a recorder instead of directly reading a voltmeter has several advantages. It allows less stringent demands on temperature stability, the performance of the measurements is facilitated and in some cases the recorder trace shows details which otherwise would easily be overlooked.

The sample contacts can be checked by displaying the current through two contacts as a function of the voltage across these contacts on an oscilloscope.

A rectifying contact can usually be made ohmic by discharging a condensor through it.

Five multiple switches serve for making the desired connections between the units described and the leads to the sample. The leads consist of thin copper wires (100 μm) and are twisted around each other in order to diminish pick-up from stray fields. The loop in the voltage circuit is fixed to one of the pole caps of the magnet and is employed for compensating the induction voltage which occurs during changing and switching of the magnetic field. With the ten-turn 100-Ω potentiometer (R) the compensation by the loop can be adjusted accurately.

Many measurements were carried out at temperatures between 77 and 350 °K in a magnet giving 5 kG. For measurement at higher field strengths a special magnet was designed in cooperation with Dr D. H. Kroon (cf. ref. 35). It attains a maximum field of nearly 23 kG in an air gap of 22 mm (at 90 A and 90 V); its weight is only 500 kg. The magnet current is obtained by rectification of a 380-V three-phase mains supply and is continuously variable.

The small air gap of this magnet necessitated a special apparatus for performing measurements at various temperatures. It is shown in fig. 2.2. The sample (1) is fixed to the cadmium-plated copper sample holder (fig. 2.2*a*) by means of four phosphor-bronze springs (2) pressing against the electrical con-

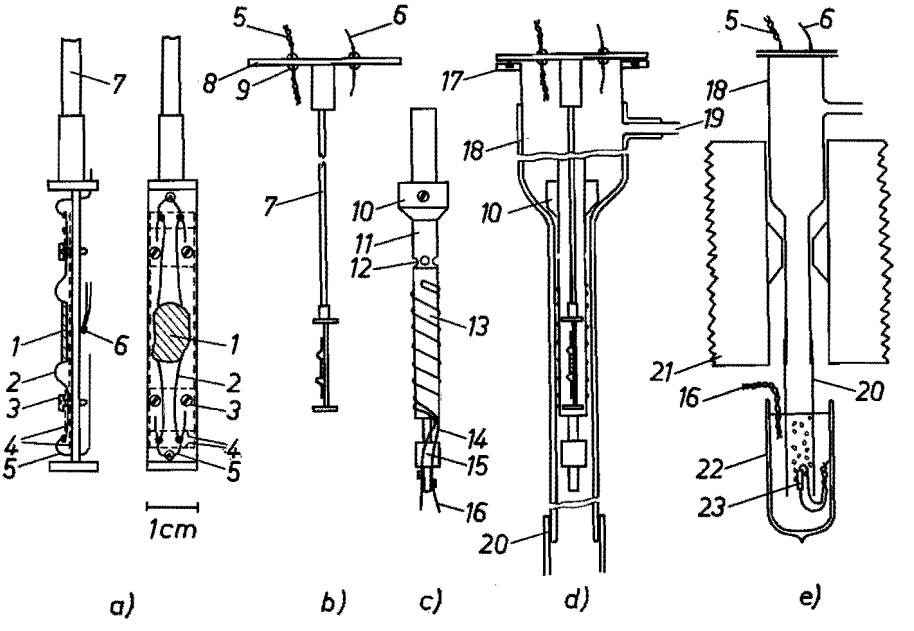

Fig. 2.2. Apparatus for Hall-effect measurements between 200 and 350 °K in magnet (21) with 22-mm air gap. For explanation, see text.

tacts of the sample. Thin mica discs (dashed lines 4) fix the springs by turning on the screws (3) and serve for electrical insulation. The lead wires (5) are soldered to the springs. The sample holder is connected to a metal disc (8) by means of a novotex rod (7), fig. 2.2*b*. The measuring leads (5) and a thermocouple (6) pass through the disc (8) via thin molybdenum tubes sealed in glass (9).

After the sample has been mounted the sample holder is lowered into an open double-walled glass tube (18), fig. 2.2*d*. This tube is silvered internally and the interspace is evacuated (the seal is not shown). It is provided with a metal flange (17) to which the disc (8) is fastened. In the tube the sample holder is surrounded by the heating element, fig. 2.2*c*. Its lower part (13) consists of a copper tube covered with an insulating layer of Al_2O_3 on which a heating wire (14) is wound. This wire is connected to leads (16) by means of screws in an asbestos block (15) which also serves for centring the heating element in the glass tube. The upper part (11) of the heating element is made of stainless steel and contains four holes (12). The asbestos piece (10) serves for suspending the heating element in the glass tube.

For cooling the sample a rubber tube (20) reaching into a Dewar vessel (22), fig. 2.2*e*, has been fitted to the lower part of the glass tube. The Dewar vessel can be filled with liquid nitrogen which will evaporate in proportion to the heat developed in a resistor (23) located within the rubber tube. The nitrogen vapour passes along the lower part of the heating element which now mainly serves for protecting the sample from rapid temperature fluctuations. Due to the asbestos part (10) the vapour is forced to flow through the holes (12) and through the upper part of the heating element. This reduces the heat inflow from above along the measuring leads and thermocouple. The vapour leaves the apparatus through the outlet (19).

To avoid cracking, the temperature difference between the inner and the outer glass tube may not be too large, so that only a limited temperature range around room temperature can be covered. Sufficient stability of the sample temperature is obtained by a constant heat input in the heating element (13) for measurements above room temperature, or in the resistor (23) in the nitrogen bath for measurements at lower temperature. In the latter case it is necessary, however, to maintain a constant nitrogen level in the Dewar vessel.

2.1.2. *Seebeck effect*

In conducting materials a temperature difference ΔT creates an electromotive force ΔV. For small temperature differences the ratio $\Delta V/\Delta T$ is called the Seebeck coefficient or thermoelectric power, and will be denoted by S.

Thermocouples are conveniently used for measuring the temperature difference. Two elementary ways of obtaining S using thermocouples are shown in fig. 2.3. In both cases the sample is clamped between two (metal) blocks which are maintained at different temperatures.

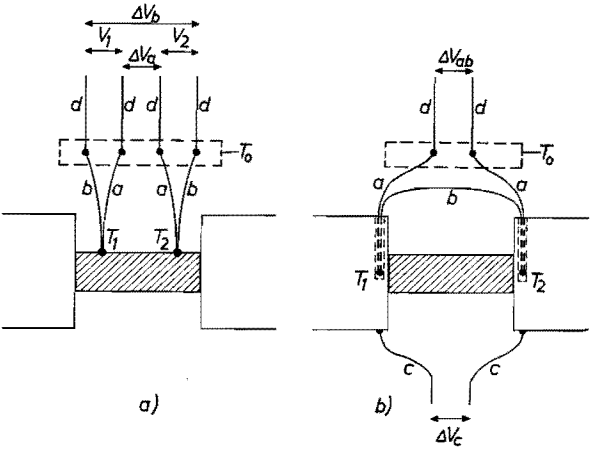

Fig. 2.3. Two common arrangements for measuring the Seebeck coefficient. The sample is clamped between two blocks which can be held at different temperatures; a and b are thermocouple branches, c and d measuring leads. Junctions between thermocouple wires and measuring leads are kept at a same temperature T_0. In case *a* the thermocouples are in electrical contact with the sample. In case *b* they are electrically insulated from the sample.

In case (*a*) the thermocouples are fixed to the sample in such a way that they make good thermal as well as good electrical contact with the sample. Denoting the measured voltages as shown in the figure, one finds the Seebeck coefficient of the sample from

$$S = \frac{\Delta V_a}{V_1 - V_2}(S_a - S_b) + S_a = \frac{\Delta V_b}{V_1 - V_2}(S_a - S_b) + S_b, \qquad (2.1)$$

where S_a and S_b are the Seebeck coefficients of the thermocouple wires a and b, respectively, at the average temperature $T = T_0 + \frac{1}{2}(V_1 + V_2)/(S_a - S_b)$. The total thermoelectric power of the thermocouples, $S_a - S_b$, can be obtained by differentiating their calibration curve. One branch should consist of a metal with known Seebeck coefficient in order that the corrections S_a and S_b in eq. (2.1) can be applied.

In case (*b*) the thermocouples are used differentially. In order to avoid short-circuiting the thermal e.m.f. of the sample, at least one of the thermocouples has to be electrically insulated from the sample.

The advantages of method (*b*) over method (*a*) are that it gives a direct reading of $\Delta V_{ab} = V_1 - V_2$, and that when measuring different samples only the samples have to be changed. With method (*b*) smaller samples can also be handled than with method (*a*). On the other hand, method (*b*) is less accurate because of possible heat resistance at the contacts between the sample and the

heating blocks *). In case (*a*) this heat resistance does not affect the measurements.

An accurate measurement of the Seebeck coefficient of a low-ohmic sample of MnTe (0·02 Ω cm at room temperature) has been obtained by employing a method proposed by Dauphinee and Mooser [36,37]). This method combines the advantages of methods (*a*) and (*b*) by giving a direct reading of ΔV_{ab} with the absence of troublesome heat resistance. The principle of the measurement is shown in the upper part of fig. 2.4. The sample and

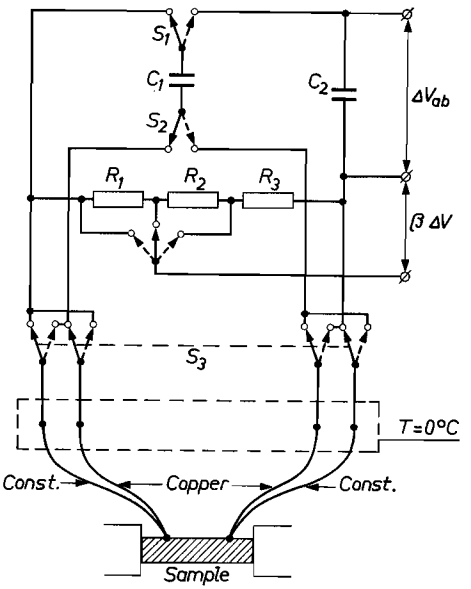

Fig. 2.4. Dauphinee-Mooser circuit used for accurate measurements of the Seebeck coefficient. Switches S_1 and S_2 vibrate simultaneously at a rate of about 40 cycles per second, charging condenser C_2 to voltage ΔV_{ab}. Resistances $R_1 = 20$ kΩ, $R_2 = 7$ kΩ and $R_3 = 3$ kΩ permit fraction $\beta = 1$, 1/3 and 1/10 of the thermal e.m.f. ΔV to be measured on the same scale of the voltmeter as ΔV_{ab}.

thermocouples are mounted as for method (*a*). The motor-driven "break-before-make" switches S_1 and S_2 vibrate simultaneously at a rate of about 40 cycles per second. In this way the condensor C_1 is charged to the voltage delivered by the thermocouple to the left, $C_1 + C_2$ to the voltage delivered by the thermocouple to the right. The difference between the two voltages ΔV_{ab} will then be found across C_2. This voltage is measured by a Keithley 150A connected to a Philips recorder, as for the measurement of the Hall effect.

*) Such heat resistance shows up as a hysteresis effect in the ΔV vs ΔT curve. It is noted that in all cases it is necessary to measure ΔV as a function of ΔT in order to eliminate small differences in the thermoelectric power of the thermocouples as well as spurious e.m.f.s in the measuring circuit. These effects cause the ΔV vs ΔT curve not to pass through the origin.

The double reversal switch S_3 permits of the measurement of the thermal e.m.f. ΔV of the sample with respect to the copper as well as to the constantan wires of the thermocouples. With the resistances R_1, R_2 and R_3 a known fraction β of ΔV can be supplied to the voltmeter so that $\beta \Delta V$ and ΔV_{ab} may be read with the same range setting. Being much larger than all other resistances in the circuit they introduce negligible errors in the results. The connections between the thermocouple wires and their lead wires were immersed in an ice bath in order to protect them from temperature variations. This was also convenient for using the thermocouples for determining the temperature of the sample.

To perform the measurements we clamped the sample between two copper blocks (fig. 2.5). The thermocouple junctions were immersed in a small amount of

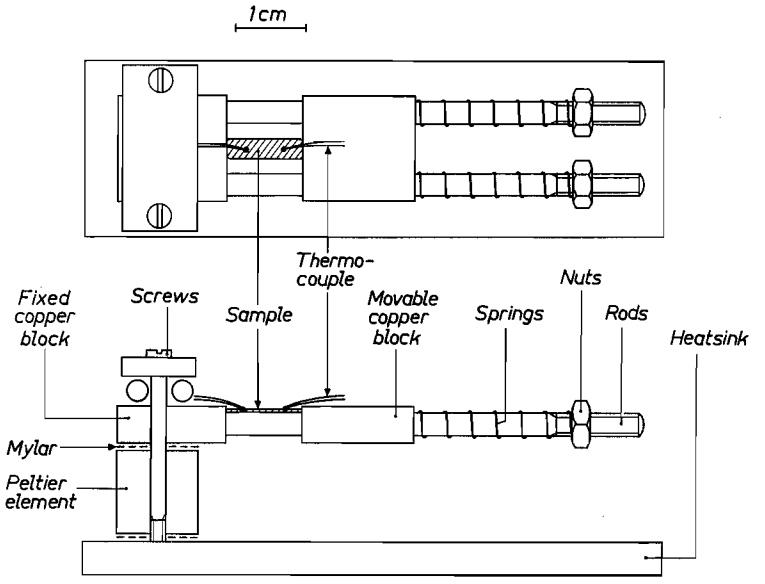

Fig. 2.5. Device used for creating a temperature gradient in a sample by means of a Peltier element.

a liquid metal alloy which had been brought into two grooves made in the sample. One of the copper blocks was clamped on top of a Bi_2Te_3 Peltier element and was cooled or heated depending on the direction of the current passed through this element. The whole device was placed in a copper tube whose temperature could be controlled between 77 and 330 °K.

The voltages ΔV_{ab} and $\beta \Delta V$ could be recorded alternately during 3 and 7 seconds, respectively, the duty cycle of 10 seconds being obtained by means of a motor-driven microswitch. A drawing of a typical recorder trace during some successive reversals of the current through the Peltier element (and a continuous

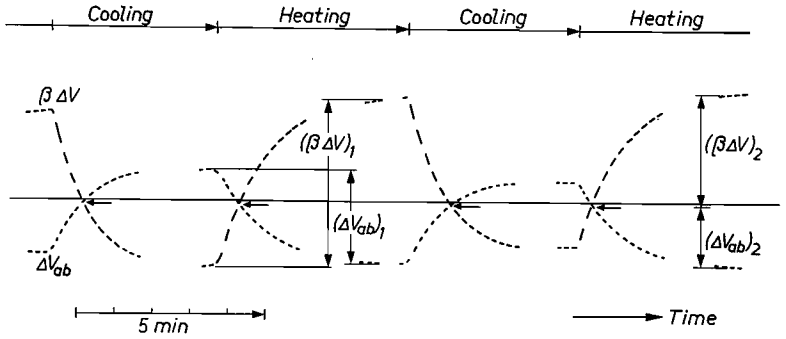

Fig. 2.6. Recorder trace obtained with apparatus shown in figs 2.4 and 2.5; ΔV_{ab} and $\beta \Delta V_a$ are recorded alternately during 3 and 7 seconds, respectively. Cooling and heating refer to the top of the Peltier element (cf. fig. 2.5). During the time that no trace is shown, measurements of temperature and resistivity were taken. Horizontal arrows indicate crossings of ΔV_{ab} and ΔV_a traces and show absence of thermal hysteresis. Vertical arrows indicate two ways of obtaining the relevant data for calculating the Seebeck coefficient of the sample.

change of the overall temperature of the measuring device) is shown in fig. 2.6. The ΔV_{ab} and $\beta \Delta V$ traces intersect at the same distance below the zero axis for both directions of the current through the Peltier element, which shows the absence of a hysteresis effect due to a possible poor thermal contact between the thermocouples and the sample. That the two traces do not intersect on the zero axis is due to spurious e.m.f.s in the circuit and/or inequality of the thermocouples (cf. footnote above).

During the time for which fig. 2.6 shows no traces the voltages ΔV_{ab}, $\beta \Delta V$, ΔV_1 and ΔV_2 were read directly on the voltmeter for both positions of the switch S_3 (for determining the resistivity the change of $\beta \Delta V$ was also observed when a given current was passed through the sample via the copper blocks; actually these measurements were usually made after the temperature difference across the sample had been made constant by adjusting the current through the Peltier element). From these readings the Seebeck coefficient was obtained from the voltages indicated in fig. 2.6 by the vertical arrows $(\beta \Delta V)_1$ and $(\Delta V_{ab})_1$. Another possibility is indicated by the vertical arrows $(\beta \Delta V)_2$ and $(\Delta V_{ab})_2$.

From the readings for the two positions of the switch S_3 it was possible to calculate the Seebeck coefficient of the sample both with respect to copper, $S - S_{Cu}$, and with respect to constantan, $S - S_{const}$ (cf. eq. (2.1)). For all measurements the relation

$$(S - S_{Cu}) = (S - S_{const}) + (S_{const} - S_{Cu}) \qquad (2.2)$$

was satisfied within two per cent. An impression of the reproducibility of the method is given by fig. 2.7, which shows the results of measurements at various temperatures on the MnTe sample mentioned. Below 200 °K the Bi_2Te_3

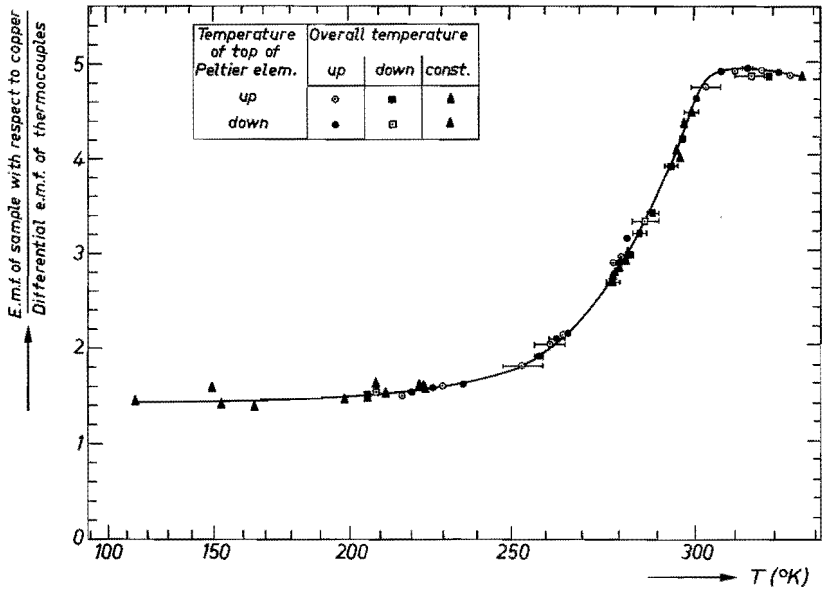

Fig. 2.7. Result of measurements of the Seebeck coefficient of an MnTe sample. For some points the change of average sample temperature during the measurement is indicated.

element was less effective in producing temperature differences across the sample and the measurements were somewhat less accurate than at higher temperatures.

It is remarked that with the device used at a constant ambient temperature one obtains a difference in average sample temperature for the two current directions through the Peltier element which is often much larger than ΔT. When, however, measurements are carried out while continually changing the ambient temperature, every second measurement can be made in such a way that it refers to a nearly constant average sample temperature. This is shown, e.g., by the four successive measurements between 254 and 263 °K. The Seebeck coefficient of the sample is given below in fig. 3.2*a*.

2.2. A method for determining the anisotropy of the resistivity

2.2.1. *The Van der Pauw method*

In an earlier paper [38]) a method was described by which the components of the resistivity of an anisotropic conductor can be obtained by means of a customary four-probe resistivity measurement (equally spaced probes in a collinear or square arrangement). This method requires samples with dimensions large compared to the spacing of the probes, otherwise complicated corrections have to be applied. In the present section another method will be discussed which does not impose such a condition and which, furthermore, has been found to be more sensitive.

The method may be regarded as a special case of the Van der Pauw method [33,34]) for measuring resistivities. For applying the latter method a flat sample (of arbitrary shape but with no holes in it) is provided with four contacts P, Q, R and S at its circumference and two "resistances" R_1 and R_2 are measured. R_1 is defined as $R_{PQ,RS}$, i.e. the voltage across the contacts R and S per unit current passed through the contacts P and Q. Similarly $R_2 = R_{QR,SP}$. If the sample is isotropic it can be shown that R_1 and R_2 do not change by conformal mapping of the sample onto some other shape. Taking for this other shape a half-plane, as e.g. in fig. 2.8*d*, it follows from elementary theory that

$$R_1 = R_{PQ,RS} = \frac{\varrho}{\pi d} \ln\left(\frac{R'P'}{R'Q'} \cdot \frac{S'Q'}{S'P'}\right), \tag{2.3a}$$

$$R_2 = R_{QR,SP} = \frac{\varrho}{\pi d} \ln\left(\frac{S'Q'}{S'R'} \cdot \frac{P'R'}{P'Q'}\right), \tag{2.3b}$$

where ϱ and d are the resistivity and the thickness of the sample, respectively; R'P' denotes the distance between the image points of R and P, etc.. Van der Pauw proceeds by noting that

$$\frac{R'Q'}{R'P'} \cdot \frac{S'P'}{S'Q'} + \frac{S'R'}{S'Q'} \cdot \frac{P'Q'}{P'R'} = 1, \tag{2.4}$$

so that

$$\exp(-\pi R_1 d/\varrho) + \exp(-\pi R_2 d/\varrho) = 1, \tag{2.5}$$

which may also be written as

$$\varrho = \frac{\pi d}{2 \ln 2} (R_1 + R_2) f(R_1/R_2), \tag{2.6}$$

$f(R_1/R_2)$ being a complicated function of the ratio R_1/R_2 which is given by Van der Pauw in graphical form *). The surprising element in the method is that the shape of the sample and the position of the contacts need not be known. These geometrical factors enter into the calculation of ϱ only in so far as they determine the ratio R_1/R_2.

The method for measuring anisotropic resistivities proposed here is based on the fact that

---

*) Some parts of the curve as reproduced in Van der Pauw's paper [33]) deviate from the correct curve by a few per cent. A useful parametric relation for calculating the curve is

$$f(R_1/R_2) = \frac{\log \frac{1}{4}}{\log(\frac{1}{2} + x) + \log(\frac{1}{2} - x)}; \quad \frac{R_1}{R_2} = \frac{\log(\frac{1}{2} - x)}{\log(\frac{1}{2} + x)},$$

with $-\frac{1}{2} < x < \frac{1}{2}$ (cf. eq. (2.20)).

(1) for an isotropic sample of simple geometry the ratio R_1/R_2 of the Van der Pauw method can be calculated explicitly, and

(2) an anisotropic sample with resistivities ϱ_i $(i = 1, 2, 3)$ along the three principal (mutually orthogonal) axes x_i is electrically equivalent to an isotropic sample whose dimensions x_i' are related to the dimensions x_i of the anisotropic sample by [34,39])

$$x_i' = (\varrho_i/\varrho)^{1/2}\, x_i \tag{2.7}$$

and whose resistivity is

$$\varrho = (\varrho_1\, \varrho_2\, \varrho_3)^{1/3}. \tag{2.8}$$

Calculations will be given below for rectangular and circular samples.

2.2.2. *Rectangular samples*

Consider a flat, anisotropic, rectangular sample of length l_1, width l_2 and thickness l_3 with its edges parallel to the directions of the principal resistivities ϱ_1, ϱ_2 and ϱ_3, and provided in a symmetrical way with two pairs of contacts at distances $a\, l_1$ apart $(a \leqslant 1)$ as shown in fig. 2.8*a*. According to eqs (2.7) and (2.8) the sample is electrically equivalent to an isotropic sample with resistivity $\varrho = (\varrho_1\, \varrho_2\, \varrho_3)^{1/3}$ and dimensions $l_i' = (\varrho_i/\varrho)^{1/2}\, l_i$ (fig. 2.8*b*).

It is well known (see e.g. refs 40 and 41) that the sine-amplitude function

$$w = \mathrm{sn}\,(z,k) \tag{2.9}$$

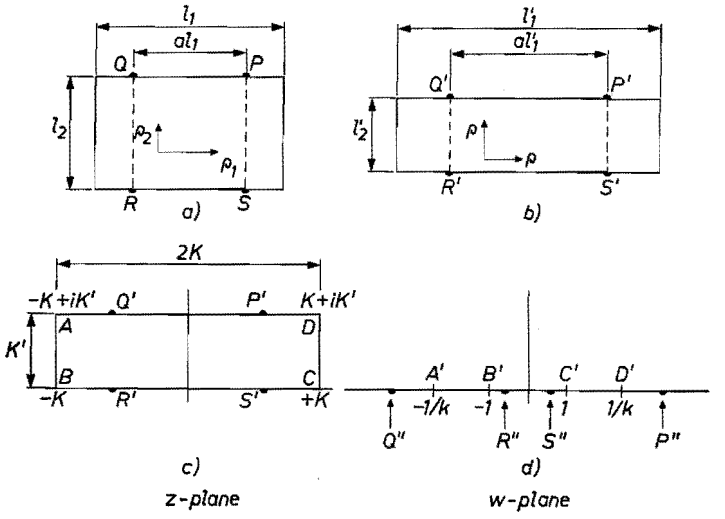

Fig. 2.8. Anisotropic rectangular sample with edges parallel to principal directions of ϱ; (*a*): the sample, (*b*): transformed into an electrically equivalent isotropic sample, (*c*): isotropic sample in z-plane, (*d*): sample mapped onto Im $w \geqslant 0$.

conformally maps the interior of a rectangle with sides $2\,K(k)$ and $K'(k)$ situated in the z-plane as shown in fig. 2.8*c*, onto the upper half of the w-plane (fig. 2.8*d*). Here $K(k)$ and $K'(k)$ are the complete elliptic integrals of the first kind and its associate, respectively. They are functions of the *modulus* k. The shape of the rectangle is determined by the ratio $K(k)/K'(k)$, i.e. by the value of k. Compilations of mathematical tables usually do not give $K(k)/K'(k)$ as a function of k, but rather the *gnome* $q(k) \equiv \exp\{-\pi\, K(k)/K'(k)\}$ as a function of k or of arcsin k.

A trivial transformation preserving the ratio l_1'/l_2' maps the sample of fig. 2.8*b* conformally onto the rectangle of fig. 2.8*c* so that the appropriate value of k for the sample considered can be obtained from the tables of $q(k)$ with

$$q(k) \equiv \exp\left(-\pi \frac{K'}{K}\right) = \exp\left(-2\,\pi \frac{l_2'}{l_1'}\right) = \exp\left(-2\,\pi \frac{l_2}{l_1} \sqrt{\frac{\varrho_2}{\varrho_1}}\right). \quad (2.10)$$

Here, as in the formulae given below, we omit in the notation the explicit dependence of the various elliptic functions of k, it being understood that in all expressions k has the same value, viz. that determined by eq. (2.10).

With the transformation (2.9) and the properties of the sine-amplitude function the position of the images of the contacts in the w-plane become (fig. 2.8*d*)

$$w(\mathrm{P}'') = \mathrm{sn}\,(a\,K + i\,K') = \{k\,\mathrm{sn}\,(a\,K)\}^{-1}, \quad (2.11a)$$

$$w(\mathrm{Q}'') = \mathrm{sn}\,(-a\,K + i\,K') = -\{k\,\mathrm{sn}\,(a\,K)\}^{-1}, \quad (2.11b)$$

$$w(\mathrm{R}'') = \mathrm{sn}\,(-a\,K) = -\mathrm{sn}\,(a\,K), \quad (2.11c)$$

$$w(\mathrm{S}'') = \mathrm{sn}\,(a\,K). \quad (2.11d)$$

Substituting the distances $\mathrm{P}''\mathrm{Q}'' \equiv w(\mathrm{Q}'') - w(\mathrm{P}'')$, etc. in eqs (2.3a) and (2.3b) one finds that

$$R_1 = \frac{(\varrho_1\,\varrho_2)^{1/2}}{\pi\, l_3}\; 2 \ln \frac{1 + k\,\mathrm{sn}^2\,(a\,K)}{1 - k\,\mathrm{sn}^2\,(a\,K)}, \quad (2.12a)$$

$$R_2 = \frac{(\varrho_1\,\varrho_2)^{1/2}}{\pi\, l_3}\; 2 \ln \frac{1 + k\,\mathrm{sn}^2\,(a\,K)}{2\,k^{1/2}\,\mathrm{sn}\,(a\,K)}. \quad (2.12b)$$

From these equations the ratio R_1/R_2 has been calculated as a function of $(l_1^2\,\varrho_1)/(l_2^2\,\varrho_2)$ for $a = 1$, 5/6, 2/3, 1/2, 1/3 and 1/6. The result is shown in fig. 2.9. These curves permit ϱ_1/ϱ_2 to be obtained from measured values of R_1/R_2, l_1/l_2 and a. The value of $\varrho_1\varrho_2$ follows from replacing ϱ by $(\varrho_1\,\varrho_2)^{1/2}$ in eq. (2.6).

It should be noted that the application of this method requires the knowledge of the directions of the principal axes of the resistivity tensor. If the plane of

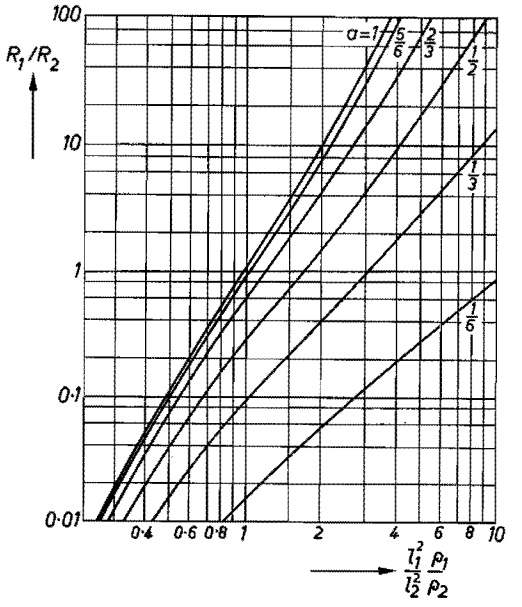

Fig. 2.9. R_1/R_2 for rectangular samples as a function of $l_1^2\varrho_1/l_2^2\varrho_2$ for different values of the fraction a (see fig. 2.8*a*).

the sample is not perpendicular to the direction of ϱ_3 the results obtained refer to the principal "sheet resistances" ϱ_1 and ϱ_2 in the plane of the sample.

2.2.3. *Circular samples*

A flat anisotropic circular sample (fig. 2.10*a*) of radius r and thickness d with its plane perpendicular to the direction of the principal resistivity ϱ_3 is electrically equivalent to an isotropic elliptic sample with semi-axes $a = r\,(\varrho_1/\varrho)^{1/2}$ and $b = r\,(\varrho_2/\varrho)^{1/2}$, and with a thickness $d' = d\,(\varrho_3/\varrho)^{1/2}$, ϱ being again equal to $(\varrho_2\,\varrho_1\,\varrho_3)^{1/3}$. The circumference of this ellipse may be represented in the z-plane (fig. 2.10*b*) by

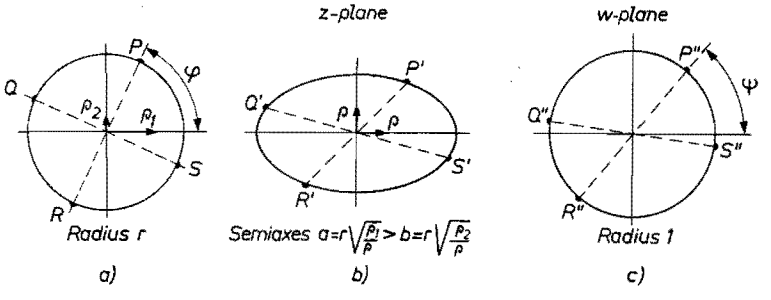

Fig. 2.10. Anisotropic circular sample; (*a*): the sample, (*b*): transformed into an elliptical, electrically equivalent isotropic sample, (*c*): the sample conformally mapped onto the unit circle.

$$z = a\cos\varphi + i\,b\sin\varphi = (a^2 - b^2)^{1/2}\cos(\varphi - ic), \tag{2.13}$$

(supposing $\varrho_1 > \varrho_2$) with

$$\exp(-c) = (a-b)(a^2-b^2)^{-1/2} = (\varrho_1^{1/2} - \varrho_2^{1/2})(\varrho_1 - \varrho_2)^{-1/2}. \tag{2.14}$$

This ellipse will first be transformed conformally into a unit circle (fig. 2.10*c*), which is achieved by

$$w = k^{1/2}\,\mathrm{sn}\left(\frac{2K}{\pi}\arcsin\frac{z}{(a^2-b^2)^{1/2}}, k\right) \tag{2.15}$$

if the modulus k satisfies

$$q(k) \equiv \exp\left(-\frac{\pi K'}{K}\right) = \exp(-4c) = \frac{(\varrho_1^{1/2} - \varrho_2^{1/2})^4}{(\varrho_1 - \varrho_2)^2}. \tag{2.16}$$

Like eq. (2.10) the later again determines the appropriate value of k for a given ratio ϱ_1/ϱ_2.

By substituting (2.13) and $4c = \pi K'/K$ (cf. (2.16)) into (2.15) (and using the properties of the sine amplitude and related functions), the image of a point $r\exp(i\varphi)$ on the circumference of the original circle on the unit circle $w = \exp(i\psi)$ is found to be

$$\begin{aligned} w &= k^{1/2}\,\mathrm{sn}\,(2K\varphi/\pi + K - iK'/2, k) = \\ &= \frac{(1+k)\,\mathrm{sn}\,(u+K) - i\,\mathrm{cn}\,(u+K)\,\mathrm{dn}\,(u+K)}{1 + k\,\mathrm{sn}^2\,(u+K)} = \\ &= \frac{\mathrm{cn}\,u\,\mathrm{dn}\,u + i(1-k)\,\mathrm{sn}\,u}{1 - k\,\mathrm{sn}^2\,u}. \end{aligned} \tag{2.17}$$

The functions $\mathrm{cn}\,(u,k)$ and $\mathrm{dn}\,(u,k)$ are related to $\mathrm{sn}\,(u,k)$ by $\mathrm{cn}^2\,u = 1 - \mathrm{sn}^2\,u$ and $\mathrm{dn}^2\,u = 1 - k^2\,\mathrm{sn}^2\,u$. In the last parts of (2.17) the modulus k has been omitted in the notation and u has been written short for $2K\varphi/\pi$.

The interior of the unit circle $|w| = 1$ is mapped conformally onto the upper half-plane $\mathrm{Im}\,t \geqslant 0$ by, e.g.,

$$t = \frac{w - i}{-iw + 1}. \tag{2.18}$$

This gives

$$t = \frac{\cos\psi}{\sin\psi + 1} \tag{2.18a}$$

for a point on the circumference, $w = \exp(i\psi)$. The final formula for the image of any point of the original circle $r \exp(i\varphi)$ on the axis $\mathrm{Im}\, t = 0$ is obtained by substituting (2.17) into (2.18). Using eqs (2.3a) and (2.3b), R_1 and R_2 can then be calculated for any arrangement of the contacts and any value of ϱ_1 and ϱ_2 (as in the case of the rectangular samples, ϱ_3 does not enter into the final results).

It will, of course, be advantageous to choose a simple geometrical arrangement. If the contacts are placed in such a way that they lie on two perpendicular diameters, a rather long but elementary calculation gives the simple result

$$R_1 = \frac{(\varrho_1 \varrho_2)^{1/2}}{\pi d} \ln \frac{2}{1 - k \,\mathrm{sn}\,(2u)}, \tag{2.19a}$$

$$R_2 = \frac{(\varrho_1 \varrho_2)^{1/2}}{\pi d} \ln \frac{2}{1 + k \,\mathrm{sn}\,(2u)}, \tag{2.19b}$$

where $u = 2K(k)\,\varphi/\pi$, φ being the angle between one of the principal axes of the resistivity and a line connecting two opposite contacts.

Figure 2.11, on a normalized scale, shows the dependence of R_1/R_2 on φ for various values of ϱ_1/ϱ_2. Using this figure it is possible to determine the directions of the principal axes by making measurements rotating the contacts (at angles $\pi/2$ apart) around the circumference of the sample. If the results of

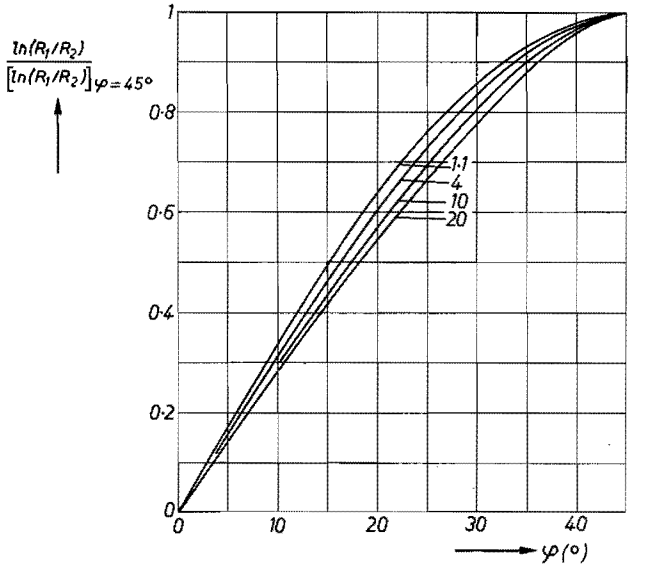

Fig. 2.11. Dependence of $\ln(R_1/R_2)$ on angle of rotation φ for anisotropic circular samples with $\varrho_1/\varrho_2 = 1{\cdot}1$, 4, 10 and 20, respectively.

such measurements deviate from the expected curve, the sample must be inhomogeneous.

The maximum value of R_1/R_2 occurs if $\varphi = \pi/4$, for which $\mathrm{sn}\,(2\,u) = 1$. In that case

$$(R_1)_{\max} = \frac{(\varrho_1\,\varrho_2)^{1/2}}{\pi\,d} \ln \frac{2}{1-k}, \tag{2.20a}$$

$$(R_2)_{\min} = \frac{(\varrho_1\,\varrho_2)^{1/2}}{\pi\,d} \ln \frac{2}{1+k}, \tag{2.20b}$$

$$(R_1/R_2)_{\max} = \frac{\ln\{\frac{1}{2}(1-k)\}}{\ln\{\frac{1}{2}(1+k)\}}; \tag{2.20c}$$

$(R_1/R_2)_{\max}$ is shown as a function of ϱ_1/ϱ_2 in fig. 2.12.

2.2.4. *Sensitivity of the method*

In fig. 2.12 the dependence of R_1/R_2 on ϱ_1/ϱ_2 for the proposed methods (curves 1 and 2) and the earlier ones [38]) (curves 3 and 4) are compared. The figure demonstrates the extreme sensitivity of the new methods. It should be remarked, however, that the accuracy of the determination of ϱ_1/ϱ_2 also depends on the accuracy achieved in obtaining the proper geometry.

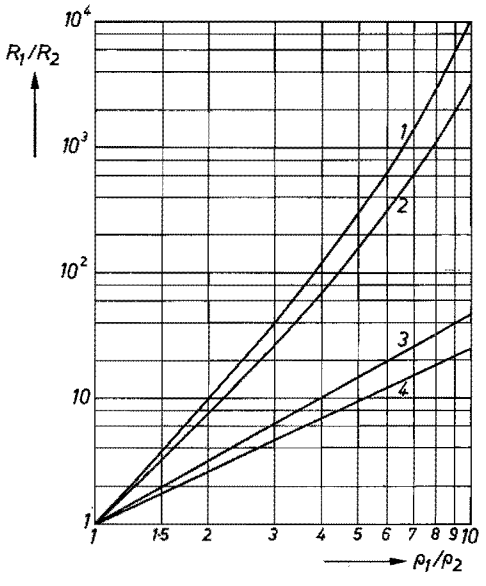

Fig. 2.12. Comparison of different methods of determining ϱ_1/ϱ_2 from R_1/R_2; (1): square sample with contacts at the corners, (2): circular sample with $\pi = \varphi/4$, (3) and (4): four probes in a square on a large thick and a large thin sample [38]).

The influence of deviations from the proper geometry and of the finite dimensions of the contacts have not been investigated. The fact that in the case of rectangular samples the R_1/R_2 vs ϱ_1/ϱ_2 curves for $a = 1$ and $a = 5/6$ lie close together (fig. 2.9) suggests that for these geometries the factors mentioned should not influence the results very drastically. The maximum at $\varphi = 45°$ in the curves of fig. 2.11 also ensures that for circular samples the 45° positions of the contacts with respect to the resistivity axes are not extremely critical.

2.2.5. *Applications*

The method discussed has been applied to rectangular and circular samples of MnTe (see fig. 3.10) and to rectangular samples of SiC [42]). As an illustration of the application to magnetoresistance measurements fig. 2.13 shows some results obtained on a circular ceramic sample of α-Fe_2O_3 doped with about 5.10^{-4} at.% Ti *). The figure relates to measurements performed in a field of 20 kG which was applied parallel to a line connecting two neighbouring contacts (see inset) or perpendicular to the plane of the sample. In the former case both the transverse effect $\Delta\varrho_\perp$ and the longitudinal effect $\Delta\varrho_{||}$ are obtained without changing the orientation of the sample (other, off-diagonal, magneto-

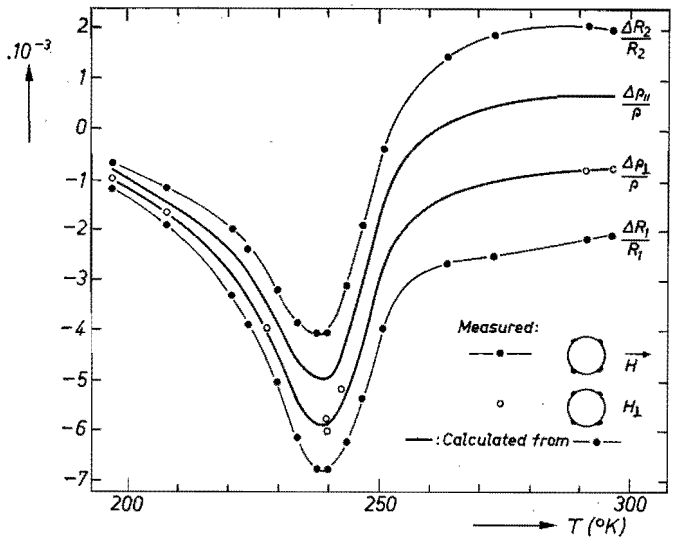

Fig. 2.13. Transverse and longitudinal magnetoresistance of a polycrystalline sample of α-Fe_2O_3 in a field of 20 kG at temperatures between 200 and 300 °K. The circular sample has four contacts 90° apart. Dots: $\Delta R_1/R_1$ and $\Delta R_2/R_2$ measured with the magnetic field parallel to the line connecting two neighbouring contacts. Thick curves: $\Delta\varrho_{||}/\varrho$ and $\Delta\varrho_\perp/\varrho$ calculated from the dots with eqs (2.25a) and (2.25b). Open circles: $\Delta R_1/R_1 = \Delta R_2/R_2 = \Delta\varrho_\perp/\varrho$ measured with the magnetic field perpendicular to the plane of the sample.

*) The sample, 8 mm in diameter and 1 mm thick, was kindly put at our disposal by Dr Bosman of our laboratory.

resistance effects should be absent in perfectly disordered polycrystalline material). Denoting the resistivity at zero field by ϱ_0 one may put

$$\varrho_1 = \varrho_0 + \Delta\varrho_\perp \equiv \varrho_0 (1 + \delta_\perp), \tag{2.21a}$$

$$\varrho_2 = \varrho_0 + \Delta\varrho_{||} \equiv \varrho_0 (1 + \delta_{||}). \tag{2.21b}$$

Since the resistance changes are small eq. (2.16) may be expanded in powers of k and of the δs. Retaining first terms only one has

$$q(k) \approx \frac{k^2}{16} = \frac{(\varrho_1^{1/2} - \varrho_2^{1/2})^4}{(\varrho_1 - \varrho_2)^2} \approx \frac{(\delta_\perp - \delta_{||})^2}{16}, \tag{2.22}$$

that is

$$k \approx \delta_\perp - \delta_{||}. \tag{2.23}$$

The direction of the magnetic field considered corresponds to $\varphi = \pi/4$, i.e. $\mathrm{sn}\,(2u) = 1$ and (2.19) reduces to

$$R_1 \approx \frac{(\varrho_1 \varrho_2)^{1/2}}{\pi d} (\ln 2 + k), \tag{2.24a}$$

$$R_2 \approx \frac{(\varrho_1 \varrho_2)^{1/2}}{\pi d} (\ln 2 - k). \tag{2.24b}$$

Using $(\varrho_1 \varrho_2)^{1/2} \approx \varrho_0 (1 + \frac{1}{2}\delta_\perp + \frac{1}{2}\delta_{||})$ and combining eqs (2.21), (2.23) and (2.24) one finds that the relative changes $\delta_\perp$ and $\delta_{||}$ of the resistivity follow from the observed relative changes $r_1 = \Delta R_1/R_1$ and $r_2 = \Delta R_2/R_2$ according to

$$\delta_\perp = r_1 - 0{\cdot}327\,(r_1 - r_2), \tag{2.25a}$$

$$\delta_{||} = r_2 + 0{\cdot}327\,(r_1 - r_2), \tag{2.25b}$$

where $0{\cdot}327 \equiv \frac{1}{2} - (\ln 2)/4$.

As fig. 2.13 shows, the values obtained for $\delta_\perp = \Delta\varrho_\perp/\varrho$ with these equations from the measurements with the magnetic field in the plane of the sample are in good agreement with the values directly observed with the magnetic field perpendicular to the plane of the sample.

(The physical significance of these measurements will not be discussed; it is only noted that the temperature of the maximum of $|\Delta\varrho/\varrho|$ roughly coincides with the transition point from antiferromagnetism to weak ferromagnetism.)

Haas et al. [43]) have used the method described above to establish the fact that the exceedingly large magnetoresistance of n-type $CdCr_2Se_4$ around 120 °K is essentially isotropic.

3. EXPERIMENTAL RESULTS AND DISCUSSION

In the first section of this chapter the main experimental data on the electrical properties of *p*-type MnTe between 77 and 350 °K are presented and their most prominent features are briefly reviewed. The sections which follow discuss in detail the Hall coefficient, the resistivity and Seebeck coefficient, and the mobility. Finally, measurements on the anisotropy of the resistivity are presented and some remarks are made on magnetoresistance effects.

3.1. Survey of main experimental results

3.1.1. *Measurements of Hall coefficient, resistivity and Seebeck coefficient*

Figures 3.1*a* and *b* show a number of resistivity $\varrho(T)$ and Hall-coefficient $R_H(T)$ curves obtained at temperatures between 77 and about 350 °K. The curves are representative of more numerous results of measurements on other samples performed with the conventional Van der Pauw method. The lower curves (1 to 3) refer to Na-doped MnTe, the higher ones (11 to 13) to Cr-doped MnTe. The other samples (4 to 10) were not intentionally doped. Symbols $\perp$ and // mark curves relating to samples whose plane was oriented perpendicular or parallel to the crystallographic *c*-axis. The difficulty in obtaining good electrical contacts to high-ohmic samples prohibited the determination of the Hall coefficient of the Cr-doped samples (11 to 13). Most Hall-effect measurements were carried out in a field of 5 kG applied perpendicularly to the plane of the samples. Only for samples 1 to 3 was the Hall effect measured in fields up to 23 kG at temperatures above 200 °K (see sec. 3.2).

Figure 3.2*a*, shown below, gives the Seebeck coefficient $S(T)$ of one of our Na-doped samples as well as of two similarly doped samples reported in the literature. The resistivity of these samples is given in fig. 3.2*b*. Other $S(T)$ and $\varrho(T)$ curves obtained by Miller [6]) are reproduced in fig. 3.3. The choice of scales for S and ϱ is motivated by eq. (3.8) given below. The measurements taken from literature were made on sintered samples and the compositions quoted probably refer to the starting material. Our crystalline sample contained 0·3 at.% Na (according to spectrochemical analysis) and was measured with the temperature gradient and the electrical current perpendicular to the *c*-axis.

3.1.2. *Theoretical formulae*

In the interpretation of the experimental data reported above, the possibility of mixed conduction by holes as well as electrons may be disregarded for a number of reasons, such as the wide energy gap of about 1·2 eV, the wide range of resistivities and Seebeck coefficients found for different samples, and the approximate temperature independence of the resistivity and Seebeck coefficient

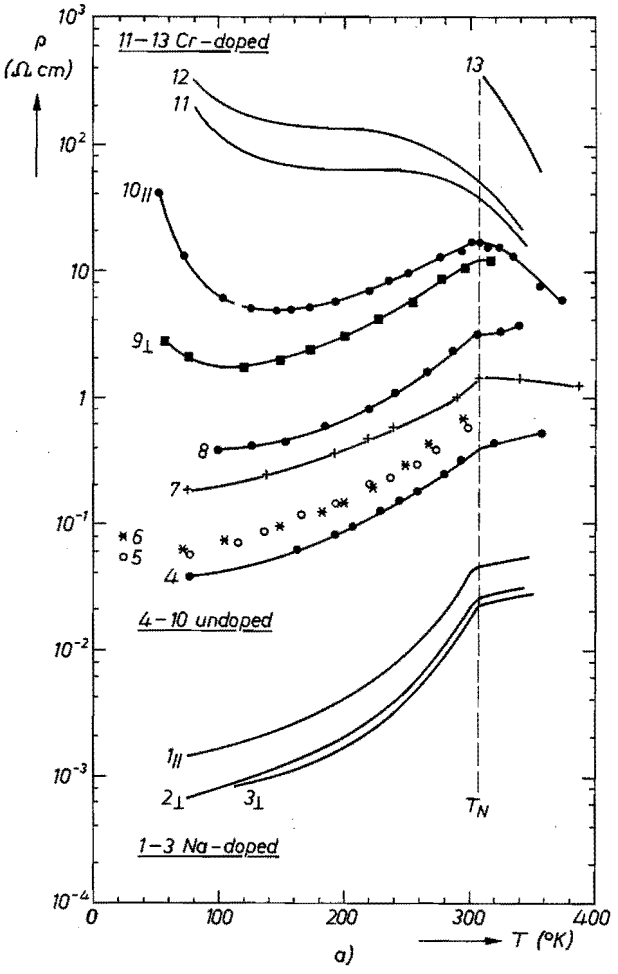

Fig. 3.1. (*a*) Resistivity ϱ and (*b*) (next page) Hall coefficient R_H of some MnTe samples as determined by the Van der Pauw method. Samples 1 to 3 contained 0·3 at. % Na, samples 11 to 13 were doped with Cr; the other samples were not intentionally doped but had received different heat treatments. Symbols $\perp$ and $\parallel$ label samples having their plane perpendicular and parallel to the *c*-axis, respectively. All Hall coefficients were positive except for samples 2 and 3 at temperatures above 305 °K.

at temperatures well above T_N (cf. fig. 3.3). The positive sign of S (as well as of $R_H^{//}$) indicate *p*-type conduction, i.e. conduction by holes.

The standard equations (see e.g. refs 44 and 45) for interpreting the Hall coefficient, resistivity and Seebeck coefficient for a semiconductor with hole concentration p, and mobility μ determined by a scattering mechanism leading to a mean free path of a hole with energy E proportional to E^r are *)

*) Usually the "scattering parameter" r has a value between 0 (e.g. for scattering by acoustical phonons) and 2 (for ionized-impurity scattering).

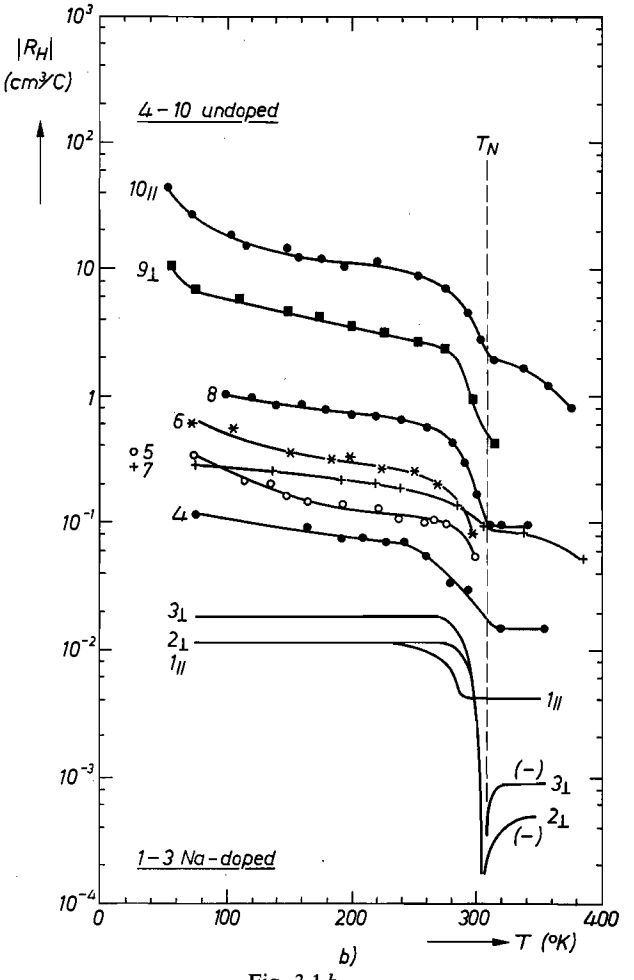

Fig. 3.1 *b*.

$$R_H = \gamma_H / p\, e, \tag{3.1}$$

$$\varrho = 1/p\, e\, \mu, \tag{3.2}$$

$$S_e = (k/e)\left\{(r+2)\frac{F_{r+1}(\eta)}{F_r(\eta)} - \eta\right\} \qquad \text{with } \eta = E_F/kT, \tag{3.3}$$

$$\approx (k/e)\,\{r + 2 + \ln(N_v/p)\} \qquad \text{for } \eta \ll 0, \tag{3.3a}$$

$$\approx (k/e)\frac{\pi^2}{3}\left(\frac{4}{3\pi^{1/2}}\right)^{2/3}(r+1)\,(N_v/p)^{2/3} \qquad \text{for } \eta \gg 0. \tag{3.3b}$$

The Hall coefficient is a third-rank tensor [46]). Its symmetry properties allow it to be reduced to a second-rank pseudotensor, whose diagonal elements refer to measurements made with the magnetic field applied perpendicular to the

plane of the sample. For these diagonal elements the "Hall-coefficient factor" γ_H usually has a value between 1 and 2, depending on the dominant scattering mechanism.

k is Boltzmann's constant, N_v is the effective density of states of the valence band,

$$N_v = 2\left(\frac{2\pi m_d^* k T}{h^2}\right)^{3/2} = 2{\cdot}51.10^{19}\left(\frac{m_d^*}{m_0}\frac{T}{300}\right)^{3/2} \text{cm}^{-3}, \tag{3.4}$$

m_d^* being the density-of-states effective mass of the valence band, $(m_d^*)^3 = \nu(m_i m_j m_k)$, where ν is the number of equivalent valence-band maxima for each of which the diagonalized effective-mass tensor has components m_i, m_j, m_k. For a single valence-band maximum ($\nu = 1$) we shall write m_d instead of m_d^*. Unspecified components of the diagonalized effective-mass tensor will be denoted by m, the free-electron mass by m_0. For discussions involving the Seebeck coefficient it may be advantageous to introduce a "Seebeck effective density of states" N_S and a "Seebeck effective mass" m_S according to

$$N_S \equiv e^r N_v \approx (r+1)^{3/2} N_v, \tag{3.5a}$$

$$m_S \equiv e^{2r/3} m_d^* \approx (r+1) m_d^*, \tag{3.5b}$$

where the $\approx$ sign obtains for all values of r of common interest, $0 \leqslant r \leqslant 2$ *).

$F_n(\eta)$ represents a Fermi integral of order n as a function of the reduced Fermi energy $\eta = E_F/kT$ (see e.g. ref. 45),

$$F_n(\eta) = \frac{1}{\Gamma(n+1)}\int_0^\infty \frac{\varepsilon^n \, d\varepsilon}{1+\exp(\varepsilon-\eta)}, \tag{3.6}$$

$$\approx \exp\eta \qquad \text{for } \eta \ll 0, \tag{3.6a}$$

$$\approx \{\eta^{n+1}/\Gamma(n+2)\}\left\{1+\frac{\pi^2}{6}(n+1)\,n\,\eta^{-2}+\ldots\right\} \quad \text{for } \eta \gg 0. \tag{3.6b}$$

The top of the valence band is taken as the zero point of the energy scale and energies are counted positive (negative) when below (above) the top of the valence band.

For the present discussions E_F or η may be considered as a measure for the hole concentration,

*) The usefulness of such substitutions is demonstrated e.g. by the method of estimating the maximum thermoelectric figure of merit of a semiconductor which we described in ref. 47.

$$p = N_v F_{1/2}(\eta) \tag{3.7}$$

$$\approx N_v \exp \eta \qquad \text{for } \eta \ll 0, \tag{3.7a}$$

$$\approx \frac{4}{3\pi^{1/2}} N_v \eta^{3/2} = (2 m_d^* E_F)^{3/2}/3\pi^2 \hbar^3 \quad \text{for } \eta \gg 0. \tag{3.7b}$$

Material for which $p \gg N_v$, i.e. $\eta \gg 0$ is called degenerate. For non-degenerate material, $p \ll N_v$ and $\eta \ll 0$. For $r = 0$ eq. (3.3a) is valid within 10% of S_e if $S > 160$ μV/deg or $p < 1{\cdot}4\, N_v$, and eq. (3.3b) if $S_e < 130$ μV/deg or $p > 2{\cdot}1\, N_v$.

It is noted that eqs (3.3) refer to the "purely electronic" contribution S_e to the Seebeck effect arising from the thermodiffusion of charge carriers in a temperature gradient. Other contributions to the Seebeck coefficient may arise from the phonon- or magnon-drag effects, which originate from the dragging of the charge carriers by the thermodiffusion current of phonons or magnons, respectively. These effects are discussed in chapter 5.

Strictly speaking, for a given scattering mechanism the Hall-coefficient factor γ_H and the mobility μ also depend on the degree of degeneracy (cf. eq. (4.12) given below). This dependence is neglected in the present chapter.

3.1.3. *Preliminary discussion*

A remarkable feature of the measurements presented is the change of sign of the Hall coefficient which for some samples (e.g. samples 2 and 3 in fig. 3.1b) occur near 300 °K. Normally such a change of sign would indicate the onset of mixed conduction, but as already remarked there are many arguments showing that this interpretation is unlikely. It is noted that this change of sign only occurs in samples cut perpendicular to the c-axis. In samples cut parallel to the c-axis (e.g. like samples 1 and 10) the Hall coefficient does decrease between 240 °K and about 300 °K, but not to the extent that it changes sign. This different temperature dependence of the Hall coefficient in samples of different orientation shows that R_H is highly anisotropic at temperatures near and above T_N. Since normal transport theory cannot account for this unusual behaviour some additional measurements have been carried out. These are reported below in sec. 3.2. As discussed in that section it appears that in the temperature region indicated, $T > 240$ °K, there is an "extraordinary" or "anomalous" contribution to the Hall coefficient which is related to the antiferromagnetic properties of MnTe. This contribution seems to be absent below 240 °K and at these temperatures the hole concentration can be estimated in the normal way from the Hall coefficient. According to fig. 3.1*b* the hole concentration of the Na-doped and most undoped samples (samples 1 to 8) is thus nearly independent of temperature.

Apart from the anomaly in the Hall coefficient, other interesting features of

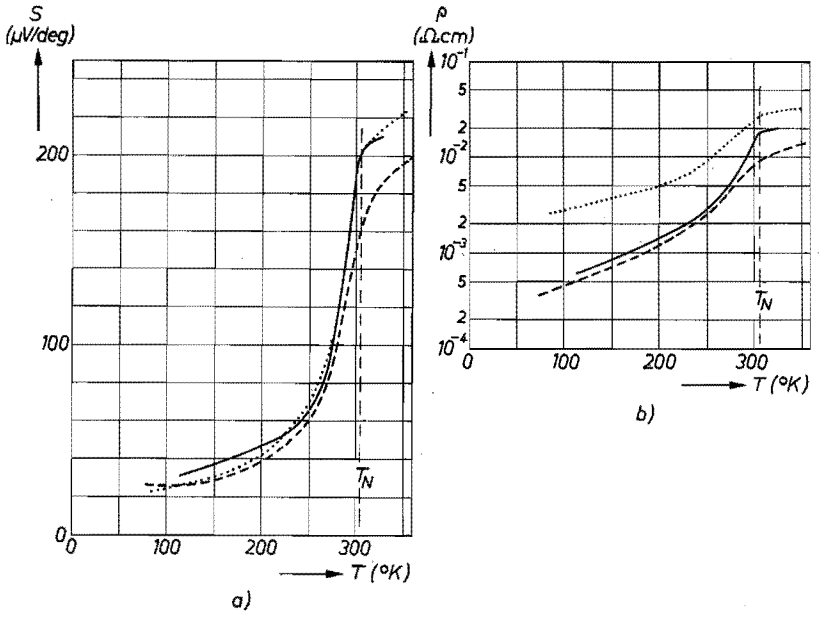

Fig. 3.2. (*a*) The Seebeck coefficient of Na-doped samples;
—— our measurements (cf. fig. 2.7), - - - - measurements by Miller [6]) on $Na_{.01}Mn_{.99}Te$, ... measurements by Deviatkova et al. [8]) on $Na_{.01}Mn_{.99}Te$.
(*b*) The resistivity of these samples.

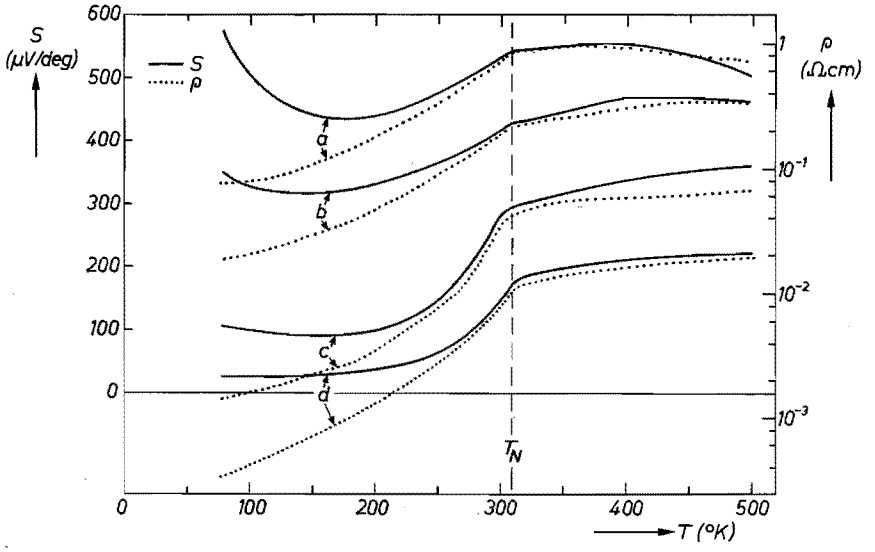

Fig. 3.3. Seebeck coefficient and resistivity of four samples of different composition reported by Miller [6]). The S and ϱ scales have been chosen such that 198 μV/°K in S corresponds to one decade in ϱ (cf. discussion to eq. (3.8)). The ϱ scale has been shifted vertically in such a way that the ϱ curves nearly coincide with the S curves at 320 °K.

the data are the strong increase in resistivity and in the Seebeck coefficient at temperatures near T_N, and the change of slope of $\varrho(T)$ and $S(T)$ at T_N; this behaviour is shown most clearly by the low-ohmic samples (1 to 3 in fig. 3.1*a*; c and d in fig. 3.3), but is also apparent in more high-ohmic samples (4 to 8 in fig. 3.1*a*; a and b in fig. 3.3).

Because of its anomalous behaviour the Hall coefficient cannot be used to determine the hole concentration at temperatures above 240 °K and in the absence of other data the behaviour of the resistivity and Seebeck coefficient can be interpreted in different ways.

In explaining the temperature dependence of the resistivity and Seebeck coefficient near T_N in terms of broad-band conduction, two basically different assumptions can be made. First (case (1)), it may be supposed that no appreciable change occurs in the structure and shape of the valence band near T_N. In that case there is no reason why the acceptor-level depth should change, and the hole concentration in undoped and Na-doped samples will be essentially independent of temperature above 240 °K, as it is at temperatures below 240 °K. On this assumption the temperature dependence of the resistivity is mainly determined by the mobility, and the Seebeck coefficient can only be understood if there is some additional contribution at temperatures above 240 °K. Because of the similarity between the $\varrho(T)$ curves for MnTe and ferromagnetic metals it would seem likely that the mobility originates from spin-disorder scattering. As shown previously [13,14]) the additional contribution to the Seebeck coefficient may be ascribed to magnon drag.

It may also be supposed (case (2)) that near T_N the shape of the valence band depends in some way on the magnitude of the sublattice magnetization (cf. sec. 4.3.2). In this case one has to reckon with the possibility that both the effective mass and the acceptor-level depth may change markedly near T_N. A change in effective mass affects the theoretical mobility as well as the electronic contribution to the Seebeck coefficient. A variation in the acceptor-level depth may affect the hole concentration. The observed $S(T)$ and $\varrho(T)$ curves suggest that just below T_N with rising temperature the hole concentration decreases (i.e. the acceptor-level depth increases) and/or the effective mass increases.

Elimination of p from eqs (3.2) and (3.3a) gives for non-degenerate samples

$$S = (k/e)\,\{r + 2 + \ln(N_v\,\mu\,e\,\varrho)\} = 198 \log_{10}(\varrho/\varrho_0)\ \mu\text{V/deg}, \qquad (3.8)$$

with $\varrho_0^{-1} = e^{r+2}\,N_v\,\mu\,e$.

According to fig. 3.3 this relation between resistivity and Seebeck coefficient is reasonably well satisfied at temperatures above 240 °K with the same temperature-independent value of ϱ_0 for all samples. This means that in this temperature region the same temperature dependence of the hole concentration required to explain the Seebeck effect would also explain the resistivity if $N_v\,\mu$ is independent of the temperature. This condition is satisfied for acoustical-phonon

scattering and, according to the theory presented in sec. 4.1.2, also roughly satisfied for spin-disorder scattering in antiferromagnetic semiconductors. For these scattering mechanisms $N_v \mu \propto m^{-1}$, so that the data of fig. 3.3 above 240 °K cannot be accounted for solely by a change of effective mass. A more detailed discussion of the resistivity and Seebeck coefficient is given in sec. 3.3.

At temperatures below 240 °K eq. (3.8) is not obeyed by the data of fig. 3.3. For the low-ohmic samples this is clearly due to the fact that by being degenerate ($S < 160$ μV/deg, see comment to eq. (3.7)) eq. (3.3a) no longer applies and eq. (3.3b) should be used instead. It is noted, however, that at low temperatures, according to their Hall coefficient, the low-ohmic samples have a temperature-independent hole concentration so that S should be proportional to T. Figure 3.2*a* shows that this is not quite the case. This behaviour, as well as the low-temperature variation in the Seebeck coefficient of more high-ohmic samples, may be attributed to magnon drag (see chapter 5).

3.2. The Hall coefficient

3.2.1. *Further measurements on the anisotropy of* R_H

The remarkable dependence of the Hall coefficient on the orientation of the sample with respect to the crystallographic *c*-axis has been investigated more closely on five samples cut from an Na-doped ingot. Measured values of $R_H\perp$ (for samples cut perpendicular to the *c*-axis) and of $R_H//$ (for samples cut parallel to the *c*-axis) are shown in fig. 3.4.

Below 240 °K the Hall coefficient of these samples was independent of tem-

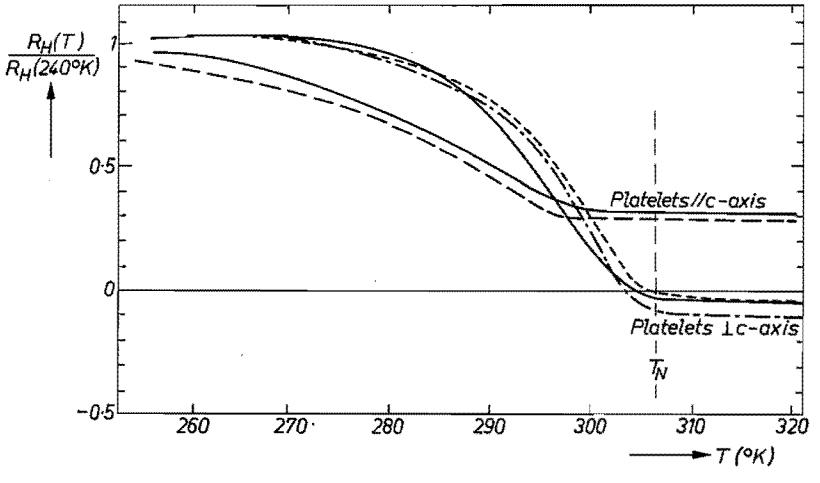

Fig. 3.4. Temperature dependence of the Hall coefficient R_H of Na-doped samples cut perpendicular or parallel to the *c*-axis.

perature and had values between 0·1 and 0·2 cm^3/C. There is no correlation between these values and the orientation of the samples with respect to the c-axis, which indicates that R_H is isotropic below 240 °K. Apparently the ingot from which the samples were taken was not quite homogeneous.

Because of the unusual anisotropy of the Hall coefficient above 240 °K some additional measurements were made. Between 200 an 350 °K it was verified that for both orientations the Hall effect was proportional to the magnetic field up to 23 kG (for the low negative values of $R_H^{\perp}$ the accuracy of this check was, however, poor).

By shaping a sample in the form of a bar with square cross-section and with one of the short edges parallel to the c-axis it was possible to obtain both $R_H^{\perp}$ and $R_H^{//}$ for one and the same sample. Although the unfavourable geometry of this sample did not allow very accurate measurements, the results were in agreement with those represented in fig. 3.4.

Since above 300 °K the Hall coefficient is relatively small and the Seebeck coefficient relatively large, a considerable Ettingshausen contribution to the measured Hall voltage might be possible. If the Ettingshausen effect [44]) creates a temperature difference ΔT across the Hall probes, and S and S_a are the Seebeck coefficients of the sample and the measuring leads, respectively, the measured Hall voltage becomes

$$V_H = V_H^{\circ} + (S - S_a)\,\Delta T, \tag{3.9}$$

V_H° being the true Hall voltage. In order to detect the possible presence of such an effect we have measured the Hall effect in some samples twice, using voltage probes consisting of thin copper and thin constantan wires, respectively. Care was taken that the probes made good thermal contact with the sample. In the temperature region of interest $60 < S < 210$ μV/deg, while $S_{Cu} \approx 2$ μV/deg and $S_{constantan} \approx 40$ μV/deg. For the two measurements, therefore, the last term differs by at least 20%. Since, nevertheless, no difference was found in V_H, the Ettingshausen contribution to the Hall effect can only be small.

Although we have studied the anisotropy of R_H only for Na-doped samples in some detail, the anisotropy is also apparent from the temperature dependence of R_H of samples 9 and 10. The decrease in R_H for sample 9, cut perpendicular to the c-axis, sets in at a higher temperature than for sample 10 whose plane was parallel to the c-axis. For the latter sample, R_H could still be measured at temperatures above 300 °K, which was not so for the former sample. The anisotropy in undoped samples has also been observed by Janssen [48]).

3.2.2. *The anomalous Hall effect*

For the interpretation of the Hall effect a clue is provided by the fact that in our Na-doped samples the Na concentration has been found from spectrochemical analysis to be about 6.10^{19} Na atoms per cm^3. The low-temperature

Hall coefficient of these samples is isotropic and has values of 0·1 to 0·2 cm³/C, which corresponds to a hole concentration of $p = 1/R_H e = 6$ to 3.10^{19} cm³. Since it is not unreasonable to assume that each Na atom gives rise to one hole by being incorporated as an Na^+ ion on the site of an Mn^{2+} ion, it is concluded that between 77 and 240 °K the Hall coefficient may be interpreted in the usual way as $R_H \approx (p\,e)^{-1}$.

Judging from their resistivity and Seebeck coefficient it seems very unlikely that in the Na-doped samples the hole concentration increases between 240 °K and T_N. Therefore both the decrease of $R_H \perp$ and of $R_H /\!/$ above 240 °K is anomalous.

Maranzana [16]) has attributed this anomaly to the interaction between the angular momentum of a charge carrier with respect to a magnetic ion and the spin S of this ion (denoting the ionic d-electrons by d, and the carrier by s, this may be called a d-spin, s-orbit interaction). For antiferromagnets this interaction is shown to lead to a Hall coefficient of the form

$$R_H = R_H^\circ \{1 + A\,B(T)\}, \tag{3.10}$$

R_H° being the normal Hall coefficient, roughly equal to $(p\,e)^{-1}$, as in eq. (3.1). The anomalous contribution to the Hall coefficient is $A\,B(T)\,R_H^\circ$. Here A is a dimensionless constant depending on the strength of the d-spin, s-orbit interaction, and $B(T)$ a function of temperature shown in fig. 3.5. In calculating the effect Maranzana only takes account of "spin-flip" scattering processes (cf. end of sec. 4.1.1) which he deals with in the approximation given by eq.

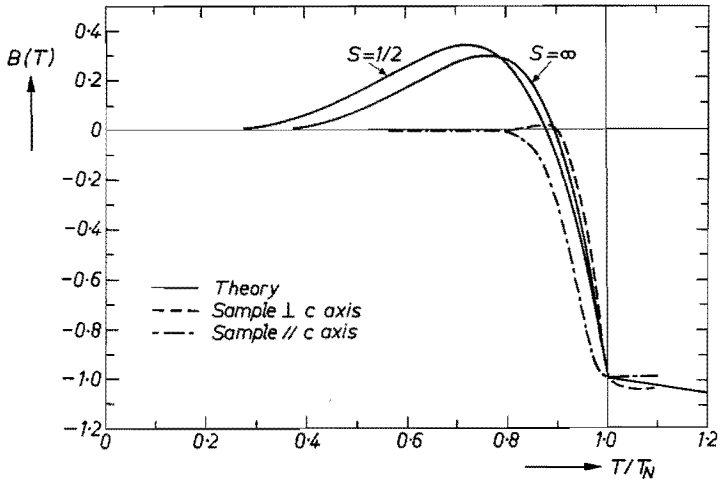

Fig. 3.5. The function $B(T)$ describing the anomalous contribution to the Hall effect in antiferromagnets according to Maranzana [16]) (see eq. (3.10)). The theoretical curves were calculated with $S = \frac{1}{2}$ and with $S = \infty$ (i.e. using the Langevin function instead of a Brillouin function). The dashed curves are calculated from the experimental curves of fig. 3.4.

(4.16). For temperatures below T_N Maranzana has only considered the case that the external magnetic field is applied in the direction of the sublattice magnetization.

Our measurements on MnTe do not satisfy the latter condition because the small magnetic anisotropy in the *c*-plane causes the sublattice magnetization to orient itself mainly perpendicularly to an applied magnetic field [31]). It seems, however, reasonable to suppose that in this case a formula similar to eq. (3.10) applies, with perhaps a slightly different value of A and a slightly different function $B(T)$. Above T_N the distinction between the cases of the field perpendicular or parallel to the sublattice magnetization does not exist, so that the functions $B(T)$ for the two cases are identical for $T \geqslant T_N$.

In fig. 3.5 we give the quantity

$$\{R_H(T) - R_H(77\ ^\circ\mathrm{K})\}/\{R_H(77\ ^\circ\mathrm{K}) - R_H(T_N)\}$$

as calculated from the data of fig. 3.4 for both orientations of the Na-doped samples with respect to the *c*-axis. Supposing R_H° to be independent of T this quantity is identical with

$$\{B(T) - B(77\ ^\circ\mathrm{K})\}/\{1 + B(77\ ^\circ\mathrm{K})\}$$

(using $B(T_N) = -1$). It is seen that the experimental temperature dependence of $B(T)$ calculated in this way roughly agrees with the theoretical temperature dependence of this function for the case considered by Maranzana, in particular with regard to its behaviour above 0·8 T_N. The value of $A\,B(T)$ for temperatures below 240 °K cannot be derived from our measurements because of the inhomogeneity of the ingot from which the Na-doped samples were taken. Since it is found that $R_H \approx (e[\mathrm{Na}])^{-1}$ for $T < 240$ °K, it seems nevertheless unlikely that this quantity differs much from zero at these temperatures.

Inserting appropriate values for the quantities determining the constant A, one finds a much smaller value than the measurements require. No solution has yet been found for this discrepancy (which, as Maranzana remarks, also exists for the anomalous Hall effect in ferromagnetic metals, both in his own theory and, for instance, in the theory proposed by Kondo [49])). We also note that the theory does not account for the anisotropy of R_H in the paramagnetic region. This anisotropy, occurring at temperatures where both the resistivity and susceptibility are isotropic, might perhaps provide a clue to the solution of the theoretical problem.

3.3. Resistivity and Seebeck coefficient

We again consider our Na-doped samples, for which it was shown that the hole concentration below 240 °K is of the order of 6.10^{19} cm^{-3}. The Seebeck coefficient S of one of these samples is given in fig. 3.2*a*. At low temperatures S is very small, in fact so small that the sample must be considered degenerate

(cf. comment to eq. (3.7)). For degenerate semiconductors eqs (3.3b) and (3.4) require that the Seebeck coefficient for a constant carrier concentration is proportional to the absolute temperature. This is only approximately the case for the $S(T)$ curves of fig. 3.2*a* below about 200 °K. With $r = 0$ and $p = 6.10^{19}$ cm^{-3} the highest possible value of the density-of-states effective mass consistent with our curve is $m_d^* = 0{\cdot}53\, m_0$. This is a reasonable value. In fact, from optical measurements Zanmarchi and Haas [21]) find $m_\perp = 0{\cdot}4\, m_0$ and $m_{||} = 1{\cdot}6\, m_0$, or $(m_\perp^2\, m_{||})^{1/3} = 0{\cdot}6\, m_0$. Comparison of these values suggests that the valence band of MnTe does not have different equivalent maxima.

As mentioned in sec. 3.1.3 two different causes may be envisaged in order to explain the $\varrho(T)$ and $S(T)$ curves at temperatures near T_N. In case (1) it is assumed that spin-disorder scattering and magnon drag are the main effects giving rise to the observed temperature dependence of the resistivity and Seebeck coefficient. The possibility of maintaining this relatively simple explanation constitutes the main subject of chapters 4 and 5. In case (2) the temperature dependence of resistivity and Seebeck coefficient near T_N is attributed to changes in acceptor-level depth and/or effective mass. We now calculate the magnitude of these effects as if each acted separately.

Case (2a). The explanation of the Seebeck coefficient and resistivity in terms of a change in hole concentration p requires that p decreases between 240 °K and T_N. This would imply that for some reason or another the energy level E_A of the acceptors rises with increasing temperature. Supposing that the donor concentration is small compared to the Na-acceptor concentration N_A and to the hole concentration, one has [45])

$$p = N_v F_{1/2}(\eta) = \frac{N_A}{1 + \frac{1}{2}\exp(E_A/kT + \eta)} \tag{3.11}$$

(E_A is counted positive when above the valence-band top). The pre-exponential factor $\frac{1}{2}$ in eq. (3.11) is the acceptor-level spin degeneracy which has the value indicated because the Na^+ ion, corresponding to the situation that it has accepted an electron from the valence band, has spin-paired electrons only. For our Na-doped samples $N_A \approx 6.10^{19}$ cm^{-3}. From the density-of-states effective mass $m_d^* = 0{\cdot}53\, m_0$ it follows that $N_v = 1.10^{19}\,(T/300)^{3/2}$ cm^{-3}. With these values it is possible to calculate E_A using the value of η which follows from the Seebeck coefficient (cf. eq. (3.3)). The result for an assumed value $r = 0$ is shown in fig. 3.6 *) (for temperatures above 320 °K the Seebeck coefficient of

*) With $p = 6.10^{19}$ cm^{-3} and $m_d^* = 0{\cdot}53\, m_0$ the Fermi level for complete degeneracy is $E_F = \frac{1}{2}\hbar^2\,(3\pi^2 p)^{3/2}/m_d = 0{\cdot}1$ eV below the top of the valence band. In order that all Na acceptors have trapped an electron their energy level must be well below E_F, which explains the negative values of E_A at temperatures below 285 °K. Negative values of E_A are not improbable if the Na levels are derived from Mn 3*d*-states supposed to lie well below the top of the Te 5*p*-valence band.

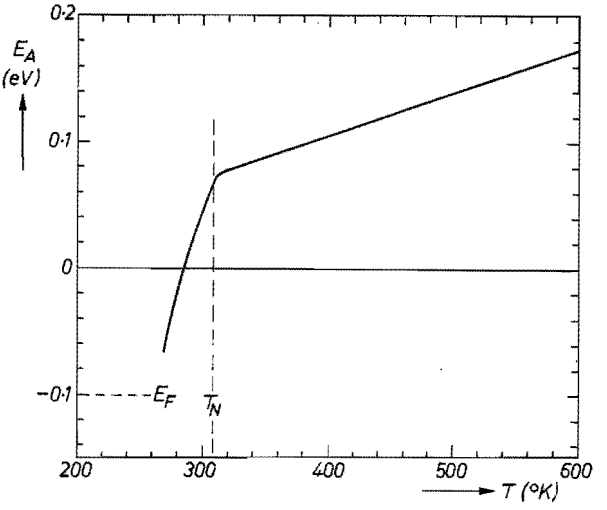

Fig. 3.6. The Na acceptor-level depth as a function of temperature if the variation of the Seebeck coefficient with temperature is due to a change in hole concentration. The curve is derived from our experimental curve of the Seebeck coefficient given in fig. 3.2*a* using eqs (3.11) and (3.3) with $N_A = 6.10^{19}$ cm^{-3}, $N_D = 1.10^{19}$ $(T/300)^{3/2}$ cm^{-3} and $r = 0$.

the sample considered was extrapolated using the temperature dependence of the Seebeck coefficient of Miller's samples c and d, fig. 3.3). The corresponding decrease in hole concentration is from 6.10^{19} cm^{-3} for $T < 240$ °K to $0{\cdot}8.10^{19}$ cm^{-3} for $T_N < T < 600$ °K.

Case (2b). As remarked in sec. 3.1.3, the temperature dependence of the resistivity and Seebeck coefficient near T_N cannot be explained in terms of a temperature dependence of the effective mass alone. However, the theoretical mobility may contain other temperature-dependent factors (cf. sec. 4.3.2) and also the scattering parameter might change near T_N. Figure 3.7 shows the effective mass as calculated from our experimental curve for an Na-doped sample, fig. 3.2*a*, using eq. (3.3) and assuming $p = 6.10^{19}$ cm^{-3} and $r = 0$. For other values of the scattering parameter r the curve given is nearly identical with the "Seebeck effective mass" defined in eq. (3.5b).

In order to be able to decide which of the interpretations is correct, further experimental information is necessary. Such information might be obtained from optical measurements, were it not that these too admit of different interpretations. In Na-doped MnTe the reflection minimum due to free-carrier resonance shifts towards longer wavelengths when the temperature is raised [19–21]). This shift may be caused by a (second-order) magnon-drag effect, as suggested by Zanmarchi and Haas [21]), by a decrease in hole concentration, as suggested by Callen [50]), as well as by an increase in effective mass, as suggested by Zanmarchi [19]). These three interpretations correspond precisely to the cases (1), (2a) and (2b), respectively.

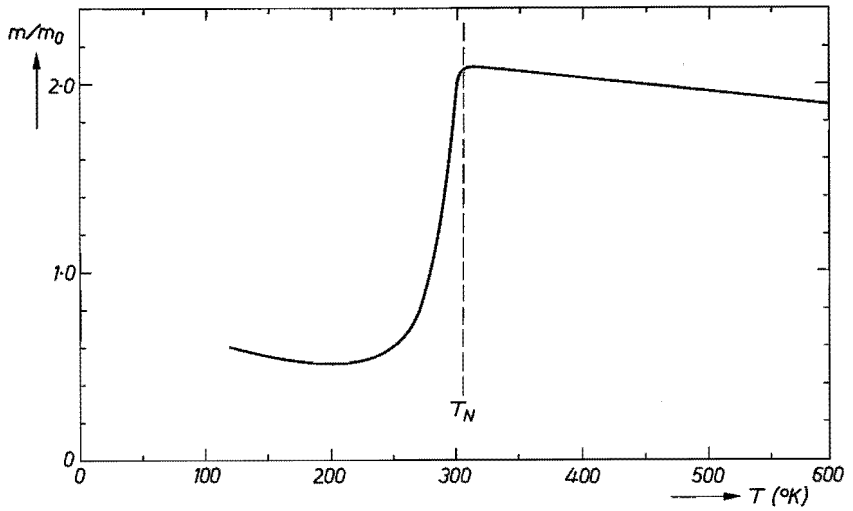

Fig. 3.7. The effective mass as a function of temperature if the variation of the Seebeck coefficient with temperature is due to a change in effective mass. The curve is calculated from our experimental curve of the Seebeck coefficient given in fig. 3.2*a* using eq. (3.3) with $p = 6.10^{19}$ cm^{-3} and $r = 0$.

In the following we shall base the interpretation of the experimental data on the most simple assumptions of case (1). Comparison with the theoretical predictions for the mobility and magnon drag will then decide whether or not these assumptions can be maintained.

3.4. The "experimental" mobility

In the preceding sections only Na-doped samples were considered. For the undoped samples the Hall coefficient cannot be compared to a chemically determined impurity concentration or deviation from stoichiometry. It seems reasonable, however, that for these samples too the Hall coefficient may be interpreted in the normal way below 240 °K, but not at higher temperatures (where for several samples the Hall curves show the same orientation-dependent decrease as the Na-doped samples).

Assuming that the acceptor-level depth does not change with temperature between 240 °K and T_N, the hole concentration will roughly be equal to $(e\,R_H^*)^{-1}$, where below 240 °K R_H^* is the measured Hall coefficient and above 240 °K it is an extrapolation of the low-temperature $R_H(T)$ curve. The log $R_H(T)$ curve of several undoped samples shows only a weak dependence on T below 240 °K whose extrapolation should not introduce serious errors. The quantity $\mu^* = R_H^*/\varrho \approx (p\,e\,\varrho)^{-1}$ will be called the "experimental" mobility (or, where no confusion is possible, simply: mobility). It is shown for some samples in fig. 3.8.

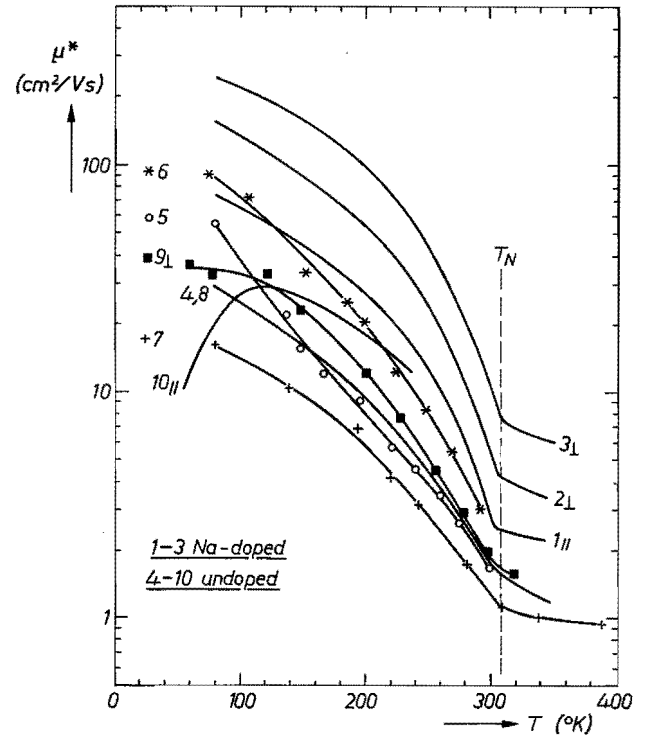

Fig. 3.8. The "experimental" mobility $\mu^*(T)$ for some samples. Below 240 °K $\mu^*(T)$ is equal to the Hall mobility, at higher temperatures it is calculated using extrapolated values of the Hall coefficient.

At temperatures below 240 °K the experimental mobility is equal to the (drift) mobility $\mu \equiv (p\, e\, \varrho)^{-1}$ if $\gamma_H^{-1}\,\{1 + A\,B(T)\}$ has the value 1 (cf. eqs (3.1), (3.2) and (3.10)). Above 240 °K the equality of μ^* and μ further requires that the hole concentration does not change in an anomalous way.

Because μ^* is small for $T \gtrsim T_N$ one would have expected at these temperatures to find in fig. 3.8 a curve representing the lattice mobility of the holes in MnTe, independent of the purity of the samples. At lower temperatures the mobility is larger and impure samples could show smaller mobilities than pure ones due to impurity scattering, while an additional difference should occur for differently oriented samples because of the anisotropy of the resistivity below T_N (see next section, fig. 3.10). Since the measurements were performed according to the Van der Pauw method and $1 \leqslant \varrho_{\parallel}/\varrho_{\perp} < 3$, this anisotropy can give at the most a difference of a factor $3^{1/2} = 1{\cdot}7$ at low temperatures. Although the spread in the experimental mobilities is indeed somewhat larger at low temperatures than at high temperatures, it is still considerable for $T \gtrsim T_N$. Furthermore the highest mobilities occur in the most heavily doped samples, or in any case in the samples with the smallest resistivities. This is true both at high and at low

temperatures. With respect to this behaviour of the experimental mobility the following remarks may be made.

The difficulty of preparing good single crystals of MnTe due to the phase transition at 1312 °K has been mentioned already in sec. 1.2. It has been remarked also that the Na-doped samples though originating from the same ingot showed different Hall coefficients at low temperatures, while they also show different resistivities, even near T_N where the resistivity is isotropic. The three undoped samples used to determine the resistivity anisotropy (see fig. 3.10 below) were taken from an ingot which was considered to be of the best available quality, and nevertheless show significant differences in the values of $\varrho_\perp/\varrho_{||}$ obtained below 230 °K. These observations may imply that the spread of the experimental mobilities is due to crystal imperfections and inhomogeneities giving rise to erroneous measurements of the resistivity and/or the Hall coefficient. That the highest mobilities are found in the Na-doped samples might be caused by crystal imperfections and inhomogeneities influencing the measurements less in material with low resistivity than in material with higher resistivity. It may also be possible that Na promotes the crystal growth of the NiAs phase at the phase transition *).

In drawing final conclusions from the comparison of theory and experimental data, a point of considerable interest is the different change of slope at T_N which the experimental mobility shows for undoped and Na-doped samples. This difference is completely due to a different temperature dependence of the resistivity in the two types of samples near T_N and is clearly visible in figs 3.1*a* and 3.3 (see also fig. 4.4). Because figs 3.1*a* and 3.3 refer to crystalline and sintered samples, respectively, it seems unlikely that this difference is due to sample quality. From fig. 3.3 it is seen that a similar difference obtains for the Seebeck coefficient.

3.5. Some additional data

3.5.1. *Anisotropy of the resistivity*

Resistivity measurements on the five Na-doped samples used to investigate the anomalous Hall effect also revealed a temperature-dependent anisotropy of the resistivity. This is shown in fig. 3.9, which gives their resistivities $\varrho_\perp$ and $(\varrho_{||}\,\varrho_\perp)^{1/2}$ as determined by the usual Van der Pauw method. The specialized Van der Pauw method described in sec. 2.2 was applied to one circular and two rectangular (undoped) samples. The results are shown in fig. 3.10. Although these measurements themselves are rather accurate (the ratio $\varrho_{||}/\varrho_\perp$ of 0·45 at 100 °K for the circular sample corresponds to $R_1/R_2 = 10$) inhomogeneities

*) The reverse effect is, however, known to occur in MnSe. In this compound the transition from the high-temperature NaCl phase to the low-temperature NiAs phase is inhibited by the incorporation of 2% Li [51]).

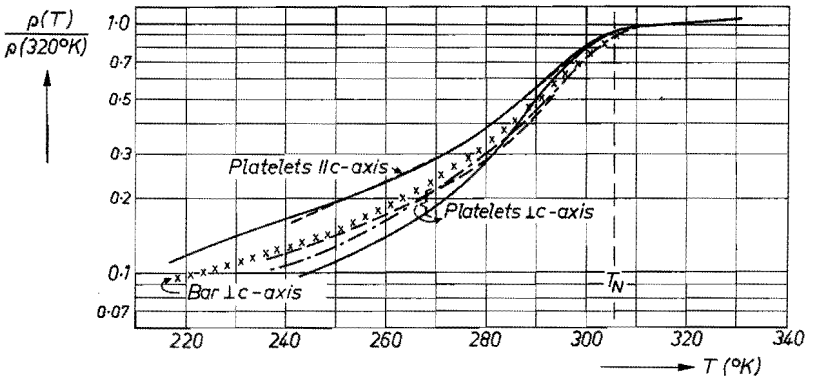

Fig. 3.9. Temperature dependence of the resistivity of the Na-doped samples of fig. 3.4. The lower curves refer to $\varrho_\perp$ as found from a bar-shaped sample, or from platelets cut perpendicular to the c-axis using the Van der Pauw method. The two upper curves refer to $(\varrho_\perp\ \varrho_{||})^{1/2}$ as obtained with the Van der Pauw method from platelets cut parallel to the c-axis.

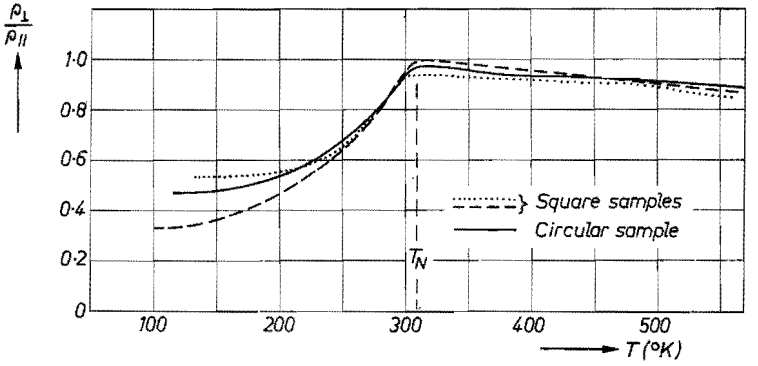

Fig. 3.10. Anisotropy of the resistivity, $\varrho_\perp/\varrho_{||}$, as determined in three samples using the method described in sec. 2.2.

or small cracks could, in principle, appreciably influence the results. The nearly identical curves found for the three samples at temperatures above 230 °K suggest that such influences manifest themselves only below this temperature. The curves of fig. 3.9 are consistent with those of fig. 3.10, both figures indicating that $\varrho_\perp$ depends more strongly on temperature than $\varrho_{||}$.

3.5.2. *Magnetoresistance*

During the measurements of the Hall effect it appeared that in many cases the voltage $V_0 + \Delta V(H)$ across the Hall probes (V_0 is the misalignment voltage) was not a symmetric function of the applied field H, i.e. $\Delta V(H) \neq -\Delta V(-H)$. The voltage V_H corresponding to the Hall effect is an odd function of H and was obtained from the difference

$$V_H = \tfrac{1}{2}\{\Delta V(H) - \Delta V(-H)\}. \tag{3.12}$$

As mentioned already, in the samples considered here V_H was found to be proportional to H. The sum of $\Delta V(H)$ and $\Delta V(-H)$ corresponds to a magnetoresistance effect which is an even function of H,

$$V_{\Delta\varrho} = \tfrac{1}{2}\{\Delta V(H) + \Delta V(-H)\}. \tag{3.13}$$

This effect was briefly examined in some of the Na-doped samples. These samples did not have a suitable form for applying the method described in sec. 2.2. It was found that at temperatures between 230 and 350 °K $V_{\Delta\varrho}$ was roughly proportional to $|H|^{1.4}$ for fields between 5 and 23 kG. In a sample cut parallel to the c-axis the constant of proportionality had the same temperature dependence as the resistivity; in a sample cut perpendicular to the c-axis the effect rapidly vanished for temperatures below T_N. Above T_N in both samples $V_{\Delta\varrho}$ was of the same order of magnitude as V_H. In the sample whose plane contained the c-axis the change of the Van der Pauw resistances R_1 and R_2 was measured also. One of these increased and the other decreased upon application of the field. This indicates that the transverse magnetoresistance is quite anisotropic (although not necessarily to the extent that the effect has different signs for different directions). The peculiar field dependence of the magnetoresistance effect seems to indicate that it is not caused by the same mechanisms as in non-magnetic semiconductors. Since no detailed measurements have been made the magnetoresistance effect will not be discussed further.

4. SPIN-DISORDER SCATTERING

In our earlier papers [13,14]) the temperature dependence of the mobility near T_N was qualitatively attributed to spin-disorder scattering. The main argument used was that the large change of slope of the mobility vs temperature curve at the Néel temperature reflects the rapid change of long-range magnetic order near T_N. Recently, however, the spin-disorder mobility in magnetic semiconductors has been calculated by Haas [18]) on the basis of a model which seems quite appropriate to MnTe. According to this theory the change of slope in $\mu(T)$ at T_N should be much smaller than found in MnTe, while it also does not explain the temperature-dependent anisotropy of the resistivity in MnTe. This chapter contains the following parts: a description of Haas' model and calculation, a comparison with the experimental result, and some considerations on possible ways in which the theory might be extended.

In view of the discussion of magnon drag in chapter 5 spin-disorder scattering is also calculated in terms of magnon scattering.

4.1. Haas' theory of spin-disorder scattering

4.1.1. *The physical model*

As in several theories of spin-disorder scattering in metals (see e.g. refs 52-55) it is assumed in Haas' theory that, to a first approximation, the charge carriers responsible for the electrical properties and the electrons responsible for the magnetic properties may be considered as independent of each other. Next, an exchange interaction between the spin of a charge carrier and the total spins of the "magnetic" electrons is introduced, from which, among other things, the spin-disorder mobility is calculated using perturbation theory.
This model is briefly outlined in the following.

As in the theory of magnetic insulators [56]) the magnetic properties are attributed to the fact that the atoms (or ions) of one of the constituent elements have a fixed, whole, number of electrons in a partially filled shell. Due to this partial filling these electrons have the possibility to combine their spins and angular momenta in different ways, and according to Hund's first rule, exchange interactions usually result in a ground state in which the total spin S of these electrons is as large as possible. Supposing orbital contributions to be quenched by the crystal field, the magnetic moment associated with each magnetic ion is $g\mu_B \mathbf{S}$, μ_B being the Bohr magneton and $g \approx 2$. Only this case is considered in the following.
This restriction has no consequences for the application of the theory to MnTe since the ground state of the five electrons occupying half of the available orbitals of the $3d$-shell of the Mn ions have a ${}^6S$ ground state, which has zero angular momentum.

Similar to the exchange interaction which causes the energy of the electrons in a partially filled shell to depend on the relative orientation of their spins, there are exchange interactions which give rise to a coupling between the total spins $\mathbf{S}_i$ and $\mathbf{S}_j$ of two magnetic ions. This interaction is usually assumed to be of the Heisenberg form

$$H_{ij} = 2 J_{ij} \mathbf{S}_i \cdot \mathbf{S}_j. \tag{4.1}$$

The exchange integrals J_{ij} can be negative, favouring the parallel orientation of $\mathbf{S}_i$ and $\mathbf{S}_j$, as well as positive, which promotes their anti-parallel orientation. For reasons of simplicity we shall only consider the case of ferromagnets or two-sublattice antiferromagnets with one type of magnetic ions situated at crystallographically equivalent lattice sites.

The charge carriers are described in terms of the usual band theory of solids. They have Bloch wave functions (see e.g. refs 57 and 58)

$$\varphi_{b\mathbf{k}}(\mathbf{r}) = u_{b\mathbf{k}}(\mathbf{r}) \exp(i\mathbf{k} \cdot \mathbf{r}), \tag{4.2}$$

which extend throughout the whole crystal. These are characterized by a wave vector $\mathbf{k}$ and a function $u_{b\mathbf{k}}(\mathbf{r})$ which is invariant for all fundamental translations of the crystal lattice. The index b labels the various energy bands.

In the case of p-type MnTe the charge carriers are holes occupying states of a valence band which may be assumed to originate mainly from the outer $5p$-orbitals of Te atoms. An energy-band scheme showing the relative positions of the energy levels of the localized "magnetic" electrons and those of the band electrons has been given by Albers and Haas [10–12]).

The interaction between a charge carrier and the magnetic spins, which ultimately gives rise to the scattering, is assumed to be of the form

$$H = \sum_i J(\mathbf{r} - \mathbf{R}_i)\, \mathbf{s} \cdot \mathbf{S}_i, \tag{4.3}$$

where $\mathbf{s}$ and $\mathbf{r}$, $\mathbf{S}_i$ and $\mathbf{R}_i$ are the spin and position of the carrier and a magnetic ion, respectively. The thermal motion of the magnetic ions is disregarded, as well as the possible effect of the presence of the charge carriers on the interactions between the magnetic spins.

Only that part of the potential (4.3) will contribute to the scattering of the charge carriers which does not have the periodicity of the lattice. The part of (4.3) which does have the periodicity of the lattice affects the band structure. For ferromagnets the periodic potential *)

*) The thermal average of a quantity X_i pertaining to the ions (i) of a (sub)lattice is denoted as $\langle X_i \rangle$ or simply as $\langle X \rangle$. For a thermal average over the ions of a given sublattice (a) the notation $\langle X_a \rangle$ will be used as well.

$$H_0^{\mathrm{F}} = \mathbf{s} \cdot \langle \mathbf{S}_i \rangle \sum_i J(\mathbf{r} - \mathbf{R}_i) \tag{4.4}$$

lifts the spin degeneracy of the electron energy bands, which results in different bands for charge carriers with spin parallel or antiparallel to $\langle \mathbf{S}_i \rangle$. The splitting of a given band extremum is to first order independent of $\mathbf{k}$ and proportional to $\langle \mathbf{S}_i \rangle$.

In an antiferromagnet with sublattice magnetizations $\langle \mathbf{S}_b \rangle = -\langle \mathbf{S}_a \rangle$ (subscripts a and b label the two sublattices) the periodic part of (4.3) is

$$H_0^{\mathrm{AF}} = \mathbf{s} \cdot \langle \mathbf{S}_a \rangle \{ \sum_j J(\mathbf{r} - \mathbf{R}_{aj}) - \sum_l J(\mathbf{r} - \mathbf{R}_{bl}) \}. \tag{4.5}$$

If the crystallographic unit cell contains a single magnetic ion this potential constitutes a superstructure as a result of which the original Brillouin zone is halved, and a band discontinuity may develop at the new zone boundary. This effect perhaps plays a role in the semiconductor-to-metal transition in VO and related compounds [59]). In the case of MnTe the crystallographic unit cell contains two Mn atoms, one of each magnetic sublattice, and the antiferromagnetic order does not introduce a new zone boundary. Since, furthermore, the magnetic structure of MnTe has a centre of inversion (viz. each Mn ion) the spin degeneracy of the bands cannot be lifted (cf. ref. 57, p. 184). These observations, however, do not exclude the possibility that the wave functions, and thus the band structure, may depend on the sublattice magnetization. This effect will be discussed below (sec. 4.3.2) and is neglected in the following.

Subtracting its periodic part, (4.4) or (4.5), from the potential (4.3) one obtains the scattering potentials for both ferro- and antiferromagnets

$$H' = \sum_i J(\mathbf{r} - \mathbf{R}_i) \, \mathbf{s} \cdot \tilde{\mathbf{S}}_i, \tag{4.6}$$

where $\tilde{\mathbf{S}}_i$ represents the spin deviation $\mathbf{S}_i - \langle \mathbf{S}_i \rangle$ on the ion at $\mathbf{R}_i$.

Before giving explicit results of mobility calculations based on this scattering potential it may be noted that there are two distinct types of scattering processes, viz. those in which the carrier's spin is reversed, and those in which this does not occur. They will be called spin-flip and non-spin-flip processes, respectively. In the former type the total quantum number of the magnetic system with respect to the direction of magnetization is changed by $\Delta M_{\mathrm{total}} = \pm 1$, while it remains unchanged in the latter case. In the following this distinction will be seen to have two consequences.

(1) For ferromagnets below the Curie temperature the band splitting is usually much larger than the energy which is exchanged between carriers and magnetic system during scattering processes. In that case only interband scattering through non-spin-flip scattering processes can occur.

(2) If the magnetic disorder is described in terms of magnons, the emission or absorption of a magnon corresponds to $\Delta M_{\text{total}} = \pm 1$, so that scattering of a charge carrier by a single magnon is a spin-flip process. Non-spin-flip processes involve two, or four, etc., magnons.

4.1.2. *The theoretical mobility*

In Haas' calculation [18]) of the spin-disorder mobility arising from the scattering potential (4.6) the following additional assumptions are made.

— The change $\mathbf{k}' - \mathbf{k}$ in wave vector of a charge carrier due to a scattering process is generally small compared to the wave vectors at the Brillouin-zone boundary, i.e. $|\mathbf{k}' - \mathbf{k}| \ll \pi/2a$, where a is a representative dimension of the crystallographic unit cell. This restricts the calculation to scattering in semiconductors which, furthermore, should be of the type illustrated in figs 4.1*a* and 4.1*c*. The calculation does not apply to the type of intervalley scattering shown in fig. 4.1*b*.

— The energy transfers between a charge carrier and the magnetic system are generally small compared with kT, i.e. the scattering is quasi-elastic.

— The range of the exchange integral $J(\mathbf{r} - \mathbf{R}_i)$ is small compared with representative values of $|\mathbf{k}' - \mathbf{k}|^{-1}$.

— The energy band in which the carriers move may be considered parabolic.

With these assumptions a relaxation time for scattering exists and is given by

$$\frac{1}{\tau_{\uparrow\downarrow}(E)} = \frac{\pi}{\hbar} g'(E) \frac{J^2}{4N} \frac{kT}{N g^2 \mu_B{}^2} 2\chi^{\perp}, \tag{4.7}$$

$$\frac{1}{\tau_{\uparrow\uparrow}(E)} = \frac{\pi}{\hbar} g'(E) \frac{J^2}{4N} \frac{kT}{N g^2 \mu_B{}^2} \chi^{//}. \tag{4.8}$$

Here $\tau_{\uparrow\downarrow}(E)$ and $\tau_{\uparrow\uparrow}(E)$ are the relaxation times for a carrier of energy E due to spin-flip and non-spin-flip scattering, respectively, $g'(E)$ is the density of states at the energy E of the band to which the carrier is scattered, $\chi^{\perp}$ and $\chi^{//}$ are the magnetic susceptibility measured with the magnetic field perpendicular and parallel to the direction of (sublattice) magnetization, respectively *), and J is

$$J = N \int u_{b'\mathbf{k}'}{}^* \, u_{b\mathbf{k}} \, J(\mathbf{r} - \mathbf{R}_i) \exp\{i(\mathbf{k} - \mathbf{k}') \cdot (\mathbf{r} - \mathbf{R}_i)\} \, \mathrm{d}r \tag{4.9}$$

(the $u_{b\mathbf{k}}(\mathbf{r})$ are normalized to unit volume, which contains N magnetic atoms). Because of the assumption made with regard to the scattering wave vector $\mathbf{k}' - \mathbf{k}$ and the range of $J(\mathbf{r} - \mathbf{R}_i)$, the integral is, to a first approximation,

*) This definition requires some further specification in the case of ferromagnets below T_c, which is given in Haas' paper.

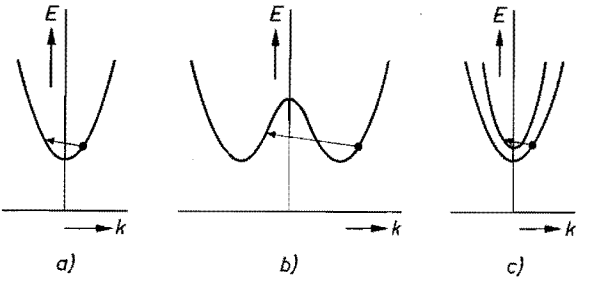

Fig. 4.1. (*a*): Intraband scattering, (*b*): interband scattering between states of equivalent band extremes, (*c*): interband scattering between states of non-equivalent band extremes situated at the same value of **k**. Arrows indicate the scattering vector $\mathbf{k}' - \mathbf{k}$. For reasons of simplicity the energy bands are shown for a one-dimensional lattice.

independent of **k** and **k**′. It is independent of i as well (but not in the case discussed in sec. 4.3.2).

Only scattering processes are considered that take place within a single band (fig. 4.1*a*). One then has, with $m_d = (m_x m_y m_z)^{1/3}$,

$$g'(E) = g(E) = (2 m_d{}^3 E)^{1/2}/\pi^2\hbar^3, \tag{4.10a}$$

except in the case of $\tau_{\uparrow\downarrow}(E)$ in a ferromagnet below T_C for which

$$g'(E) = 0, \tag{4.10b}$$

corresponding to the fact that the band splitting prevents the occurrence of spin-flip processes (the energy E is counted from the top of the highest valence band or the bottom of the lowest conduction band in p- and n-type material, respectively).

In order to arrive at a simple formula for the mobility we introduce the parameter T^* which has the dimension of a temperature and which is equal to

$$T^* = S(S+1)\frac{N g^2 \mu_B{}^2}{k \chi''} \tag{4.11a}$$

for ferromagnets below T_C and equal to

$$T^* = S(S+1)\frac{N g^2 \mu_B{}^2}{k(2\chi^\perp + \chi'')} \tag{4.11b}$$

otherwise. According to simple theories of the susceptibility, T^* may for example have the following values

$$T^* = T - T_C \qquad \text{(ferro, } T > T_C\text{)}, \tag{4.11c}$$

$$T^* = T + \theta \qquad \text{(antiferro, } T \geqslant T_N\text{)}, \tag{4.11d}$$

$$T^* = \tfrac{2}{3}(T_N + \theta) \qquad \text{(antiferro, } T = 0\text{)} \tag{4.11e}$$

(θ is the asymptotic Curie temperature of the antiferromagnet).

For obtaining an expression valid for arbitrary degeneracy of the carrier system (cf. sec. 3.1.2) we define another temperature, T', according to

$$k\,T' = \frac{9\,\pi}{16}\,[E^{-1/2}]^{-2} = \{F_0(\eta)/F_{1/2}(\eta)\}^{-2}\,k\,T, \tag{4.12}$$

$$\approx k\,T \qquad \text{(non-deg.)}, \tag{4.12a}$$

$$\approx \frac{9\,\pi}{16}\,E_F = \frac{9\,\pi}{16}\,\frac{\hbar^2\,(3\,\pi^2\,p)^{2/3}}{2\,m_d} \quad \text{(deg.)}, \tag{4.12b}$$

where p is the carrier concentration and [ ] denotes the usual average in the case of Fermi-Dirac statistics.

With the above expressions the mobility in a direction $i = x,y,z$ becomes

$$\mu_i = \frac{e}{m_i}\,[\tau(E)] = \frac{8\,(2\,\pi)^{1/2}\,e\,\hbar^4}{3\,m_i\,m_d^{3/2}}\,\frac{N}{J^2\,S\,(S+1)}\left(\frac{T^*}{T}\right)\left(\frac{1}{k\,T'}\right)^{1/2} \tag{4.13a}$$

$$= \frac{10{\cdot}3{\cdot}10^{22}\,N}{m_i\,m_d^{3/2}/m_0^{5/2}}\,\frac{1}{J^2\,S\,(S+1)}\left(\frac{T^*}{T}\right)\left(\frac{300}{T'}\right)^{1/2} \text{cm}^2/\text{V s} \tag{4.13b}$$

(N in cm^{-3}, J in eV). These equations contain two temperature-dependent factors, T^*/T and $1/T'$. The former, T^*/T, is shown by the curves labelled 1 in fig. 4.2. These curves were calculated with molecular-field expressions for

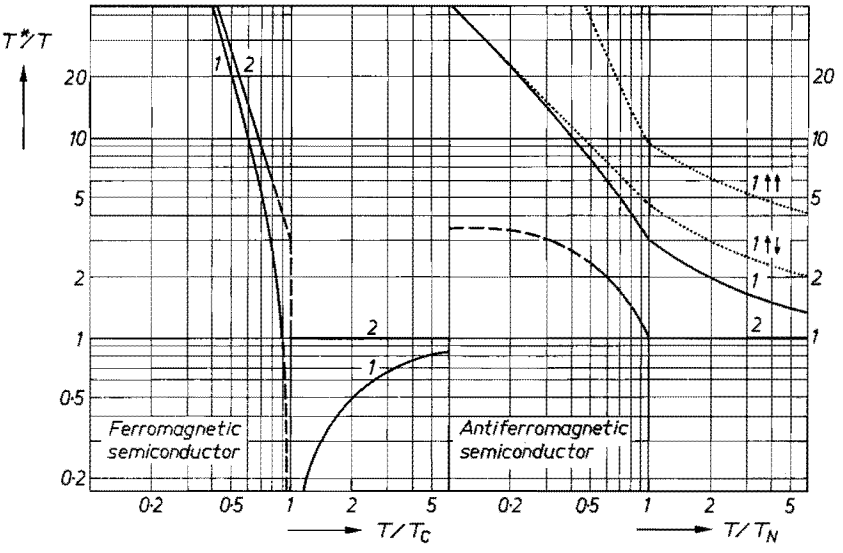

Fig. 4.2. The temperature dependence of the function T^*/T in eqs (4.13a) and (4.13b). Curves 1: calculated according to Haas' theory from eqs (4.11a) and (4.11b) for $S = 5/2$. Curves 2: calculated from eqs (4.17a) and (4.17b) for $S = 5/2$. For the antiferromagnetic semiconductor the asymptotic Curie temperature is taken to be twice the Néel temperature. Curves labelled $1\uparrow\downarrow$ and $1\uparrow\uparrow$ correspond to spin-flip scattering and non-spin-flip scattering separately.

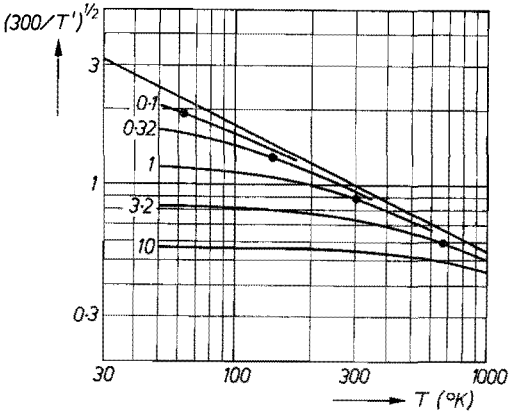

Fig. 4.3. The temperature dependence of the function $(300/T')^{1/2}$ in eq. (4.13b) indicating the effect of degeneracy. Numbers labelling the curves are values of $p/N_v(300)$, where $N_v(300) = 2{\cdot}5.10^{19}\ (m/m_0)^{3/2}$ cm^{-3} is the effective density of states at 300 °K. Dots refer to the temperature where $p = N_v(T)$.

the susceptibilities using in χ'' below T_C and T_N the Brillouin functions for $S = 5/2$, and in the case of the antiferromagnet $\theta = 2\,T_N$. Figure 4.3 shows the temperature dependence of $(300/T')$ for some values of $p/2{\cdot}5.10^{19}\ (m_d/m_0)^{3/2}$.

Other consequences of Haas' calculation are the following.

According to eq. (4.10a) the relaxation times are proportional to $E^{-1/2}$. It follows that the scattering parameter r, defined by $l(E) \propto E^{1/2}\,\tau(E) \propto E^r$, is equal to zero. As remarked in sec. 3.1.2 the knowledge of this value is of importance for calculating the electronic contribution of the Seebeck coefficient.

It is seen also that the relaxation times are isotropic, i.e. they do not depend on the directions of $\mathbf{k}$ and $\mathbf{k}'$. This implies that, as shown also by eqs (4.13), any anisotropy in the mobility can only be due to an anisotropic effective mass.

4.1.3. *Additional remarks*

The susceptibility occurs in eqs (4.7) and (4.8) because in the calculation of transition probabilities double sums arise of the form

$$\sum_n \sum_m \langle \tilde{S}_n^{\,i}\, \tilde{S}_m^{\,j} \rangle \exp\{i\,\mathbf{q}\,.\,(\mathbf{R}_n - \mathbf{R}_m)\} \tag{4.14a}$$

$(i,j = x,y,z;\ \mathbf{q} = \mathbf{k}' - \mathbf{k})$ which are equal to [60])

$$\frac{k\,T}{g^2\,\mu_B{}^2}\,\chi^{ij}(\mathbf{q}), \tag{4.14b}$$

$\chi^{ij}(\mathbf{q})$ being a generalized susceptibility. For small values of q this susceptibility can be expanded as

$$1/\chi^{ij}(\mathbf{q}) = 1/\chi^{ij} + A^{ij}\,q^2, \tag{4.15}$$

where χ^{ij} is the value for homogeneous magnetic fields. In Haas' calculation the terms in q^2 are neglected, which is the main reason why this theory only pertains to small values of $\mathbf{k}' - \mathbf{k}$.

For large scattering wave vectors it may be argued [54]) that interference effects due to correlation between different ionic spins may be neglected. Following Maranzana [16]) we put

$$\langle S_n^i S_m^j \rangle = \langle S_n^i \rangle \langle S_m^j \rangle \quad \text{for} \quad n \neq m, \tag{4.16}$$

and it is easily found that the expression (4.14a) then leads to

$$\frac{1}{\tau_{\uparrow\downarrow}(E)} = \frac{\pi}{\hbar} g'(E) \frac{J^2}{4N} \{S(S+1) - \langle M^2 \rangle \pm \tfrac{1}{2}(\langle M_a \rangle + \langle M_b \rangle)\}, \tag{4.17a}$$

$$\frac{1}{\tau_{\uparrow\uparrow}(E)} = \frac{\pi}{\hbar} g'(E) \frac{J^2}{4N} \{\langle M^2 \rangle - \langle M \rangle^2\}, \tag{4.17b}$$

where M has been written for the eigenvalue of S^z, and where the term $\frac{1}{2}(\langle M_a \rangle + \langle M_b \rangle)$ vanishes for an antiferromagnet and should be taken equal to $\langle M \rangle$ for a ferromagnet. Except for some minor details these expressions have been obtained by several authors who considered spin-disorder scattering in ferromagnetic metals [52–55]). In the paper by Van Peski-Tinbergen and Dekker [55]) account is taken of non-elasticity in spin-flip processes. This removes the difference in relaxation times for carriers with opposite spin directions to which the $\pm$ sign in eq. (4.17a) refers (in ferromagnetic metals spin-flip scattering can occur because the band splitting due to the potential (4.4) is smaller than E_F).

The curves labeled 2 in fig. 4.2 were calculated from eqs (4.17) using molecular-field expressions for $\langle M \rangle$ and $\langle M^2 \rangle$, while, as before, only non-spin-flip scattering was assumed to occur below T_C for the ferromagnet. At low temperatures the curve shown for the antiferromagnet is dashed because in that temperature region molecular-field theory does not apply, while moreover explicit account has to be taken of spin-wave theory.

Curve 2 for the antiferromagnetic semiconductor of fig. 4.2 shows a considerable change of slope at T_N. This change is roughly similar to that found in ferromagnetic metals. For a qualitative explanation of such behaviour one is easily led to associate the mobility with long-range magnetic order (which changes rapidly below T_N and T_C, and is absent above these temperatures). The correct relation between scattering and magnetic order is given, however, by the expression (4.14a), or the susceptibility $\chi(\mathbf{q})$, which has a quite different temperature dependence as long-range magnetic order. This is clearly shown by curves 1 in fig. 4.2 which pertain to $\chi(q = 0)$. For the antiferromagnetic semiconductor curve 1 exhibits only a very small change of slope at T_N.

If long-range magnetic order is an irrelevant, though plausible, quantity, one may ask why it is the susceptibility that determines the behaviour of the

mobility. Perhaps one might reason as follows. According to the term $\mathbf{s} \cdot \mathbf{S}_i$ in the interaction (4.3), the spin of a carrier acts on the magnetic system in a similar way as a magnetic field, and the ease with which it can create a disturbance in the magnetic system is proportional to the susceptibility. The creation of a disturbance means, however, that the carrier is scattered. In this way there is a direct proportionality between scattering probability and susceptibility.

A more detailed description is needed to explain that it is rather $\chi(\mathbf{q})$ that counts than $\chi(\mathbf{k})$.

4.2. Comparison with the experimental mobility in MnTe

It has already been mentioned that Haas' theory leads to a small change of slope at T_N in the mobility vs temperature curve. A much larger change is found experimentally for p-type MnTe. This is clearly demonstrated in fig. 4.4, which shows the temperature dependence of both the theoretical curve and some curves of experimental mobilities (see sec. 3.4).

That there is also a difference in temperature dependence at low temperatures may be due to the presence of other scattering mechanisms or, in particular for the undoped samples, to unreliable results of the Hall measurements because of imperfect crystalline quality (cf. sec. 3.4). These may also be reasons that degenerate samples (1 to 3) seem to have higher mobilities than non-degenerate samples (4 to 8), while according to fig. 4.3 theory predicts the opposite.

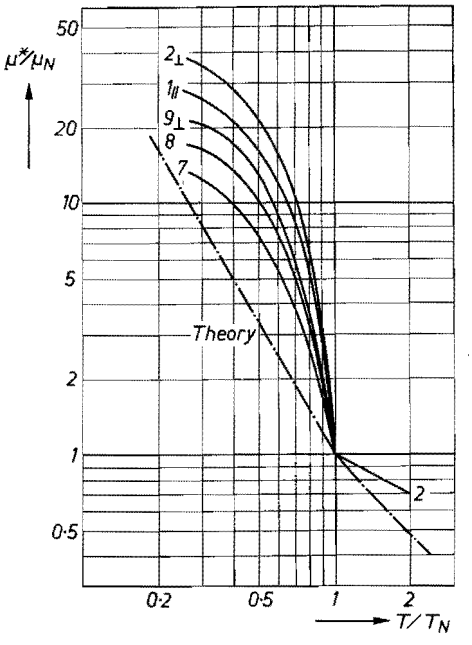

Fig. 4.4. Theoretical and experimental curves of the mobility normalized a $T_N = 307\,^\circ\mathrm{K}$.

The temperature-dependent anisotropy of the mobility, as shown in fig. 3.10 poses another problem. With an isotropic relaxation time an anisotropic mobility can only be due to an anisotropic effective mass. At low temperatures we have indeed $\mu_\perp/\mu_{||} \approx 0{\cdot}3$ which is roughly equal to $m_{||}/m_\perp \approx 0{\cdot}25$ as determined from optical measurements [21]). At temperatures near and above T_N, on the other hand, $\mu_\perp/\mu_{||} \approx 1$. This may indicate that $m_\perp$ and $m_{||}$ depend on temperature, or, more specifically, on the magnetic order. That such a dependence is not a priori impossible is discussed in sec. 4.3.2. Other mechanisms which may have to be considered are discussed in sec. 4.3.1.

4.3. Possible improvements of the theory

4.3.1. *Various mechanisms*

Beside mechanisms which the theory discussed in the foregoing has not taken into account and whose incorporation may result in a better agreement with experiment, there are also a number which might at first sight seem relevant, but are not so. Some examples of the latter are discussed first.

It has been mentioned already in sec. 4.1.1 that antiferromagnetic order can give rise to a *new Brillouin-zone boundary* along which an energy gap could be created, but that this does not occur in MnTe.

The theory given does not apply to *inelastic scattering*. The condition of elastic scattering is more readily satisfied in semiconductors than in metals (cf. sec. 4.4.2), and in the latter case it has been shown [54,55]) that for simple ferromagnets quasi-elastic scattering obtains at temperatures near and above T_C. In antiferromagnets one might perhaps have the complication of the presence of "*optical*" *magnetic excitations* (at low temperatures: optical magnons), which could give rise to inelastic scattering and, possibly, to a behaviour of the mobility as observed in MnTe. In simple two-sublattice antiferromagnets such as MnTe there are two branches of magnon states which are, however, both of the acoustical type (cf. ref. 57, p. 60).

Comparison of the two curves of $\tau(E)$ for antiferromagnets in fig. 4.2 shows that *intervalley scattering* of the type indicated in fig. 4.1*b* can give rise to a mobility with a sharper change of slope at T_N. Since the (density-of-states) effective mass derived from the Seebeck coefficient is not larger than the optically determined effective mass (cf. sec. 3.3) the existence of different equivalent maxima in the valence band of MnTe seems unlikely.

Having excluded the above possibilities one may consider the invalidity of one or more of the assumptions made.

The *use of perturbation theory* is strictly permitted only if the uncertainty in energy $\Delta E = \hbar/\tau$ connected with the finite time τ between scattering events is less than $k\,T$ (see e.g. ref. 58, p. 212). In terms of the mobility this condition reads

$$\mu > 44 \frac{300}{T} \frac{m_0}{m} \text{ cm}^2/\text{V s}, \tag{4.18}$$

which is clearly violated by the experimental mobility, especially near and above T_N (cf. fig. 3.8). This may indicate that at these temperatures a magnetic analogue of the large polaron is a more appropriate starting point for theoretical interpretation [61]).

The *form of the exchange interaction* (4.3) may be too simple in the case of MnTe. Assuming a valence band made up of predominantly 5*p*-orbitals of Te atoms, we have to do with *p*-electrons (or holes). The angular momentum of such electrons may also contribute to the exchange interaction *). In order to account for the observed anisotropy in the resistivity, the relaxation time due to this interaction should be an anisotropic function of the wave vector **k**, the anisotropy depending on temperature.

The other assumptions made in connection with eq. (4.3) would seem of minor importance. This is also the case as regards the neglect of the dependence of J and χ on $\mathbf{k}' - \mathbf{k}$ (eqs (4.9) and (4.15)).

4.3.2. *Magnetization-dependent band parameters*

According to eq. (4.5) antiferromagnetic order introduces a lattice-periodic potential H_0^{AF} in the crystal which is proportional to the sublattice magnetization. As is seen from its form, this potential causes a charge carrier with a given spin direction to be attracted by one sublattice and to be repulsed by the other, and the carrier will adapt its wave function accordingly. It can do so because for each ion there is another equivalent ion in the unit cell; wave functions therefore occur in pairs which in chemical terms may be labelled as bonding and antibonding (see fig. 4.5). By forming linear combinations of these wave functions the desired adaptation can be achieved. In terms of band theory this means that in the antiferromagnetic phase H_0^{AF} causes a mixing of states of different bands. Although for MnTe this mixing cannot give rise to a splitting of the bands (as it may do in the case of different crystallographic and magnetic unit cells, cf. sec. 4.1.1) it can change the shape of the bands and therefore also for instance the effective mass. Since H_0^{AF} depends on the sublattice magnetization $\langle \mathbf{S}_a \rangle$ the temperature dependence of such changes might be strong just below T_N. It will be difficult, however, to estimate the magnitude of the effect since it will depend critically on the (unknown) band structure of MnTe.

In principle the temperature dependence of the experimental mobility and its anisotropy would be explained if the effective mass were isotropic in the paramagnetic region, $T > T_N$, and if $m_\perp$ (and perhaps also $m_{||}$, though less markedly) decreased with increasing sublattice magnetization in the antiferro-

*) The author is indebted to Dr C. Haas for pointing out this possibility.

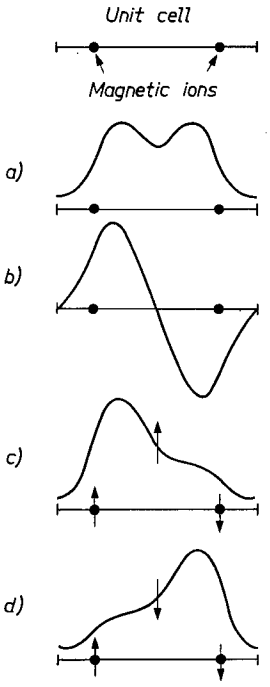

Fig. 4.5. A bonding orbital (*a*) and an antibonding orbital (*b*) can mix in such a way that the wave function of a charge carrier with a given spin direction is larger at the positions of the ions of one magnetic sublattice than at those of the other sublattice, (*c*) and (*d*).

magnetic region, $T < T_N$. It should be noted, however, that apart from a temperature-dependent effective mass other effects arise which must also be taken into account in calculating the mobility. Temperature-dependent wave functions imply, for instance, that the exchange integral J, eq. (4.9), depends on temperature. Even more important may be the fact that with different wave functions for opposite spin directions one obtains different exchange integrals J. It can be readily shown that such different values of J lead in the expression for $1/\tau(E)$ to additional terms which contain the "staggered" susceptibilities $\chi\perp(0,0,2\pi/c)$ and $\chi//(0,0,2\pi/c)$. These susceptibilities would be found if a spatially varying magnetic field having one direction on the one sublattice and the opposite direction on the other were applied. They are similar in magnitude and temperature dependence to the static susceptibilities $\chi\perp$ and $\chi//$ of ferromagnets and can become very large.

Another possibility contained in the present model is that the change in shape of the bands may result in a change of acceptor-level depth. This, in turn, may lead to an anomalous temperature dependence of the hole concentration near T_N. The model of magnetization-dependent band parameters, therefore, includes the most prominent features of case (2) considered in sec. 3.3.

In sec. 5.4.3 we shall come back to the question which of the proposed modifications of the theory possibly plays the major role in determining the electrical properties of MnTe.

4.4. Magnon scattering in antiferromagnetic semiconductors

In Haas' theory the scattering probability is directly connected with the general expression for the susceptibility. This theory is independent, therefore, of the model used for the description of the magnetic system and it will be valid also in the temperature region where spin disorder should be described in terms of spin waves (magnons).

In view of the considerations on magnon drag in chapter 5 we consider in this section the reverse problem, viz. the question up to what temperature does magnon scattering give the correct mobility. Only the case of one-magnon scattering processes in antiferromagnets is discussed. Such processes dominate those involving two or more magnons, in any case at low temperatures (the fact that in fig. 4.2 the curve $1_{\uparrow\downarrow}$ for spin-flip scattering lies below the curve $1_{\uparrow\uparrow}$ for non-spin-flip scattering agrees with this observation). Furthermore, as explained in sec. 5.2.2, the main contribution to magnon-drag effects is expected to arise from one-magnon scattering processes.

One of the conditions for the validity of Haas' theory is that the scattering may be regarded as quasi-elastic. This condition is easily formulated in the case of magnon scattering and will be treated briefly too.

4.4.1. *Calculation of magnon scattering*

We consider an antiferromagnet having $N/2$ magnetic ions of one sublattice at positions $\mathbf{R}_{aj}$ and $N/2$ magnetic ions of the other sublattice at (equivalent) positions $\mathbf{R}_{bl}$. With the exchange integral J of eq. (4.9) the relevant matrix element for the scattering of a charge carrier with wave function $\varphi_{\mathbf{k}}(\mathbf{r})$ and spin $m_s = +\frac{1}{2}$ to a state with $\varphi_{\mathbf{k}'}(\mathbf{r})$ and $m_s = -\frac{1}{2}$ is found to be

$$M = M(\mathbf{k},+\tfrac{1}{2},\mu;\mathbf{k}',-\tfrac{1}{2},\mu') \tag{4.19}$$

$$= \frac{J}{N}\sum_{j,l}\langle -\tfrac{1}{2},\mu'|\tfrac{1}{2}s^{-}\,[S_{aj}{}^{+}\exp\{i(\mathbf{k}-\mathbf{k}')\cdot\mathbf{R}_{aj}\}+ S_{bl}{}^{+}\exp\{i(\mathbf{k}-\mathbf{k}')\cdot\mathbf{R}_{bl}\}]|+\tfrac{1}{2},\mu\rangle,$$

where the symbol μ represents the magnon system and $S^{\pm} = S^{x} \pm iS^{y}$.

For evaluating this matrix element the following expressions from the standard, linear, theory of antiferromagnetic magnons are used (see e.g. ref. 57, chapter 4; a slightly different convention with regard to the sign of the wave vectors is used here: the creation and annihilation operators for a magnon with wave vector $\pm\mathbf{q}$ are denoted as $\alpha_{\pm\mathbf{q}}{}^{+}$ or $\beta_{\pm\mathbf{q}}{}^{+}$ and $\alpha_{\pm\mathbf{q}}$ or $\beta_{\pm\mathbf{q}}$, respectively.)

$$S_{aj}^{+} = 2\left(\frac{S}{N}\right)^{1/2} \sum_{\mathbf{q}} \exp\left(i\,\mathbf{q}\,.\,\mathbf{R}_{aj}\right).\left(u_{\mathbf{q}}\,\alpha_{\mathbf{q}} + v_{\mathbf{q}}\,\beta_{-\mathbf{q}}^{+}\right), \tag{4.20a}$$

$$S_{bl}^{+} = 2\left(\frac{S}{N}\right)^{1/2} \sum_{\mathbf{q}} \exp\left(i\,\mathbf{q}\,.\,\mathbf{R}_{bl}\right).\left(u_{\mathbf{q}}\,\beta_{-\mathbf{q}}^{+} + v_{\mathbf{q}}\,\alpha_{\mathbf{q}}\right), \tag{4.20b}$$

$$u_{\mathbf{q}} = \cosh\chi = u_{-\mathbf{q}}; \quad v_{\mathbf{q}} = \sinh\chi = v_{-\mathbf{q}}, \tag{4.21a}$$

$$\tanh 2\chi = \frac{-\omega_e\,\gamma_{\mathbf{q}}}{\omega_e + \omega_A}, \tag{4.21b}$$

$$\gamma_{\mathbf{q}} = \sum_{\delta} \exp\left(i\,\mathbf{q}\,.\,\boldsymbol{\delta}\right) = \gamma_{-\mathbf{q}} \tag{4.22}$$

$$\approx 1 - \sum_{i=x,y,z} a_i^{2}\,q_i^{2} \qquad \text{(for small } q\text{)}, \tag{4.22a}$$

$$\hbar\,\omega_e = 2\,J_{12}\,z\,S = 3\,k\,T_{\mathrm{N}}/(S+1), \tag{4.23}$$

$$\hbar\,\omega_A = g\,\mu_{\mathrm{B}}\,H_A, \tag{4.24}$$

$$\hbar\,\omega_{\mathbf{q}} = \hbar\left\{(\omega_e + \omega_A)^2 - \omega_e^{2}\,\gamma_{\mathbf{q}}^{2}\right\}^{1/2} \tag{4.25}$$

$$\approx \hbar\,\omega_e\,(2\sum a_i^{2}\,q_i^{2})^{1/2} \quad \text{if} \quad \omega_A < 2\,\omega_e \sum a_i^{2}\,q_i^{2} < 2\,\omega_e \tag{4.25a}$$

(J_{12} is the exchange integral between the z nearest neighbours of a given magnetic ion to which they are connected by the vectors $\boldsymbol{\delta}$; H_A is the anisotropy field; the a_i are interatomic distances multiplied by numerical constants).

When substituting (4.20a) and (4.20b) into (4.19) use can be made of the general relation

$$\sum_{j=1}^{N/2} \exp\left\{i\,(\mathbf{k} - \mathbf{k}' + \mathbf{q})\,.\,{}_{aj}\mathbf{R}\right\} = \sum_{l=1}^{N/2} \exp\left\{i\,(\mathbf{k} - \mathbf{k}' + \mathbf{q})\,.\,\mathbf{R}_{bl}\right\} = \frac{N}{2}\,\delta_{\mathbf{k}'-\mathbf{k},\mathbf{q}+\mathbf{G}}, \tag{4.26}$$

$\mathbf{G}$ being 2π times a fundamental vector of the reciprocal lattice. In semiconductors, however, it is usually not necessary to consider Umklapp processes, i.e. scattering processes for which $\mathbf{G} \neq 0$. Neglecting these one finds

$$M = \frac{J}{2}\left(\frac{S}{N}\right)^{1/2} (u_{\mathbf{q}} + v_{\mathbf{q}})\,\langle\mu'\,|\alpha_{\mathbf{q}} + \beta_{-\mathbf{q}}^{+}|\,\mu\rangle, \tag{4.27}$$

with $\mathbf{q} = \mathbf{k}' - \mathbf{k}$. The terms in the operators $\alpha_{\mathbf{q}}$ and $\beta_{-\mathbf{q}}^{+}$ correspond, respectively, to a scattering process of the charge carrier in which an α magnon with wave vector $\mathbf{q}$ is absorbed and one in which a β magnon with wave vector $-\mathbf{q}$ is emitted. Upon squaring the matrix element one obtains

$$M^2 = \frac{J^2\,S}{4\,N}\,(u_{\mathbf{q}} + v_{\mathbf{q}})^2\,\{n^{\mathbf{q}\alpha} + (n_{-\mathbf{q}}{}^{\beta} + 1)\}. \tag{4.28}$$

If the magnon distribution in $\mathbf{q}$-space is not significantly disturbed by the electrical current *) the occupation numbers $n_{\mathbf{q}}$ and $n_{-\mathbf{q}}$ are given by the Bose-Einstein distribution, and

$$n_{\mathbf{q}}{}^{\alpha} + n_{-\mathbf{q}}{}^{\beta} + 1 = \coth(\hbar\omega_{\mathbf{q}}/2\,\boldsymbol{k}\,T) \tag{4.29}$$

$$\approx 2\,\boldsymbol{k}\,T/\hbar\,\omega_{\mathbf{q}} \quad \text{for} \quad \hbar\,\omega_{\mathbf{q}} < 2\,\boldsymbol{k}\,T, \tag{4.29a}$$

$$\approx 1 \qquad\quad \text{for} \quad \hbar\,\omega_{\mathbf{q}} > 2\,\boldsymbol{k}\,T. \tag{4.29b}$$

In connection with these equations it should be remarked that for $\hbar\,\omega_{\mathbf{q}} > \boldsymbol{k}\,T$ the scattering processes are not quasi-elastic so that the transport equations normally used for semiconductors cannot be applied (see next section). For the present we are interested in the high-temperature case, $\hbar\,\omega_{\mathbf{q}} < \boldsymbol{k}\,T$. Here the scattering processes may be regarded as quasi-elastic, but for large values of $n_{\mathbf{q}}$ magnon theory should generally take account of higher-order terms in $\alpha_{\mathbf{q}}$ and $\beta_{\mathbf{q}}$, which have been omitted in eqs (4.20a) and (4.20b). Nevertheless, we shall now make use of eq. (4.29a), on the argument that we are concerned with magnons of small wave vector and that for these the approximation of the linear magnon theory appears to be less serious than for magnons with large wave vectors (see e.g. ref. 62).

From eqs (4.21a), (4.21b) and (4.25) we obtain

$$(u_{\mathbf{q}} + v_{\mathbf{q}})^2 = \omega_{\mathbf{q}}\,(\omega_e + \omega_A + \omega_e\,\gamma_{\mathbf{q}})^{-1}, \tag{4.30}$$

so that the squared matrix element becomes

$$M^2 = \frac{J^2\,S}{4\,N}\,\frac{\omega_{\mathbf{q}}}{\omega_e + \omega_A + \omega_e\,\gamma_{\mathbf{q}}}\,(2\,n_{\mathbf{q}} + 1) \tag{4.31}$$

$$\approx \frac{J^2\,S}{4\,N}\,\frac{2\,\boldsymbol{k}\,T}{\hbar\,(\omega_e + \omega_A + \omega_e\,\gamma_{\mathbf{q}})} \tag{4.31a}$$

$$\approx \frac{J^2\,S}{4\,N}\,\frac{\boldsymbol{k}\,T}{\hbar\,\omega_e} \tag{4.31b}$$

$$= \frac{J^2}{4\,N}\,\frac{\boldsymbol{k}\,T}{N g^2\,\mu_{\mathrm{B}}{}^2}\,2\,\chi^{\perp}(T < T_{\mathrm{N}}), \tag{4.31c}$$

where the approximation (4.29a) is introduced in (4.31a), where in (4.31b) the terms ω_A and $\omega_e \sum a_i{}^2\,q_i{}^2$ have been neglected with respect to ω_e, and where in (4.31c) use has been made of

*) The violation of this condition leads to the second-order drag effects described in chapter 5.

$$\frac{\hbar\,\omega_e}{S} = \frac{3\,k\,T_N}{S(S+1)} = \frac{2\,\chi^{\perp}(T < T_N)}{N g^2\,\mu_B{}^2} \tag{4.32}$$

for nearest-neighbour interaction only ($\chi\perp(T < T_N)$ represents the perpendicular susceptibility for temperatures below T_N).

Because M^2 does not depend on $\mathbf{q}$, the relaxation time due to the scattering is given by $1/\tau_{\text{magnon}}(E) = (\pi/\hbar)\,g(E)\,M^2$, and comparison with eq. (4.7) for $\tau_{\uparrow\downarrow}(E)$ shows that for the case considered

$$\tau_{\text{magnon}} = \tau_{\uparrow\downarrow} \quad \text{for} \quad T < T_N. \tag{4.33}$$

This result may easily be generalized to interactions between arbitrary neighbours in a two-sublattice antiferromagnet. In that case $2\,T_N$ in eq. (4.23) is replaced by $T_N + \theta$, while due to interactions within one and the same sublattice an additional term $-\omega_e' \sum b_i{}^2\,q_i{}^2$ should be included in ω_A. If this term and the term $\omega_e \sum a_i{}^2\,q_i{}^2$ are retained in eq. (4.31a), one obtains a result which is in complete agreement with the form of the expansion of $\chi^{ij}(\mathbf{q})$ given in eq. (4.15).

We have thus arrived at the conclusion that in antiferromagnetic semiconductors the scattering of charge carriers by single magnons — described in terms of the simple, linear magnon theory — leads to the same mobility as Haas' theory *up to the Néel temperature*. An analogous result has been obtained for a similar problem in connection with neutron scattering in ferromagnets (ref. 60, p. 131).

4.4.2. *The condition of elastic scattering*

The calculation of magnon scattering as well as that of spin-disorder scattering discussed in this chapter requires that the scattering processes be regarded as quasi-elastic, i.e. that on the average they change the energy of a carrier by an amount less than $k\,T$. This condition will be briefly considered.

Assuming an energy-independent magnon velocity, eq. (4.25a), the consequences of the laws of conservation of energy and crystal momentum are the same as for acoustical-phonon scattering. For an isotropic magnon velocity, c, and an isotropic effective mass, m, one thus finds (see e.g. ref. 63, p. 530) that a carrier of wave vector k can only be scattered by magnons with wave vector

$$q < q_m = 2\,k + m\,c/\hbar. \tag{4.34}$$

In non-degenerate semiconductors a "thermal" carrier has a wave vector $k_T = (2\,m\,k\,T)^{1/2}/\hbar$ and its energy can at the most be changed by an amount $\hbar\,c\,q_m = 2\,\hbar\,c\,k_T + m\,c^2$. Requiring that this be less than $k\,T$ implies that the temperature should be higher than

$$T_0 \approx 9\,m\,c^2/k = 60\left(\frac{c}{10^6}\right)^2 \frac{m}{m_0}\ ^{\circ}\text{K} \tag{4.35}$$

(c in cm/s). In degenerate semiconductors, $q_m = 2\,k_F + m\,c/\hbar \approx 2\,k_F = 2\,(3\,\pi^2\,p)^{1/3}$. In this case the temperature should be higher than

$$T_0' = 2\,\hbar\,c\,k_F/k = 47\,\frac{c}{10^6}\left(\frac{p}{10^{18}}\right)^{1/3}\ °\mathrm{K} \qquad (4.36)$$

(c in cm/s; p in cm^{-3}).

For MnTe c is $1{\cdot}4.10^6$ cm/s [21]) so that T_0 is 72 °K for $m = 0{\cdot}6\,m_0$, while T_0' is 260 °K for $p = 6.10^{19}$ cm^{-3}. This shows that in highly Na-doped samples effects of inelasticity may become important. On the other hand it is known in the case of metals that large deviations from the "classical" linear temperature dependence of the resistivity only occur at temperatures well below the Debye temperature. Since this temperature plays the same role as T_0' in our case [64]), large effects are not expected to occur in the temperature range considered, especially if other scattering processes too occur at low temperatures.

5. MAGNON DRAG

In this chapter we reconsider the magnon-drag explanation previously given for the anomalous behaviour of the Seebeck coefficient in MnTe [13,14]). It will be seen that a detailed analysis is impossible, mainly due to the lack of sufficiently accurate mobility data. Therefore only the simplest theoretical model will be considered, neglecting anisotropies in effective mass, mobility and magnon velocity. Nor do we discuss in any detail the difficult theoretical question with regard to the description of magnetic excitations in terms of magnons at temperatures comparable to T_N. The treatment includes, however, the "second-order" drag effects, which Zanmarchi and Haas [21]) have used to explain optical phenomena in MnTe.

5.1. Physical description of the drag effects

The phonon- [65]) and magnon-drag [15]) effects arise as a consequence of the law of conservation of crystal momentum for scattering processes between charge carriers and phonons or magnons. In its strict sense this law is not valid for scattering between (quasi) particles having large wave vectors, in which case Umklapp processes may occur (cf. comment to eq. (4.26)). In such processes a considerable amount of momentum is transferred to or withdrawn from the crystal as a whole. In the following we shall consider the case of a semiconductor in which the charge carriers are scattered between states of a single band extremum (fig. 4.1*a*). Since in that case the scattering processes only involve (quasi) particles with small wave vectors, the law of conservation of crystal momentum obtains in its strict sense. For the quasi particles which scatter the carriers we consider magnons, but the following discussion is valid for phonons as well. Scattering by impurities will be neglected.

5.1.1. *First-order effects*

The drag contribution Π_d to the Peltier effect may be thought to arise in the following way [65]). Due to the combined action of the electrical field and the scattering by magnons the charge carriers acquire a stationary excess amount of crystal momentum. Since crystal momentum is conserved in the scattering processes, the magnons also acquire an excess amount of crystal momentum, i.e. they are dragged along with the carrier current. The energy flux carried by the magnon current constitutes the magnon-drag contribution to the Peltier heat.

In the Seebeck effect the drag contribution $S_d = \Pi_d/T$ is due to the fact that the flow of magnons created by the temperature difference (which, in principle, contributes to the heat conduction) drags the charge carriers along, thus enhancing the carrier accumulation which already exists at the colder end of the sample due to thermodiffusion.

In the first-order effects two relaxation times are of importance. First, the relaxation time τ_1 of the charge carriers characteristic of the rate at which they loose excess momentum to the magnons and, second, the relaxation time τ_3 of the magnons characterizing the rate at which magnons dissipate excess momentum in Umklapp processes, boundary scattering, etc. (the interpretation of τ_3 is considered in more detail in sec. 5.2.2).

It will be easily understood that Π_d should be proportional to τ_3/τ_1: a large τ_3 means a long distance over which the magnons can transport excess energy, while a small τ_1 signifies a strong coupling between the carrier and magnon systems.

5.1.2. *Second-order effects*

As pointed out by Sondheimer [66]), the formulation of the drag problem which considers only the processes mentioned above leads to a violation of the Kelvin relations. In order that these be satisfied account must also be taken of the scattering of magnons (phonons) by the charge carriers. The relaxation time τ_2 for the rate at which magnons loose excess momentum to the carriers will be inversely proportional to the carrier concentration.

As a consequence of these processes it is possible that the momentum, which is transferred from a carrier to a magnon, is returned to another carrier before it is randomized (due to a process characterized by τ_3). This means that the scattering of charge carriers by magnons becomes less effective, so that the spin-disorder mobility is increased. Considering the probabilities with which the processes mentioned occur, the factor by which the mobility increases is found to be $(1 + \tau_3/\tau_2)$. This increase may also be attributed to the fact that the carriers are scattered by a magnon system which moves along with them due to the first-order drag effect (cf. footnote in connection with eq. (4.29)). Effects of this kind are called second-order effects.

It can be shown that the drag contributions Π_d and S_d are decreased by roughly the same factor $(1 + \tau_3/\tau_2)$ by which the mobility is increased. In the case of the Peltier and Seebeck coefficient the second-order effect is also called saturation effect [65]).

5.2. Simplified theory

5.2.1. *Basic equations*

A simplified calculation of the first-order drag effects has been given by Herring [65]). The simplification consists of neglecting of the energy dependence of the relaxation times. Extending this approach to the case where second-order effects are important Zanmarchi and Haas [21]) have derived the following expressions for the drag contribution S_d to the Seebeck coefficient and for the mobility:

$$S_d = \frac{k}{e}\frac{m c^2}{k T}\frac{\tau_3}{\tau_1 (1 + \tau_3/\tau_2)}, \tag{5.1}$$

$$\mu = \frac{e}{m}\tau_1 (1 + \tau_3/\tau_2), \tag{5.2}$$

(eq. (5.1) is written in the form given because it clearly shows the factor $k/e = 86$ μV/deg, the "natural" unit in which the Seebeck coefficient can be expressed; the other two factors are dimensionless). The (average) relaxation times occurring in these equations have been defined in the preceding section and, briefly, refer to the following processes:
(τ_1) scattering of carriers by magnons,
(τ_2) scattering of magnons by carriers,
(τ_3) scattering of magnons by magnons, boundaries, etc.
In eq. (5.1) c is the magnon velocity *). For the limiting case $\tau_2 \to \infty$ eq. (5.1) refers to the first-order drag effect in the Seebeck coefficient and eq. (5.2) reduces to the normal mobility due to magnon scattering. If other scattering mechanisms, characterized by a relaxation time τ_4, contribute to the mobility the present approximation gives

$$\frac{1}{\mu_{\text{tot}}} = \frac{m}{e}\left\{\frac{1}{\tau_1 (1 + \tau_3/\tau_2)} + \frac{1}{\tau_4}\right\}, \tag{5.3}$$

while S_d remains unchanged.

Because τ_1 and τ_2 relate to one and the same mechanism, viz. the mutual scattering of carriers and magnons, there must be a relation between them. From the argument that in the absence of all other scattering mechanisms the carriers and magnons must have the same drift velocity Zanmarchi and Haas find that

$$\frac{\tau_1}{\tau_2} = \frac{1}{A}\frac{m c^2}{k T}, \tag{5.4}$$

$$A = \frac{2}{3\pi^{1/2}}\frac{N_v}{p} \quad \text{(non-deg.)}, \tag{5.4a}$$

$$A = \tfrac{1}{2} \quad \text{(deg.)}, \tag{5.4b}$$

where p is the carrier concentration and N_v the effective density of states of the band in which they move. In non-degenerate material τ_1 is independent of p

*) The calculation pertains in particular to drag effects due to antiferromagnetic "acoustical" magnons and to acoustical phonons, for which c may be regarded as energy-independent. For optical magnons and phonons the group velocity c is vanishingly small so that these do not contribute to the drag effects. Some remarks concerning the drag effects in ferromagnetic semiconductors will be made in the next section.

so that τ_2 is inversely proportional to the carrier concentration, as should be expected. In degenerate material, $\tau_1 \propto k_F^{-1} \propto p^{-1/3}$ giving $\tau_2 \propto p^{-1/3}$.

Combining eqs (5.4), (5.4a) and (5.4b) with (5.1) and (5.2) one may write

$$S_d = S_d^{\circ}/(1 + S_d^{\circ}/S_M), \tag{5.5a}$$

$$S_d^{\circ} = S_d/(1 - S_d/S_M), \tag{5.5b}$$

$$\mu_1 = \mu_1^{\circ}/(1 - S_d/S_M), \tag{5.5c}$$

$$S_M = \frac{2}{3\pi^{1/2}} \frac{N_v}{p} \frac{\boldsymbol{k}}{e} \quad \text{(non-deg.)} \tag{5.5d}$$

$$= \tfrac{1}{2} \frac{\boldsymbol{k}}{e}. \quad \text{(deg.)} \tag{5.5e}$$

Here S_d° and μ_1° are the first-order quantities (for $\tau_2 = \infty$ or $S_M = \infty$), and S_d and μ_1 the quantities including second-order effects. In these expressions the factor $(1 + S_d^{\circ}/S_M) = (1 - S_d/S_M)^{-1}$ replaces the factor $(1 + \tau_3/\tau_2)$ in eqs (5.1) and (5.2). The use of eqs (5.5b) and (5.5c) is that they permit a direct estimate to be made of the importance of second-order effects by comparing the experimental drag contribution S_d with the quantity S_M. The value of the latter is a constant given by eq. (5.5e) for degenerate samples, and depends only on the carrier concentration and effective density of states for non-degenerate samples. From eqs (5.5a) and (5.5b) it follows that S_d can never exceed S_M (nor S_d°) so that, for example, according to eq. (5.5e) in degenerate samples S_d can be at most $\frac{1}{2}\boldsymbol{k}/e = 43$ μV/deg.

The above equations follow from a rather crude model based on (ill-defined) average relaxation times. Calculations in which the averaging procedures are carried out more accurately have been performed in the analogous case of phonon drag. As will be shown in sec. (5.3) these calculations result in higher values of S_M (or the coefficient A of eq. (5.4)).

One correction to the value of the coefficient A is a rather trivial one. In their calculation Zanmarchi and Haas assume a single magnon branch. Usually, however, the magnon states in antiferromagnets are doubly degenerate (neglecting magnetic anisotropy). Because, according to their calculation, the drift velocity of the magnons is inversely proportional to the number of magnons, it can be easily seen that a double degeneracy of the magnon states implies that A, and thus S_M, is twice as large as given by the above equations (one may say that the more magnons there are, the more difficult it is to give them the same drift velocity as the carriers).

5.2.2. *The magnon relaxation times in antiferromagnetic and in ferromagnetic semiconductors*

Herring [65,67]) has emphasized that in order to understand phonon drag in

semiconductors it is necessary to be aware of the fact that charge carriers of wave vector k can only be scattered by a phonon having a wave vector q if $q \lesssim 2k$ (cf. eq. (4.34)). In this way an electric current feeds surplus momentum only in the low-q modes of the phonon system. Phonon-phonon scattering next distributes the surplus momentum over all other modes, but, in general, does not destroy it *). This is because the most probable processes between low- and high-q phonons are normal, i.e. non-Umklapp, processes in which crystal momentum is conserved. The ultimate dissipation of crystal momentum in the phonon system occurs through U-processes between high-q phonons. Since, however, the relaxation time for these processes is much shorter than for the scattering of low-q by high-q phonons, it is the latter which determine the rate of loss of crystal momentum for the low-q modes. The relaxation time τ_3 for phonon drag is thus roughly equal to the average relaxation time of the phonons with wave vector $q < 2\hat{k}$, where

$$\hat{k} \equiv k_T = (2 m \boldsymbol{k} T)^{1/2}/\hbar \qquad \text{(non-deg.)}, \tag{5.6a}$$

$$\hat{k} \equiv k_F = (2 m E_F)^{1/2}/\hbar = (3\pi^2 p)^{1/3} \quad \text{(deg.)} \tag{5.6b}$$

are the wave vectors of a carrier of energy $\boldsymbol{k} T$ and E_F, respectively. For $\tau_1 \propto k^{2r-1}$ and $\tau_3 \propto q^{-s-2}$ we thus have

$$S_d \propto \hat{k}^{-2r-s-1}. \tag{5.6c}$$

Assuming that the same arguments apply to magnon drag, one finds that there should be a rather fundamental difference in the interpretation of τ_3 for antiferromagnetic and ferromagnetic semiconductors.

As mentioned in chapter 4, in the case of antiferromagnets the larger carrier relaxation time for non-spin-flip scattering as compared with the carrier relaxation time for spin-flip scattering can be understood from the argument that the former processes involve two magnons while the latter only involve a single magnon. The dominant scattering mechanism of the carriers is, therefore, the scattering by single magnons, so that for antiferromagnets τ_3 may be interpreted as the relaxation time for magnons with $q \lesssim 2\hat{k}$.

In the case of ferromagnets, however, the band splitting due to the magnetization prevents spin-flip scattering at temperatures up to nearly T_C and the mobility is practically determined by non-spin-flip processes, i.e. two-magnon processes. In that case the magnons taking part in the scattering of the carriers are not subject to the condition $q \lesssim 2\hat{k}$. This means that τ_3 wil be an average over all possible magnon modes which will be much smaller than the τ_3 for low-q modes only.

If all other quantities involved are equal one therefore expects that τ_3/τ_1,

*) Scattering of phonons (magnons) by impurities and boundaries is neglected here.

and thus the first-order magnon-drag effect, will be much smaller in ferromagnetic than in antiferromagnetic semiconductors.

With respect to second-order effects it is to be expected that these will be smaller for multi-magnon scattering than for one-magnon scattering. First because in the former case τ_3 will be smaller, and, second, because τ_2 will be larger due to the fact that also magnons with $q > 2\,\hat{k}$ have to be given the same drift velocity as the carriers (cf. the remark on the effect of the double degeneracy of the antiferromagnetic magnon states made at the end of sec. 5.2.1).

Another conclusion to be drawn from the above observations is that in antiferromagnetic semiconductors non-spin-flip scattering contributes much less than spin-flip scattering to the first-order effects in S and to the second-order effects. This may be accounted for by interpreting τ_1 as being due to spin-flip scattering only and including non-spin-flip scattering in the relaxation time τ_4 of eq. (5.3). Except in cases of extremely large second-order effects this correction is of some importance only at temperatures $T \gtrsim T_N$ since only at these temperatures are $\tau_{\uparrow\uparrow}$ and $\tau_{\uparrow\downarrow}$ of the same order of magnitude (see fig. 4.2).

It is finally noted that intervalley scattering between equivalent band extremes at different $\mathbf{k}$-values involves magnons of large $\mathbf{q}$ having a small τ_3, and is therefore expected to contribute only slightly to the drag effects.

5.2.3. *Magnon drag near and above T_N*

From the point of view of elementary theory the notion of magnons is valid only at low temperatures, while we also wish to apply the theory of magnon drag to MnTe at temperatures near and above T_N. The problems relating to magnons at high temperatures will not be discussed in this paper and the naïve point of view will be taken that for present purposes the magnon description of spin disorder is valid at all temperatures. Some support for this view is provided by the fact that neutron-scattering experiments have demonstrated the existence of magnon-like excitations at temperatures near and above T_N [68–70], while the calculation in sec. 4.4.1 also shows that the formula derived for the mobility due to (one-) magnon processes is identical with Haas' formula relating to spin-flip scattering at temperatures up to T_N. At higher temperatures the difference is only a factor $(T_N + \theta)/(T + \theta)$.

An estimate of the time of decay of a magnon with wave vector q at temperatures comparable to T_N has been given by Zanmarchi and Haas [21]:

$$\frac{1}{\tau_3(q)} = \Lambda\, q^2 = \sum_i 2\, J_i\, S\, z_i\, a_i^2\, q^2/\hbar, \tag{5.7}$$

where the J_i are exchange integrals referring to the exchange interaction between a magnetic ion and its z_i neighbours at distance a_i which all have a spin S. A similar formula (with, however, a smaller value of the diffusion constant Λ) has been given by Mori and Kawasaki [71] and by De Gennes [72].

5.3. More accurate calculations

More accurate formulae for the drag effects should be derived taking account of the wave-vector dependence of the carrier and magnon (or phonon) relaxation times $\tau_1(k)$, $\tau_2(q)$, $\tau_3(q)$ and $\tau_4(k)$. The problem to be solved has been formulated by Sondheimer [66]) in the form of two Boltzmann transport equations, one for the carriers and one for the magnons (phonons), which have to be solved simultaneously. This approach has been used by Parrott [73]) and by Appel [74]). A somewhat different treatment has previously been given by Herring [65,67]).

The papers cited consider acoustical-phonon drag. Their results should, however, apply also to magnon drag in antiferromagnetic semiconductors because the antiferromagnetic magnons have the same linear-dispersion law as acoustical phonons (neglecting the few magnons with very small wave vector, $q < \omega_A/c$, cf. eq. (4.25)).

As long as the scattering of the charge carriers may be regarded as quasi-elastic no particular difficulties arise in the calculation of the first-order drag contribution to the Seebeck coefficient. For the case that

$$1/\tau_e \equiv \{1/\tau_1(k) + 1/\tau_4(k)\} \propto E^{-r+1/2} \propto k^{-2r+1}$$

and

$$\tau_3(q) \propto q^{-(2+s)}$$

one finds [67])

$$S_d^{\circ} = \frac{\Gamma(3/2 - r - s/2)}{\Gamma(5/2)\,\Gamma(2+r)} \frac{4}{2-s} \frac{c^2\,\tau_3}{\mu_1^{\circ} T} \qquad \text{(non deg.)}, \tag{5.8a}$$

$$S_d^{\circ} = \frac{4}{2-s} \frac{c^2\,\tau_3}{\mu_1^{\circ}\,T} \qquad \text{(deg.)}, \tag{5.8b}$$

$$\tau_3 \equiv \tau_3(2\hat{k}) \tag{5.8c}$$

($\hat{k}$ is defined by eq. (5.6), μ_1° is the normal mobility due to τ_1 only). As indicated by the factor $2 - s$ these expressions are only valid if $s < 2$ *). For both the phonon case and the case of magnons near T_N one has $r = 0$ and $s = 0$, so that (5.8) reduces to

$$S_d^{\circ} = \tfrac{4}{3} \frac{c^2\,\tau_3}{\mu_1^{\circ}\,T} = \pi^{1/2}\, \frac{k}{e} \frac{m\,c^2}{k\,T} \frac{\tau_3}{\tau_1} \qquad \text{(non deg.)}, \tag{5.9a}$$

$$S_d^{\circ} = 2 \frac{c^2\,\tau_3}{\mu_1^{\circ}\,T} = 2\, \frac{k}{e} \frac{m\,c^2}{k\,T} \frac{\tau_3}{\tau_1} \qquad \text{(deg.)}, \tag{5.9b}$$

$$\tau_1 \equiv \tau_1(\hat{k}), \tag{5.9c}$$

*) If larger values of s should occur one has to take into account that magnons and phonons with a very small wave vector always have a mean free path which cannot exceed the dimensions of the sample (or, perhaps those of the magnetic domains).

the first-order mobility $\mu_1{}^0$ being given by

$$\mu_1{}^0 = \frac{4}{3\pi^{1/2}} \frac{e}{m} \tau_1 \qquad \text{(non deg.)}, \tag{5.10a}$$

$$\mu_1{}^0 = \frac{e}{m} \tau_1 \qquad \text{(deg.)}. \tag{5.10b}$$

Taking into account that the τ_3 in the present formulae is a factor of 4 smaller than the τ_3 used by Zanmarchi and Haas [21]), who put $\tau_3 \equiv \tau_3(\hat{k})$, the value of S_d predicted by eqs (5.9a) and (5.9b) is about 40% of that predicted by eq. (5.1) (with $\tau_2 = \infty$).

The problem of calculating the second-order effects is much more complicated than that of the first-order effects. In the papers cited only partial solutions with a limited range of validity were obtained.

For a small second-order effect and $\tau_1(k) \propto k^{-1}$, $\tau_4 = \infty$, $\tau_3(q) \propto q^{-2}$, Parrott [73]) finds a relative change in the mobility of non-degenerate material

$$\frac{\mu_1 - \mu_1{}^0}{\mu_1{}^0} = 0{\cdot}48 \frac{p}{N_v} \frac{m c^2}{\boldsymbol{k} T} \frac{\tau_3}{\tau_1} = \frac{0{\cdot}48}{\pi^{1/2}} \frac{p}{N_v} \frac{S_d{}^0}{\boldsymbol{k}/e}. \tag{5.11}$$

With the same approximations one finds from his equation 58 a relative change in the drag contribution to the Seebeck coefficient

$$\frac{S_d{}^0 - S_d}{S_d} = \tfrac{1}{2} \frac{p}{N_v} \frac{S_d{}^0}{\boldsymbol{k}/e}, \tag{5.12a}$$

which is equivalent to

$$S_M = 2 \frac{N_v}{p} (\boldsymbol{k}/e), \tag{5.12b}$$

S_M being defined by eq. (5.5a). It may be noted that eqs (5.5c) and (5.11) lead to a different value of S_M. In the limit of high saturation, however, eqs (5.5a) and (5.5c) must have the same S_M.

In his conference paper [65]) Herring quotes an equation, also valid for small second-order effects and non-degenerate statistics, which corresponds to

$$S_M = \pi^{1/2} \frac{N_v}{p} (\boldsymbol{k}/e). \tag{5.13}$$

This is very nearly the same result as (5.12b). In his other paper (1954b) Herring treats the case that $\tau_e \approx \tau_4(k)$ is independent of k *) while $\tau_1(k) \propto k^{-1}$ and

*) The condition $\tau_1 > \tau_4$ is implied by the replacement of β_{ex} by $\beta_{ex}{}^{(0)}$ in eq. 53 of the paper cited, which corresponds to neglecting the second-order effect on the carrier distribution.

$\tau_3(q) \propto q^{-2}$. His result for non-degenerate statistics is presented in graphical form and shows that the numerical coefficient in eq. (5.13) increases gradually with increasing importance of the second-order effect. At $S_d/S_d^{\circ} = 0{\cdot}1$, for example, one has approximately

$$S_M = 7\frac{N_v}{p}(k/e). \tag{5.14}$$

The paper also gives an explicit expression for S_d/S_d° valid for complete degeneracy and the same conditions regarding the relaxation times as above,

$$\frac{S_d}{S_d^{\circ}} = 1 - \xi + \tfrac{1}{2}\,\xi^2 \ln(1 + 2/\xi), \tag{5.15a}$$

which is equivalent to

$$\frac{S_d}{S_d^{\circ}} = \frac{1}{1 + \xi/\xi_M} \tag{5.15b}$$

with $1 \leqslant \xi_M < 4/3$ for $0 \leqslant \xi < \infty$. The parameter ξ in these equations may be written as

$$\xi = \frac{1}{f}\frac{\tau_e(k_F)}{\tau_1(k_F)}\frac{S_d^{\circ}}{k/e}, \tag{5.15c}$$

where f is the fraction due to τ_1 of the total loss of momentum of the charge carriers and neglecting second-order effects. Since $f \approx \tau_4/\tau_1$ and $\tau_e \approx \tau_4$ these equations give

$$S_M = (1 \text{ to } 4/3)\,(k/e). \tag{5.16}$$

This result can also be obtained from the considerations on phonon drag in metals by Ziman (ref. 58, p. 409). He finds $S_M = \pi^2 C_L/ek_F{}^3$, C_L being the phonon heat capacity. Assuming that only phonons with wave vector $q \leqslant 2\,k_F$ contribute to C_L it is easily shown that at high temperatures this leads to $S_M = (4/3)\,(k/e)$ per (acoustical) phonon branch. At lower temperatures, viz. $T < T_0' = 2\,\hbar c k_F/k$ (cf. eq. (4.36)), the heat capacity of the relevant phonons decreases as $D(T/T_0')/D(\infty)$, $D(x)$ being the well-known Debye function for the specific heat. At these temperatures one therefore expects

$$S_M = \tfrac{4}{3}\frac{D(T/T_0')}{D(\infty)}\frac{k}{e} \tag{5.17}$$

in degenerate samples. Towards lower temperatures this correction slowly decreases S_M to half of its original value at $T \approx 0{\cdot}25\ T_0'$; at still lower temperatures S_M diminishes more rapidly.

It is noted that a similar quantum correction should be applied for the first-order effect. Such correction might be of the form $G(T/T_0')\ D(T/T_0')/D(\infty)$, the first factor being the Grüneisen function $(\varrho/T)/(\varrho/T)_\infty$ and describing the decrease of the coupling between carriers and phonons (i.e. an increase of τ_1), and the second factor taking account of the decrease in heat capacity of the phonon system. As these corrections are not very important in the cases to be considered we have not investigated whether or not this argument is too simple.

Appel [74]) has considered the problem of second-order effects for combined phonon and ionized-impurity scattering of the carriers and a q-independent relaxation time of the phonons. This is a somewhat peculiar case because it is only due to the presence of impurity scattering that some of the relevant integrals remain finite. Because of this special feature it is doubtful whether the results of the calculations have a more general validity, and we have not analyzed them.

5.4. Magnon drag in MnTe

5.4.1. *General remarks*

As mentioned in sec. 3.1.1, only few measurements of the Seebeck coefficient in MnTe have been made. Especially in view of the shape of the $S(T)$ curve near T_N we did an accurate measurement on an Na-doped sample, the result of which agrees very well with that obtained by others on similarly doped samples (see fig. 3.2). Below we shall consider this (degenerate) sample as well as the four (degenerate and non-degenerate) samples reported by Miller [6]) (fig. 3.3). The temperature dependence of the resistivity of these samples agrees with that of our samples of comparable resistivity.

The separation of the Seebeck coefficient of the samples into contributions from the purely electronic effect and the drag effect is hampered by two circumstances. In the first place, our "experimental" mobility curves (fig. 3.8) provide no reliable data on the value of the mobility which is necessary in order to evaluate the hole concentration in Miller's samples from their resistivity. In the second place, especially near T_N, the temperature dependence of the experimental mobility deviates considerably from that predicted by Haas' theory of spin-disorder scattering. In sec. 4.3 we have proposed some possible explanations for this deviation. Each of these may affect the value of S_e at temperatures near and above T_N in some way or another, perhaps even to the extent that they are responsible for the larger part of the anomaly in S near T_N. For the moment, however, it will be assumed this is not the case and that the electronic contribution S_e may be calculated from eq. (3.3) with temperature-independent effective mass and scattering parameter, and that the "experimental" mobilities

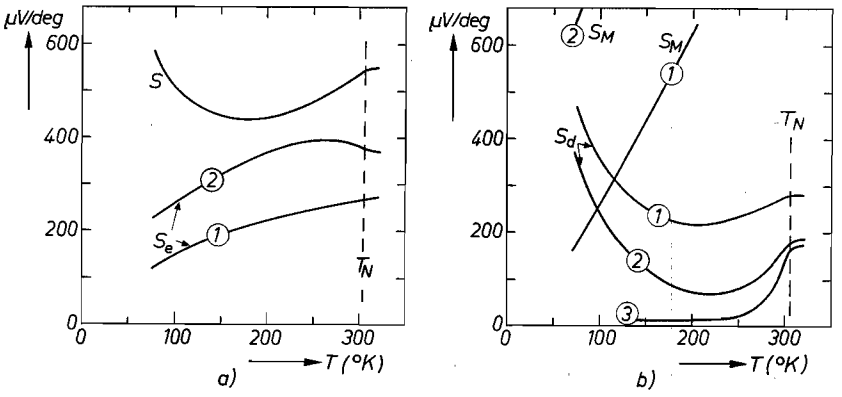

Fig. 5.1. The Seebeck coefficient of a non-degenerate sample (sample a from fig. 3.3); (*a*) measured Seebeck coefficient S, and calculated electronic contribution S_e, (*b*) drag contribution $S_d = S - S_e$, and maximum drag contribution S_M calculated using eq. (5.18a). For the curves labelled 1 the hole concentration was derived from the resistivity of the sample and the experimental mobility of samples 4 and 8 in fig. 3.8. For the curves labelled 2 a mobility was used having a value of 100 $cm^2/V\,s$ at 77 °K and the temperature dependence of the experimental mobility of Na-doped samples. For comparison curve 3 of fig. 5.2*b* is also shown.

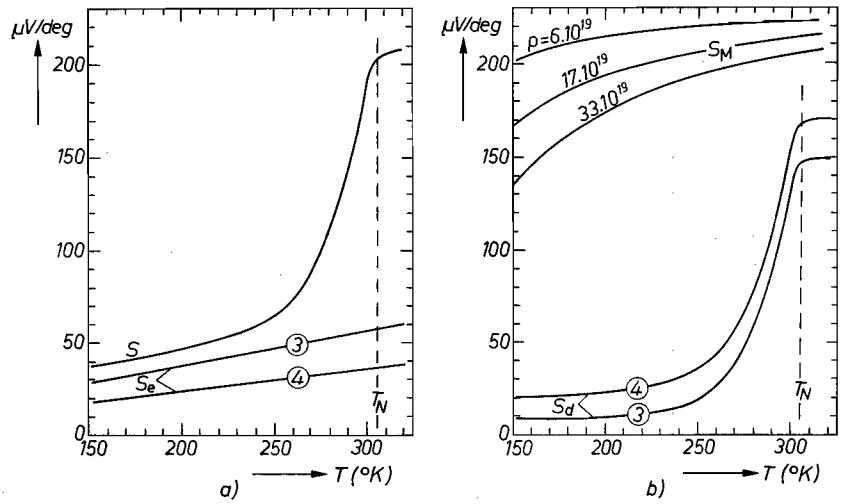

Fig. 5.2. The Seebeck coefficient of our Na-doped sample (see fig. 3.2); (*a*) measured Seebeck coefficient S, and calculated electronic contribution S_e, (*b*) drag contribution $S_d = S - S_e$, and maximum drag contribution S_M calculated using eq. (5.18b). For curves 3 and 4 the hole concentration is 17.10^{19} cm^{-3} and 33.10^{19} cm^{-3}, respectively, assuming $r = 0$ and $m = 0{\cdot}6\, m_0$.

defined in sec. 3.4 may be used to convert resistivities into hole concentrations. These are the assumptions of case (1) considered in sec. 3.1.3.

Figures 5.1*a* and 5.2*a* show the experimental Seebeck coefficient S of a non-degenerate and a degenerate sample, and some possible electronic contribu-

tions S_e. For the non-degenerate sample, curve 1 for S_e was obtained from the resistivity of the sample and the experimental mobility of samples 4 and 8 (fig. 3.8). This mobility is 30 cm^2/V s at 77 °K. Curve 2 for S_e was obtained with a mobility having a value of 100 cm^2/V s at 77 °K and the temperature dependence as found in Na-doped samples. For the degenerate sample S_e was calculated with two different temperature-independent carrier concentrations. The difference $S - S_e$ is shown in figs 5.1*b* and 5.2*b* and presumably represents the magnon-drag contribution S_d.

For a qualitative discussion of these curves we note first of all that the theory requires that S_d should be inversely proportional to the mobility. This gives a direct connection between the change of slope of $S_d(T)$ and that of the mobility at T_N.

A striking difference between figs 5.1*b* and 5.2*b* is that towards lower temperatures S_d increases strongly in the non-degenerate sample while this is not the case in the degenerate sample. This difference is due to the fact that $\tau_3(2\hat{k})/\tau_1(\hat{k})$ depends on temperature, $\hat{k}$ being equal to $k_T = (2\,m\,k\,T)^{1/2}/\hbar$ for non-degenerate samples, whereas for degenerate samples $\hat{k} = k_F = (3\,\pi^2\,p)^{1/3}$ is independent of temperature.

As follows from the correction factor $(1 - S_d/S_M)$ in eqs (5.5b) and (5.5c), second-order effects become important if the drag contribution S_d comes close to the quantity S_M. Assuming eqs (5.12b) and (5.17) to be valid and taking the double degeneracy of the magnon states into account, we have

$$S_M = 4\frac{N_v}{p}(k/e) \qquad \text{(non-deg.)}, \tag{5.18a}$$

$$S_M = \frac{8}{3}\frac{D(T/T_0')}{D(\infty)}(k/e) \qquad \text{(deg.)}. \tag{5.18b}$$

These estimates are indicated in figs 5.1*b* and 5.2*b*. They show that second-order effects should indeed be considered.

5.4.2. *Drag effects at* 77 °K

We first consider the situation at low temperatures. Figures 5.1*b* and 5.2*b* show that at low temperatures S_d remains well below S_M for the degenerate sample, but that for curves labelled 1 of the non-degenerate sample S_d considerably exceeds S_M. The latter cannot be correct. Either we have to take into account that for large second-order effects the numerical constant in eq. (5.18a) may be considerably larger than assumed (as in the case considered by Herring, eq. (5.14)), or we have used too small a mobility in calculating S_e (for a given resistivity a larger mobility means a smaller carrier concentration, a larger S_e, a smaller S_d, and a higher S_M). The second possibility may be assumed to be

the case because S_d shows no tendency to follow the temperature dependence of S_M towards lower temperatures.

Curves labelled 2 represent the case of a larger assumed mobility and, indeed, does not show the contradiction $S_d > S_M$. From this curve we find at 77 °K that $S_d = 350$ μV/deg and $S_M = 650$ μV/deg. Using eq. (5.5b) this gives $S_d^\circ = 760$ μV/deg. If the mobility is entirely due to magnon scattering, the first-order mobility calculated according to eq. (5.11) becomes $\mu_1^\circ = 60$ cm²/V s. Substituting these values and $c = 1{\cdot}4.10^6$ cm/s [21]) in eqs (5.9a) and (5.9b) we obtain $\tau_3 = 13.10^{-13}$ s. If, however, other scattering mechanisms determine the mobility at 77 °K, then μ_1° and thus τ_3 may be considerably larger. To establish a more accurate value of τ_3 and its temperature dependence it will be necessary to have more information on the mobility and the scattering prevailing at low temperatures.

In the preceding section the different temperature dependence of S_d at low temperatures in degenerate and non-degenerate samples was attributed to the different temperature dependence of $\tau_3(2\hat{k})/\tau_1(\hat{k})$ for the two cases. For the strongly degenerate sample d of fig. 3.3 (see also fig. 3.2) it is found that $S_d = S_d^\circ \approx 15$ μV/deg at 77 °K, which seems extremely low compared to the estimate $S_d^\circ = 760$ μV/deg for the non-degenerate sample considered in fig. 5.1. The difference may, however, be understood by noting that at 77 °K with $m = 0{\cdot}6\, m_0$ and $p = [\mathrm{Na}] = 2.10^{20}$ cm^{-3} (or $\mu = 90$ cm/V s) one has $k_F/k_T = 5{\cdot}6$. The ratio $760/15 = 51$ is, therefore, more than accounted for if $S_d^\circ \propto \hat{k}^{-2\cdot5}$. This implies that the scattering parameters r and s for carriers and magnons satisfy $2r + s = 1{\cdot}5$ (cf. eq. (5.6c); $\tau_1(k) \propto k^{2r-1}$, $\tau_3(q) \propto q^{-s-2}$). This relation requires no values of r and s which are a priori impossible *).

5.4.3. *Drag effects near* T_N

At temperatures near T_N second-order effects need not be taken into account for non-degenerate samples because $S_d \ll S_M$. In view of the uncertainties mentioned in sec. 5.4.1 the first-order drag contribution at 320 °K (i.e. just above T_N) has been analyzed in the following general way. Figure 5.3 shows the Seebeck coefficient and resistivity at 320 °K of the four samples of fig. 3.3. According to the figure the relation between S and ϱ may be written as

$$S = (k/e) \ln (\varrho/\varrho_0) = 198 \log_{10}(\varrho/\varrho_0) \quad \mu\mathrm{V/deg}, \tag{5.20a}$$

$$\varrho_0 \approx 1{\cdot}5.10^{-3}\ \Omega\ \mathrm{cm}. \tag{5.20b}$$

Denoting by μ_t and μ_1 the total (drift) mobility and mobility due to one-

*) In the calculation of τ_3 above it was assumed that $r = s = 0$. Other values of r and s do not, however, change the results very much, except if s would be 2 or larger, cf. eqs (5.8a) and (5.8b).

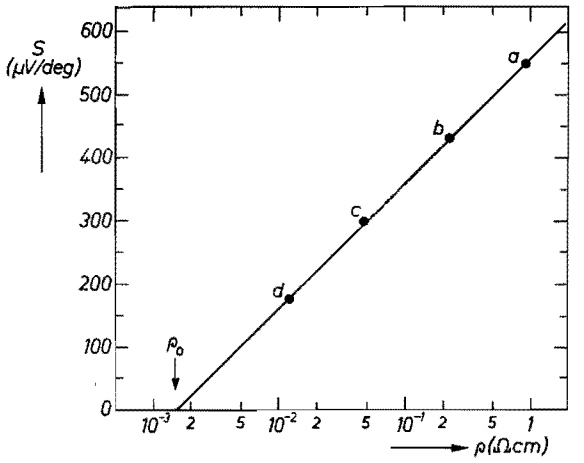

Fig. 5.3. Seebeck coefficient vs resistivity at 320 °K for samples a, b, c and d of fig. 3.3. The arrow indicates the value $1{\cdot}5.10^{-3}$ Ω cm for ϱ_0 in eq. (5.20).

magnon scattering, respectively, one also has for non-degenerate statistics, negligible second-order effects and τ_3 given by eq. (5.7),

$$S = S_e + S_d = \frac{k}{e}\left[r + 2 + \ln\left(N_v\,\mu_t\,e\,\varrho\right)\right] + \frac{c^2}{\Lambda}\,\frac{\hbar}{6\,\mu_1\,m\,k\,T^2}. \tag{5.21}$$

From the theoretical point of view the quantity of main interest is c^2/Λ. The value of this quantity and that of S_d are now determined.

Combining eqs (5.20a) and (5.21), one obtains, putting $x = \mu_t\,(T/300)^{3/2}$ and $m_S = m\,e^{2r/3}$ (cf. eq. (3.5b)):

$$S_d = \frac{k}{e}\ln\left(e^{2+r}\,N_v\,\mu_t\,e\,\varrho_0\right)^{-1}$$

$$= \frac{k}{e}\ln\frac{3{\cdot}36.10^{-2}/\varrho_0}{x\,(m_S/m_0)^{3/2}}, \tag{5.22}$$

$$\frac{c^2}{\Lambda} = \frac{6\,\mu_1\,m\,(k\,T)^2}{\hbar^2\,e}\ln\left(e^{2+r}\,N_v\,\mu_t\,e\,\varrho_0\right)^{-1}$$

$$= 5{\cdot}25.10^{12}\,e^{-2r/3}\,\frac{\mu_1}{\mu_t}\left(\frac{T}{300}\right)^{1/2} x\,\frac{m_S}{m_0}\ln\frac{3{\cdot}36.10^{-2}/\varrho_0}{x\,(m_S/m_0)^{3/2}}, \tag{5.23}$$

with x in cm²/V s, ϱ_0 in Ω cm, c^2/Λ in s^{-1}. Figures 5.4*a* and *b* show S_d and $y = \{\exp(2\,r/3)\}\,(3\,\mu_t/2\,\mu_1)\,(300/T)^{1/2}\,(c^2/\Lambda)$ as a function of x for $\varrho_0 = 1{\cdot}5.10^{-3}$ Ω cm and different relevant values of m_S. From these figures S_d and $\{\exp(2\,r/3)\}\,(3\,\mu_t/2\,\mu_1)\,(c^2/\Lambda)$ are directly evaluated once μ_t and m_S are known. They also show the effect of changing the assumed values of μ_t and m_S.

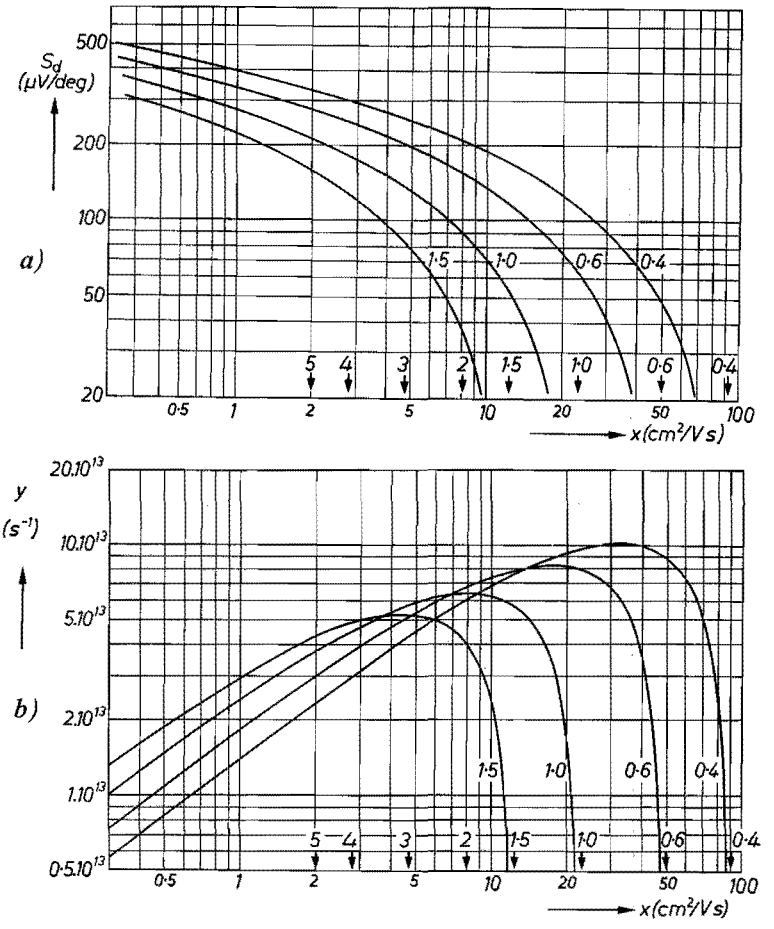

Fig. 5.4. (*a*) The drag contribution S_d and (*b*) the quantity
$y = (3/2)\, 5{\cdot}25.10^{12}\, x\, (m_S/m_0) \ln \{22\, x^{-1}\, (m_S/m_0)^{-3/2}\}$
as a function of $x = \mu_t\, (T/300)^{3/2}$ for various values of $m_S = m \exp(2\, r/3)$ acording to eqs (5.22) and (5.23) with $\varrho_0 = 1{\cdot}5.10^{-3}\ \Omega$ cm. Arrows indicate combinations of values of x and m_S for which $x\, (m_S/m_0)^{3/2} = 22$ cm^2/V s.

Miller [6]) finds from the resistivity of samples of composition $Na_\delta Mn_{1-\delta}Te$ a mobility of about 2 cm^2/V s at 320 °K (assuming that at this temperature the hole concentration is equal to $p = [Na] = 2\, \delta.10^{22}$ cm^{-3}). A mobility of 4 cm^2/V s seems a reasonable compromise between this value and our highest experimental mobility of 7 cm^2/V s at 320 °K (see fig. 3.8). With $x = 4{\cdot}5$ cm^2/V s and $m_S = 0{\cdot}6\, m_0$ figs 5.4*a* and *b* give $S_d \approx 200$ μV/deg and $\{\exp(2\, r/3)\}\, (3\, \mu_t/2\, \mu_1)\, (c^2/\Lambda) \approx 5.10^{13}$ s^{-1}.

Assuming that Haas' theory of spin-disorder scattering is valid, $r = 0$ and $2\, \mu_1/3\, \mu_t = 1$ (assuming that only spin-flip scattering contributes to the drag effect) so that $c^2/\Lambda = 5.10^{13}$ s^{-1}. The theoretical value calculated according

to eq. (5.7) with exchange integrals quoted by Zanmarchi and Haas [21]) is $1{\cdot}1.10^{13}\ s^{-1}$. As remarked in connection with eq. (5.7) other authors [71,72]) obtain somewhat smaller values of Λ than Zanmarchi and Haas. Our experimental value of $5.10^{13}\ s^{-1}$ for c^2/Λ thus appears to be in quite satisfactory agreement with theory.

It will be noted that according to fig. 5.4*b* the value of c^2/Λ is fairly insensitive to variations in mobility and Seebeck effective mass as long as $x\,(m_S/m_0)^{3/2} \lesssim 15\ cm^2/V\ s$. There is therefore a certain freedom in changing the assumed values of μ_t and m_S without coming into conflict with the theoretical value of c^2/Λ.

For a qualitative discussion of the temperature dependence of c^2/Λ near T_N it is remarked that towards lower temperatures the quantity x increases roughly as the ratio of the experimental mobility to the theoretical mobility in fig. 4.4. Above T_N the mobility in non-degenerate material is not accurately known, but it seems likely that at these temperatures x is roughly constant. Because, as just mentioned, c^2/Λ is only a weak function of x and, furthermore, ϱ_0 is constant for $T > 240\ °K$ (fig. 3.3), it follows that c^2/Λ is roughly constant for $T > T_N$ and increases only slightly towards lower temperatures. A pronounced change of c^2/Λ with temperature near T_N is not expected [21]).

We now consider degenerate samples, like the sample of fig. 5.2 and sample d of figs 3.3 and 5.3. As the latter two figures show, the resistivity and Seebeck coefficient of degenerate samples obey the same relations (5.20a) and (5.20b) as non-degenerate samples. As long as only first-order effects are considered this may be attributed to the fact that the total Seebeck coefficient $S_e + S_d^\circ$ may be rather insensitive to effects of degeneracy because these enlarge S_e and reduce S_d° (for $T \gtrsim T_N$ we have $S_d^\circ \propto \tau_3/\tau_1 \propto \hat{k}^{-1}$). Figure 5.2 shows, however, that for degenerate samples second-order effects cannot be neglected at temperatures $T \gtrsim T_N$. Making the appropriate correction according to eq. (5.5b) for $S_M = 220\ \mu V/deg$, one finds for curve 3 with $S_d = 150\ \mu V/deg$ and curve 4 with $S_d = 170\ \mu V/deg$ that S_d° is 470 and 750 μ/Vdeg, respectively. Contrary to the expectation these values are appreciably larger than the 200 $\mu V/deg$ obtained for non-degenerate samples.

Another feature of the experimental data also disagrees with the theoretical expectation concerning second-order effects. As mentioned in sec. 5.1.2 and as shown by eq. (5.5c), the mobility increases with increasing second-order effect. Therefore, the mobility in the degenerate sample should be larger than in a non-degenerate sample for $T \geqslant T_N$. This is indeed the case (cf. fig. 3.8). However, at temperatures below T_N second-order effects are negligible and both types of samples should have the same mobility (neglecting the effect of T', fig. 4.3). This should lead to only a small change of slope at T_N in the mobility for the degenerate sample, as shown by the dashed curve in fig. 5.5. Instead of a small change of slope the experimental mobility in degenerate samples shows

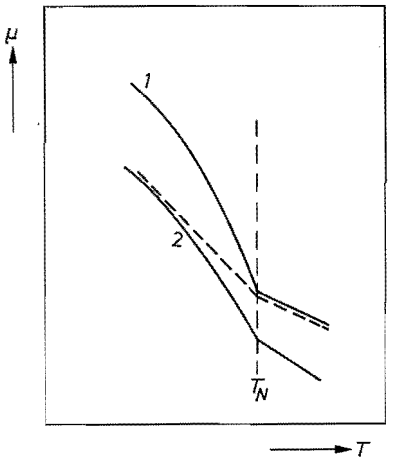

Fig. 5.5. Expected behaviour of mobility near T_N in the presence of second-order effects (schematic). Curve 1: experimental mobility in degenerate samples; curve 2: experimental mobility in non-degenerate samples; dashed curve: expected mobility in degenerate samples in the presence of second-order effects.

on the contrary a large change of slope, see fig. 4.4. The same difficulty is encountered when considering the different temperature dependence of the Seebeck coefficient in degenerate and non-degenerate samples (fig. 3.3).

The above discrepancies can be explained if it is assumed that the hole concentration in degenerate (Na-doped) samples and non-degenerate (undoped) samples depend differently on temperature between 240 °K and T_N. If in the undoped samples p increases, both $S_d°$ and the change of slope in the mobility at T_N for these samples become larger. Conversely, if in the Na-doped samples p decreases between 240 °K and T_N their $S_d°$ and change of slope in the mobility become smaller. In the latter case $S_d°$ diminishes both because S_e increases and because the correction for the second-order effect decreases. In this case, therefore, a much smaller change in p is required to satisfy the expected relations than in the case of the undoped samples. This may be an argument for assuming that the anomalous temperature dependence of the hole concentration occurs rather in the Na-doped samples than in the undoped samples.

It will be noted that the correction of the experimental mobility $\mu^*(T)$ necessitated by the proposed change in hole concentration near T_N increases the difference in μ^* at $T > 240$ °K for undoped and Na-doped samples. Since this difference is already large at temperatures below 240 °K this may not be a strong argument against the proposed interpretation, and it should probably be attributed to poor crystal quality (cf. sec. 3.4).

It thus appears that an anomalous temperature dependence of the acceptor-level depth as envisaged in case (2a) of sec. 3.3 may be a real effect occurring

in MnTe. As mentioned in sec. 4.3.2 such an effect is possible if the band parameters depend on the sublattice magnetization.

The model of magnetization-dependent band parameters also includes the possibility of a temperature-dependent effective mass (case (2b) of sec. 3.3). A temperature-dependent effective mass cannot contribute much to diminish the discrepancies discussed here, but it can contribute significantly to the temperature dependence of S_e. The proposed model need not, however, lead to a magnon-drag contribution to the Seebeck coefficient smaller than theoretically expected because of the insensitivity of c^2/Λ to variations in effective mass and mobility.

In sec. 4.3 two other modifications in the theory of spin-disorder scattering are mentioned, viz. an interaction between charge carriers and ionic spins different from that assumed by Haas, and the possible importance of magnetic-polaron effects at $T \gtrsim T_N$. In the former case the relaxation time determining the mobility is an anisotropic function, as yet unknown, of the wave vector $\mathbf{k}$. It can be easily shown that a possibly temperature-dependent effective *) scattering parameter r cannot account for the different temperature dependence of the resistivity and Seebeck coefficient in degenerate and non-degenerate samples. The magnetic-polaron model can account for this difference only if it also leads to a different temperature dependence of the hole concentration in the two types of samples, or if the model includes a mechanism that corresponds to the second-order effect but works out differently.

*) Because of the anisotropy of $\tau(\mathbf{k})$ a true scattering parameter r defined by $\tau \propto E^{r-1/2}$ may not exist.

6. CONCLUDING REMARKS

For temperatures below 240 °K the interpretation of the electrical transport properties of *p*-type MnTe seems to pose no essential problems. From a further study of the Seebeck coefficient and the dominating scattering mechanism it should be possible to obtain the value of the magnon relaxation time and its dependence on temperature and wave vector.

The origin of the interesting transport properties above 240 °K is less clear. Starting from the simple assumptions of a temperature-independent acceptor-level depth and effective mass, and assuming an interaction between the charge carriers and ionic spins proportional to $\mathbf{s} \cdot \mathbf{S}_i$, as well as the validity of a simple description of magnon drag, it has been shown that the following experimental data cannot be accounted for:

(A) the sharp change of slope at T_N (307 °K) in the "experimental" mobility as a function of temperature (see fig. 4.4),

(B) the temperature-dependent anisotropy $\mu_{||}/\mu_{\perp}$ (see fig. 3.10),

(C) the larger experimental mobility in degenerate samples than in non-degenerate samples (see fig. 3.8),

(D) the different temperature dependence of the experimental mobility (see figs 4.4 and 5.7) and of the Seebeck coefficient (see fig. 3.3) near T_N in degenerate and non-degenerate samples,

(E) the larger drag contribution to the Seebeck coefficient at $T \gtrsim T_N$ in degenerate samples (after correction for second-order effects) than in non-degenerate samples.

Point (C) may be related to imperfect crystal quality. It seems unlikely that this is also the case for the other points listed although, of course, verification by measurements on more perfect crystals would be valuable.

In connection with (A) and (B) three possible modifications of the theory of spin-disorder scattering were proposed in sec. 4.3:

(1) the interaction between charge carriers and ionic spins giving rise to spin-disorder scattering is of a more complex form than that assumed in eq. (4.3), this complexity being possibly due to spin-orbit coupling of the charge carriers,

(2) the interaction between charge carriers and ionic spins leads not only to scattering, but also to magnetization-dependent band parameters,

(3) at $T \gtrsim T_N$ the mean free path of the charge carriers due to the scattering is so small that a magnetic-polaron model is a better starting point for theoretical explanations.

In case (1) no anomalous temperature dependence of the hole concentration is expected to occur near T_N and the "experimental" mobility defined in sec. 3.4 will be equal to the drift mobility (except for the trivial effect of crystal quality, and the possibility that there is an anomalous contribution to the Hall coefficient

at low temperatures). In order to account for the observed anisotropy in the mobility, point (B), the relaxation time must be an anisotropic function, as yet unknown, of the wave vector **k**. It can be easily shown that point (E) requires the effective scattering parameter to be smaller than $-\frac{1}{2}$. Such a change in the value of r cannot, however, account for the different temperature dependence of the mobility and Seebeck coefficient in degenerate and non-degenerate material, point (D).

If the band parameters depend markedly on the sublattice magnetization (case (2)), the acceptor-level depth, and thus the hole concentration, may change anomalously near T_N. Due to this change the drift mobility is not equal to the "experimental" mobility. The drift mobility might still originate from the interaction (4.3), but account must be taken of temperature dependence of the effective mass and exchange integrals J, while the mobility will also include terms containing the staggered susceptibility. This model seems to be capable of explaining all items listed, except perhaps (C). Further theoretical work is necessary to determine whether the model does in fact lead to the required temperature dependence of the drift mobility and its anisotropy, points (A) and (B). The difficulties of points (D) and (E) would be removed if near T_N and with rising temperature the hole concentration either increases in the non-degenerate (undoped) samples or decreases in the degenerate (Na-doped) samples. As remarked in sec. 5.4.3, the fact that the mobility and the effective mass may have values different from those assumed in that section need not greatly affect the experimental value of c^2/Λ, the quantity determining the magnitude of the first-order drag effect at temperatures comparable to T_N.

In the case of magnetic polarons both the theoretical mobility and the Seebeck coefficient have to be reconsidered completely. Point (D) requires that the model leads to a temperature-dependent acceptor-level depth, or that it includes some mechanism which corresponds to the second-order drag effect and which results perhaps in a polaron effective mass depending on the hole concentration.

According to the above considerations the evidence of the available data strongly suggests that in the case of broad-band conduction the transport properties of p-type MnTe are significantly affected by a magnetization-dependent effective mass and acceptor-level depth (although the dependence need not be as large as shown in figs 3.6 and 3.7).

The optical data [19–21]) are not in disagreement with this conclusion, but neither do they provide information regarding its validity. For experimental verification of the conclusion it would be of interest to find new and independent ways of measuring the drift mobility, hole concentration or effective mass at temperatures near T_N. The drift mobility could perhaps be obtained from noise measurements [75]) or with techniques using injection pulses [76]). In spite of its anomalous behaviour a careful study of the Hall effect might still give infor-

mation regarding the possible anomalous temperature dependence of the hole concentration near T_N. If these measurements show that points (C) and (D) are real mobility effects, a polaron model with concentration-dependent effective mass deserves serious attention.

Acknowledgement

The work described in this thesis was carried out in the Philips' Research Laboratories in Eindhoven. I wish to express my sincere gratitude to the Directors of these laboratories for their permission to proceed with this work for a much longer time than originally foreseen, and to present its results as a thesis.

The investigation of MnTe was started in the group of Dr H. J. Vink at the suggestion of and in collaboration with Drs C. Haas and W. Albers. The frequent discussions with Dr Haas, now Professor at the University of Groningen, have greatly influenced many of the ideas put forward in this work. Without the care devoted by Mr A. M. J. H. Seuter to the difficult preparation of MnTe, the results presented would not have been obtained.

I am greatly indebted to Dr W. F. Knippenberg for his continuous encouragement during the writing of the manuscript. Discussions with many colleagues, in particular Drs W. van Haeringen, F. E. Maranzana and G. Zanmarchi, are gratefully acknowledged. Special thanks are due to Mrs A. Meyer-Huisman for preparation of the manuscript for publication.

REFERENCES

1) C. Herring, in G. T. Rado and H. Suhl (eds), Magnetism, Academic Press Inc., New York, 1966, Vol. 4.
2) S. Methfessel and D. C. Mattis, in S. Flügge and H. P. J. Wijn (eds), Hb. Phys., Vol. 18/1, 1968, p. 389.
3) D. Adler, Solid State Phys. **21**, 1, 1968.
4) E. Uchida, H. Kondoh and N. Fukuoka, J. phys. Soc. Japan **11**, 27, 1956.
5) R. E. Frederick and C. R. Manser, U.S. Patent 2,890,260, 1958.
6) R. C. Miller, in R. R. Heikes and R. W. Ure Jr. (eds), Thermoelectricity: science and engineering, Interscience Publishers, New York, 1961, p. 92.
7) H. Yadaka, T. Harada and E. Hirahara, J. phys. Soc. Japan **17**, 875, 1962.
8) E. D. Deviatkova, A. V. Golubkov, E. K. Kudinov and I. A. Smirnov, Soviet Phys. Solid State **6**, 1425, 1964.
9) A. J. Panson and W. D. Johnston, J. inorg. nucl. Chem. **26**, 705, 1964.
10) W. Albers and C. Haas, Phys. Letters **8**, 300, 1964.
11) W. Albers and C. Haas, Proc. int. conf. physics of semiconductors, Dunod, Paris, 1964, p. 1261.
12) W. Albers, G. van Aller and C. Haas, in Propriétés thermodynamiques, physiques et structurales des dérivés semimétalliques, Eds CNRS, Paris, 1967, p. 19.
13) J. D. Wasscher and C. Haas, Phys. Letters **8**, 302, 1964.
14) J. D. Wasscher, A. M. J. H. Seuter and C. Haas, Proc. int. conf. physics of semiconductors, Dunod, Paris, 1964, p. 1269.
15) M. Bailyn, Phys. Rev. **126**, 2040. 1962,
16) F. E. Maranzana, Phys. Rev. **160**, 421, 1967.
17) H. J. van Daal and A. J. Bosman, Phys. Rev. **158**, 736, 1967.
18) C. Haas, Phys. Rev. **168**, 531, 1968.
19) G. Zanmarchi, J. Phys. Chem. Solids **28**, 2123, 1967.
20) G. Zanmarchi and C. Haas, J. appl. Phys. **39**, 596, 1968.
21) G. Zanmarchi and C. Haas, Philips Res. Repts **22**, 389, 1968.
22) A. M. J. H. Seuter, in Propriétés thermodynamiques, physiques et structurales des dérivés semimétalliques, Eds CNRS, Paris, 1967, p. 459.
23) J. D. Wasscher, Solid State Comm. **3**, 169, 1965.
24) J. D. Wasscher, in Propriétés thermodynamiques, physiques et structurales des dérivés semimétalliques, Eds CNRS, Paris, 1967, p. 465.
25) K. Walther, Solid State Comm. **5**, 399, 1967.
26) J. van den Boomgaard, Philips Res. Repts, to be published.
27) N. Kunitomi, Y. Hamaguchi and S. Anzai, J. Phys. Radium **25**, 568, 1964.
28) S. Greenwald, Acta cryst. **6**, 396, 1953.
29) K. K. Kelley, J. Am. chem. Soc. **61**, 203, 1939.
30) K. Ozawa, S. Anzai and Y. Hamaguchi, Phys. Letters **20**, 132, 1966.
31) T. Komatsubara, M. Murakami and E. Hirahara, J. phys. Soc. Japan **18**, 356, 1963.
32) N. N. Sirota and G. J. Makovetski, Sov. Phys. Doklady **11**, 888, 1967.
33) L. J. van der Pauw, Philips Res. Repts **13**, 1, 1958.
34) L. J. van der Pauw, Philips Res. Repts **16**, 187, 1961.
35) D. H. Kroon, Laboratory magnets, Centrex, Eindhoven, 1967.
36) T. M. Dauphinee and E. Mooser, Rev. sci. Instr. **26**, 660, 1955.
37) L. J. van der Pauw, Rev. sci. Instr. **31**, 1189, 1960.
38) J. D. Wasscher, Philips Res. Repts **16**, 301, 1961.
39) J. Hornstra and L. J. van der Pauw, J. Electron. Control **7**, 169, 1959.
40) Z. Nehari, Conformal mapping, McGraw-Hill, New York, 1952.
41) P. F. Byrd and M. D. Freedman, Handbook of elliptic integrals, Springer Verlag, 1954.
42) G. Bosch, J. Phys. Chem. Solids **27**, 795, 1966.
43) C. Haas, A. M. J. G. van Run, P. F. Bongers and W. Albers, Solid State Comm. **5**, 657, 1967.
44) E. H. Putley, The Hall effect and related phenomena, Butterworths, London, 1960.
45) J. S. Blakemore, Semiconductor statistics, Pergamon Press, Oxford, 1962.
46) H. B. G. Casimir, Rev. mod. Phys. **17**, 343, 1945.
47) J. D. Wasscher, W. Albers and C. Haas, Solid-State Electronics **6**, 261, 1963.
48) C. J. G. F. Janssen, Some properties of MnTe single crystals, Thesis, University of Utrecht, 1965.
49) J. Kondo, Progr. theoret. Phys. (Kyoto) **27**, 772, 1962.

[50]) E. Callen, Phys. Rev. Letters **20**, 1045, 1968.
[51]) A. Taylor, cited by R. R. Heikes in P. H. Egli (ed.), Thermoelectricity, John Wiley and Sons, New York, 1960, p. 99.
[52]) T. Kasuya, Progr. theoret. Phys. (Kyoto) **16**, 58, 1956.
[53]) T. Kasuya, Progr. theoret. Phys. (Kyoto) **22**, 227, 1959.
[54]) P. G. de Gennes and J. Friedel, J. Phys. Chem. Solids **4**, 71, 1958.
[55]) T. van Peski-Tinbergen and A. J. Dekker, Physica **29**, 917, 1963.
[56]) P. W. Anderson, in G. T. Rado and H. Suhl (eds), Magnetism, Academic Press Inc., New York, 1963, Vol. 1, p. 25.
[57]) C. Kittel, Quantum theory of solids, John Wiley & Sons, New York, 1963.
[58]) J. M. Ziman, Electrons and phonons, Clarendon Press, Oxford, 1963.
[59]) D. Adler and H. Brooks, Phys. Rev. **155**, 826, 1967.
[60]) P. G. de Gennes, in G. T. Rado and H. Suhl (eds), Magnetism, Academic Press Inc., New York, 1963, Vol. 3, p. 115.
[61]) T. Wolfram and J. Callaway, Phys. Rev. **130**, 45, 1963.
[62]) L. R. Walker, in G. T. Rado and H. Suhl (eds), Magnetism, Academic Press Inc., New York, 1963, Vol. 1, p. 229.
[63]) W. Shockley, Electrons and holes in semiconductors, Van Nostrand Inc., Princeton, 1950.
[64]) E. H. Sondheimer, Proc. phys. Soc. **65A**, 561, 1952.
[65]) C. Herring, in Halbleiter und Phosphore, Vieweg & Sohn, Braunschweig, 1954, p. 184.
[66]) E. H. Sondheimer, Proc. roy. Soc. (London) **234**, 391, 1956.
[67]) C. Herring, Phys. Rev. **96**, 1163, 1954.
[68]) B. Jacrot and T. Riste, in P. A. Egelstaff (ed.), Thermal neutron scattering, Academic Press Inc., London, 1965, p. 251.
[69]) T. Riste, J. appl. Phys. **39**, 528, 1968.
[70]) P. Martel, R. A. Cowley and R. W. H. Stevenson, J. appl. Phys. **39**, 1116, 1968.
[71]) H. Mori and K. Kawasaki, Progr. theoret. Phys. (Kyoto) **27**, 529, 1962.
[72]) P. G. de Gennes, J. Phys. Chem. Solids **4**, 223, 1958.
[73]) J. F. Parrott, Proc. phys. Soc. **70B**, 590, 1957.
[74]) J. Appel, Z. Naturf. **13a**, 386, 1958.
[75]) G. A. Acket, On the conduction mechanism of some transition-metal oxides, Thesis, University of Utrecht, 1965. See also R. J. J. Zijlstra, F. J. Leeuwerik and Th. G. M. Kleinpenning, Phys. Letters **23**, 185, 1966.
[76]) D. J. Gibbons and W. E. Spear, J. Phys. Chem. Solids **27**, 1917, 1966.

Summary

MnTe is an antiferromagnetic semiconductor with a Néel temperature T_N of 307 °K and an energy gap of 1·2 eV. The electrical properties, Hall coefficient, resistivity and Seebeck coefficient (thermoelectric power) of *p*-type MnTe show a marked influence of the rapidly changing magnetic ordering occurring near T_N. The investigation and explanation of this influence constitutes the main subject of this thesis.

In chapter 1 some general properties of MnTe are discussed. In chapter 2 a description is given of the experimental arrangements used, and of a simple and sensitive method for measuring anisotropies in the resistivity.

The results of the measurements are presented and their interpretation is discussed in chapter 3. It is found that a pronounced anisotropic anomalous contribution to the Hall effect occurs at temperatures above 240 °K. The sign and temperature dependence of this contribution agrees with the predictions of Maranzana's theory describing the anomalous Hall effect in magnetic conductors. However, this theory does not account for the magnitude and the anisotropy of the observed effect.

Important factors for the description of the resistivity and Seebeck effect are spin-disorder scattering and magnon drag. These phenomena are discussed in chapters 4 and 5, respectively.

Disorder in the orientation of the magnetic moments causes scattering of the charge carriers due to the existence of an exchange interaction between a charge carrier and the partially filled shells of the magnetic atoms. Haas recently calculated the mobility of charge carriers in magnetic semiconductors making certain assumptions, among other things as regards the form of the interaction mentioned. It is found that this theoretical mobility cannot account for the temperature dependence of the resistivity observed in MnTe near T_N, nor for the observed temperature dependence of the anisotropy of the resistivity.

Three possible extensions of the theory of spin-disorder scattering are indicated: (1) The true form of the interaction between charge carriers and magnetic spins is more complicated than assumed. (2) The interaction causes a mixing of states of different energy bands, the amount of mixing depending on the magnitude of the (sublattice) magnetization. This may lead to a magnetization-dependent effective mass and acceptor-level depth. (3) At temperatures $T \gtrsim T_N$ the mobility is so small (of the order of 5 $cm^2/V\,s$) that a magnetic-polaron model is a better starting point for theoretical explanations.

In connection with the discussion of magnon drag a calculation is given of the mobility in antiferromagnetic semiconductors due to the scattering caused by the creation and annihilation of a magnon. The equation obtained agrees with the corresponding equation of Haas' theory at all temperatures up to T_N. At temperatures above T_N the difference between the two results is only small.

In chapter 5 both first-order and second-order magnon-drag effects are discussed. The first-order drag effect appears in the Seebeck (and Peltier) effect, and is caused by the mutual drag between currents of charge carriers and magnons resulting from the scattering of charge carriers by magnons. Second-order effects become important if the scattering of magnons by charge carriers contributes significantly to restoring equilibrium in the magnon system. This is only the case if the carrier concentration is large. Second-order effects lead to an increased mobility of the carriers and to a decreased drag contribution to the Seebeck effect.

At low temperatures (measurements have been done down to 77 °K) the magnitude and wave-vector dependence of the magnon relaxation time can be estimated from the drag contribution to the Seebeck coefficient in samples with different hole concentration. For obtaining more accurate results more information is required regarding the mobility at these temperatures.

If it is assumed that in MnTe the hole concentration and effective mass do not, or do nearly not, depend on temperature, the first-order magnon-drag effect is found to account adequately for the observed Seebeck coefficient at temperatures near and above T_N. From the measurements the diffusion constant of the magnons can be derived. The value obtained is relatively insensitive to variations in the assumed values of effective mass and mobility, and it agrees fairly well with theoretical expectation.

It is shown that at temperatures close to and above T_N second-order effects should be important in highly-Na-doped samples, which have a large hole concentration. From this fact a different temperature dependence is expected to occur in the resistivity and Seebeck coefficient of undoped and Na-doped samples. The observed difference is, however, opposite to that expected. It is concluded that probably the Na-acceptor-level depth depends on the sublattice magnetization. Also a refined magnetic-polaron model may perhaps account for the experimental data.

In the final chapter 6 the main differences between experimental data and the simple theoretical models used are reviewed and compared to the theoretical refinements proposed in chapter 4. Some suggestions for further experimental work on MnTe are made.

Samenvatting

MnTe is een antiferromagnetische halfgeleider waarvan de elektrische eigenschappen duidelijk beïnvloed worden door de sterk veranderende magnetische ordening die plaats vindt rond de Néel-temperatuur, $T_N = 307$ °K. Het voornaamste onderwerp van dit proefschrift is de bestudering en verklaring van deze invloed op de elektrische weerstand, het Hall-effekt en het Seebeck-effekt (thermokracht) in *p*-type MnTe.

Na een bespreking van enige algemene eigenschappen van MnTe in hoofdstuk 1, wordt in hoofdstuk 2 een beschrijving gegeven van de gebruikte meetmethoden. In het bijzonder wordt ingegaan op een methode om op eenvoudige en gevoelige wijze weerstandsanisotropieën te meten.

In hoofdstuk 3 worden de meetresultaten en hun mogelijke interpretaties besproken. In het Hall-effekt blijkt een sterk anisotrope anomale bijdrage op te treden bij temperaturen boven 240 °K. De temperatuurafhankelijkheid van deze bijdrage is in goede overeenstemming met Maranzana's theorie van het anomale of buitengewone Hall-effekt in magnetische geleiders. Deze theorie geeft echter geen verklaring voor de grootte en de anisotropie van het waargenomen effekt.

Belangrijk voor de beschrijving van weerstand en Seebeck-coefficient zijn spinwanorde-strooiing en magnon-drag ("magnon-meesleep-effekt"). Deze verschijnselen worden achtereenvolgens besproken in de hoofdstukken 4 en 5.

Wanorde in de orientatie van de magnetische momenten geeft aanleiding tot strooiing van ladingdragers doordat er een plaatsruil-wisselwerking is tussen een ladingdrager en de gedeeltelijk gevulde schillen van de magnetische atomen. Onder bepaalde veronderstellingen, o.a. wat betreft de vorm van genoemde wisselwerking, heeft Haas een theoretische berekening gegeven van de uit deze strooiing voortvloeiende beweeglijkheid van ladingdragers in magnetische halfgeleiders. Het verloop van deze beweeglijkheid blijkt de bij de Néel-temperatuur waargenomen temperatuurafhankelijkheid van de weerstand in *p*-type MnTe niet te kunnen verklaren. Ook geeft de theorie geen rekenschap van de gevonden temperatuurafhankelijkheid in de anisotropie van de weerstand.

Drie mogelijke uitbreidingen van de theorie voor spinwanorde-strooiing worden genoemd: (1) De werkelijke vorm van de wisselwerking tussen ladingdragers en magnetische spins kan gecompliceerder zijn dan in Haas' theorie wordt aangenomen. (2) De wisselwerking brengt een menging teweeg van toestanden uit verschillende energiebanden, waarbij de grootte van de menging afhangt van de subrooster-magnetisatie. Dit kan onder meer leiden tot een magnetisatieafhankelijkheid van effektieve massa en acceptordiepte. (3) De beweeglijkheid bij temperaturen $T \gtrsim T_N$ is zo klein (van de orde van 5 cm^2/V s) dat een magnetisch-polaronmodel een beter uitgangspunt voor theoretische beschouwingen is.

In verband met de discussie van magnon-drag-verschijnselen wordt aan het eind van hoofdstuk 4 een berekening gegeven van de beweeglijkheid in antiferromagnetische halfgeleiders veroorzaakt door strooiing ten gevolge van het creëren en annihileren van een magnon. De verkregen formule stemt in het hele temperatuurgebied tot T_N overeen met de overeenkomstige formule uit Haas' theorie. Bij temperaturen boven T_N zijn de afwijkingen tussen de uitkomsten van de twee berekeningen slechts gering.

Bij de magnon-drag-effekten worden in hoofdstuk 5 zowel de eerste- als de tweede-orde effekten besproken. Het eerste-orde effekt geeft een extra bijdrage tot het Seebeck- (en tot het Peltier-) effekt en wordt veroorzaakt doordat wegens onderlinge botsingen ladingdragers meegesleept worden door een magnonenstroom (en omgekeerd). Tweede-orde effekten zijn van belang wanneer strooiing van magnonen aan ladingdragers een aanzienlijke bijdrage levert tot het in evenwicht komen van het magnonsysteem. Dit is alleen het geval bij grote ladingdragersconcentratie. Tweede-orde effekten leiden tot een vergroting van de beweeglijkheid van de ladingdragers en tot een verkleining van de magnon-drag-bijdrage tot de Seebeck-coefficient.

Bij lage temperaturen (metingen zijn gedaan vanaf 77 tot 350 °K) kan uit de drag-bijdrage aan de Seebeck-coefficient van preparaten met verschillende gatenconcentraties een schatting gemaakt worden van de grootte en golfvektorafhankelijkheid van de relaxatietijd van de magnonen. Voor nauwkeuriger uitkomsten zijn meer gegevens betreffende de beweeglijkheid bij deze temperaturen vereist.

Indien men aanneemt dat in MnTe de gatenconcentratie en de effektieve massa niet of nauwelijks van de temperatuur afhangen, vindt men dat het eerste-orde magnon-drag effekt een goede verklaring geeft voor de waargenomen Seebeck-coefficient bij temperaturen in de buurt van of boven de Néeltemperatuur. Uit de metingen kan de diffusieconstante van de magnonen bepaald worden. De afgeleide waarde is betrekkelijk onafhankelijk van de veronderstellingen aangaande de effektieve massa en de beweeglijkheid, en zij stemt redelijk goed overeen met de theoretisch voorspelde waarde.

Men kan laten zien dat tweede-orde effekten van belang zijn in sterk met natrium verontreinigde preparaten (die een grote gatenconcentratie hebben) bij temperaturen $T \gtrsim T_N$. Hieruit volgt dat de temperatuurafhankelijkheid van de weerstand en van de Seebeck-coefficient verschillend moet zijn voor al dan niet met Na verontreinigde preparaten. Het waargenomen verschil is echter tegengesteld aan het verwachte verschil. Hieruit wordt de gevolgtrekking gemaakt dat waarschijnlijk het Na-acceptorniveau van de subroostermagnetisatie afhangt. Ook een verfijnd magnetisch-polaronmodel zou de waarnemingen misschien kunnen verklaren.

In het zesde en laatste hoofdstuk worden de voornaamste verschillen tussen de waarnemingen en de gebruikte eenvoudige theoretische modellen nog eens

kort samengevat en vergeleken met de theoretische verfijningen die in hoofdstuk 4 werden voorgesteld. Tenslotte worden enige voorstellen gedaan betreffende eventueel verder te doen experimenteel onderzoek aan MnTe.

STELLINGEN

bij het proefschrift van J. D. Wasscher,

30 sept. 1969, Technische Hogeschool, Eindhoven

I

Anisotropieën in de soortelijke weerstand kunnen zeer geschikt bepaald worden door de methode van Van der Pauw toe te passen op preparaten van eenvoudige vorm.

Dit proefschrift, hoofdstuk 2.

II

Voor een beter begrip van de elektrische geleiding in *p*-type MnTe rond de Néel-temperatuur zijn metingen gewenst waaruit de beweeglijkheid, gatenconcentratie, of acceptordiepte op onafhankelijke wijze bepaald kan worden.

Dit proefschrift, hoofdstukken 5 en 6.

III

De wijze waarop Abrikosov et al. het existentiegebied van MnTe bepaald hebben is aan bedenking onderhevig.

N. Kh. Abrikosov, K. A. Dyul'dina en V. V. Zhdanova, Inorg. Mat. **4**, 1638, 1968.

IV

De argumenten die Adler aanvoert tegen Maranzana's theorie van het anomale Hall-effect, zijn ongegrond.

D. Adler, Solid State Phys. **21**, 1, 1968.
F. E. Maranzana, Phys, Rev. **160**, 421, 1967.

V

De door Putley gegeven toelichting op de invloed die de ontaarding van een elektronengas heeft op de elektronenbeweeglijkheid, kan gemakkelijk aanleiding geven tot onjuiste gevolgtrekkingen.

E. H. Putley, The Hall effect and related phenomena (Butterworths, Londen, 1960), blz. 93 en 94.

VI

Bij hun berekeningen van de maximale „figure of merit" voor extrinsieke halfgeleiders gaan Chasmar en Stratton uit van een materiaalparameter β. Het is zinvoller uit te gaan van $\beta \exp r$, waarbij r de op bladzijde 26 van dit proefschrift gedefinieerde strooiingsparameter is.

R. P. Chasmar en R. Stratton, J. Electron. Control, **7**, 52, 1959.
J. D. Wasscher, W. Albers en C. Haas, Solid-State Electron. **6**, 261, 1963.

VII

Uit de optische en elektrische metingen van Austin et al. aan met Li verontreinigd NiO kan afgeleid worden dat de bovengrens voor de hipenergie van vrije gaten in NiO lager is dan die welke door de genoemde auteurs zelf is aangegeven.

I. G. Austin, B. D. Clay en C. E. Turner, J. Phys. C (Proc. phys. Soc.) Ser.2, **1**, 1418, 1968.

VIII

Bij de door Niilisk en Kirs bepaalde drukafhankelijkheid van de relatieve spektrale gevoeligheid van de fotogeleiding in GaSe kunnen de meetresultaten, behalve door oppervakte-effekten, ook door andere verschijnselen beïnvloed zijn.

A. J. Niilisk en J. J. Kirs, Phys. Stat. sol. **31**, K91, 1969.

IX

De juistheid van de mening van Harper en Hakki dat de door hen gemeten groene emissie van GaP-diodes bij lage temperatuur door Si(donor)-Zn(acceptor) paarrekombinatie ontstaat, is aan twijfel onderhevig.

F. E. Harper en B. W. Hakki, J. appl. Phys. **40**, 672, 1969.

X

De door Smith et al. verkregen meetresultaten betreffende de zuurstofdoorlaatbaarheid van met CaO gestabiliseerd ZrO_2, kunnen moeilijk verklaard worden met de veronderstelling dat alle calciumionen acceptoren, en alle zuurstofvakatures donoren zijn.

A. W. Smith, F. W. Meszaros en C. D. Amata, J. Am. ceram Soc. **49**, 240, 1966.